# ELESCLOMOL ALLEVIATES MENKES PATHOLOGY IN MICE BY DELIVERING CU TO BRAIN CYTOCHROME *C* OXIDASE

A Dissertation

By

LIAM M. GUTHRIE

Submitted to the Graduate and Professional School of
Texas A&M University
In partial fulfillment of the requirements for the degree of

DOCTOR OF PHILOSOPHY

| | |
|---|---|
| Chair of Committee, | James C. Sacchettini |
| Committee Members, | Sarah E. Bondos |
| | Gregg B. Wells |
| | Jerome P. Trzeciakowski |
| Head of Department, | Carol M. Vargas Bautista |

August 2022

Major Subject: Medical Sciences

# ABSTRACT

Copper is an essential micronutrient required for the proper biological function of numerous enzymes. Absorption, transportation, and elimination of copper is highly regulated due to potential pathological effects of copper overload or deficiency. Menkes Disease is an X-linked inherited defect in active, directional copper transport caused by mutations in the *ATP7A* gene that results in profound copper deficiency and subsequent neurodegeneration in hemizygous male infants. The prognosis for those diagnosed with Menkes Disease is poor with death resulting before three years of age.

Current therapeutic strategies involve parental replacement of systemic copper using histidine as the ionophoric carrier, but clinical trials have failed to significantly alter disease progression in most patients. Poor tissue penetrance and low restoration of cuproenzyme function explain the failure of histidine-based therapy in Menkes patients.

Elesclomol is a chemotherapeutic agent with highly specific copper coordinating properties. The copper (II)-elesclomol complex is highly lipophilic, penetrates the blood-brain barrier, and has demonstrated the ability to restore cuproenzyme function in copper-deficient yeast strains at very low exposure levels.

To assess the efficacy of an elesclomol-based copper replacement therapy, an intervention protocol in *mottled-brindled* mice was developed resulting in greater than 80% survival of affected male mice. Of these mice, average lifespan within the treatment group approximated wildtype length with multiple individuals surviving greater than 250 days.

Phenotypic characterization of rescued Menkes-affected males reveals subtle deficiencies in neurologic and motor performance. Quantification of tissue copper levels and cuproenzyme function demonstrate partial restoration of copper levels and function of the key cuproenzyme cytochrome *c* oxidase.

Pharmacokinetics and acute toxicity of the intervention regime were assessed. The complex exhibits biphasic distribution with slow elimination from peripheral tissues, moderate systemic exposure, and is well tolerated at low exposure levels.

Based on these results, the copper (II)-elesclomol complex shows promise as a potential therapeutic agent for the treatment of Menkes Disease.

# DEDICATION

For my family… Thank you for years of support and encouragement.

# ACKNOWLEDGEMENTS

I would like to thank my committee chair and primary investigator, Dr. James Sacchettini, and my committee members, Dr. Sarah Bondos, Dr. Gregg Wells, and Dr. Jerome Trzeciakowski, for their guidance and support throughout the course of this research. I especially thank Dr. James Sacchettini and co-primary investigator Dr. Vishal Gohil for their mentorship these past seven years. I thank Dr. Julian Leibowitz, Mrs. Mary Imran, and Mrs. Katharina Ojala for their patience and guidance throughout my time in MD/PhD Program.

Thanks also go to my friends and colleagues in Medical Sciences and the Sacchettini and Gohil Labs for making my time at Texas A&M University a great experience. I wish a special thanks to Dr. Cory Thurman and Dr. Adam Salazar for our many coffee time conversations and friendship.

Finally, thanks to my mother, Heather Guthrie, for her unwavering encouragement and to my husband, Joe Guthrie-Perez, for his patience and love. I owe you all the world and love you more than words can describe. Thank you.

CONTRIBUTORS AND FUNDING SOURCES

## Contributors

This work was supervised by a dissertation committee consisting of Dr. James Sacchettini at Texas A&M University. Committee Members consisted of Dr. Sarah Bondos, Dr. Gregg Wells and Dr. Jerome Trzeciakowski of Texas A&M Health Science Center College of Medicine.

All cardiac *CTR1* knockout mice work was conducted by Dr. Sai Yuan under the supervision of Dr. Byung-Eun Kim in the Department of Animal and Avian Sciences, University of Maryland, College Park, MD 20742. Generation of *ATP7A* knockout B16 melanoma cell line was conducted by Dr. Vinit Shanbhag and Dr. Michael Petris at the Department of Biochemistry, University of Missouri, Columbia, MO 65211.

Dr. Shivatheja Soma and Dr. Mohammad Zulkifli of the Department of Biochemistry-Biophysics at Texas A&M University assisted in tissue sample processing, quantified tissue copper levels, quantified tissue COX1, and performed RT-PCR quantification of tissue metallothionein levels. Mr. Andres Silva and Dr. Thomas Snavely assisted in animal husbandry activities, tissue harvest, and pharmacokinetic studies. Dr. Arjun Archarys at Texas A&M University synthesized and purified the copper (II)-elesclomol complex. Dr. Franklin Lopez of Texas Veterinary Medicine Diagnostics Lab generated digital histology slides and provided histopathological technical expertise. Dr. Vishal Gohil of Biochemistry-Biophysics at Texas A&M University provided guidance on copper biology.

All other work conducted for this dissertation was completed independently by Liam M. Guthrie.

**Funding Sources**

Medical Education and Graduate study was supported by a fellowship from the Texas A&M Health Science Center College of Medicine MD/PhD Program and dissertation research from the laboratory of Dr. James C. Sacchettini.

This work was made possible by the Texas A&M University System Chancellor's Research Initiative, the Welch Foundation under Grant Numbers A-0015, and the National Institutes of Health under Grant Number P01AI095208. Its contents are solely the responsibility of the authors and do not necessarily represent the official views of the Chancellor's Research Initiative, Welch Foundation, or National Institutes of Health.

# NOMENCLATURE

| | |
|---|---|
| AD | Alzheimer Dementia |
| ALS | Amyotrophic Lateral Sclerosis |
| ASPEN | American Society for Parenteral and Enteral Nutrition |
| ATOX1 | Antioxidant Protein 1 |
| ATP | Adeonosine Triphosphate |
| ATP7A | Copper Transporting ATPase 7α |
| ATP7B | Copper Transporting ATPase 7β |
| BBB | Blood-Brain-Barrier |
| BCSFB | Blood-Cerebrospinal Fluid-Barrier |
| CCS | Copper Chaperone to SOD |
| CNS | Central Nervous System |
| COA6 | Cytochrome *c* Oxidase Assembly Factor 6 |
| COX | Cytochrome *c* Oxidase Subunit |
| Cp | Ceruloplasmin |
| CTR1 | Copper Transporter 1 |
| $Cu^{+}$ | Cuprous Ion |
| $Cu^{2+}$ | Cupric Ion |
| $CuSO_4$ | Copper Sulfate |
| DMT1 | Divalent Metal Transporter 1 |
| DBH | Dopamine β-Hydroxylase |

| | |
|---|---|
| EAR | Estimated Average Requirement |
| ES | Elesclomol |
| ES-$Cu^{2+}$ | Copper (II)-Elesclomol Complex |
| FDX1 | Fe-S Protein Ferredoxin 1 |
| FTT | Failure to Thrive |
| GSH | Glutathione |
| His | Histidine |
| His-$Cu^{2+}$ | Copper (II)-Histidine Complex |
| HMN | X-Linked Distal Hereditary Motor Neuropathy |
| IMM | Inner Mitochondrial Membrane |
| IMS | Intermembrane Space |
| LBGA | Low Birthweight for Gestational Age |
| LOX | Lysyl Oxidase |
| MD | Menkes Disease |
| MS | Multiple Sclerosis |
| MT | Metallothioneins |
| NDD | Neurodegenerative Disease |
| PD | Parkinson’s Disease |
| RDA | Recommended Dietary Allowance |
| ROS | Reactive Oxygen Species |
| SCO1 | Protein Synthesis of COX1 |
| SCO2 | Protein Synthesis of COX2 |

| | |
|---|---|
| TPN | Total Parenteral Nutrition |
| TYR | Tyrosinase |
| UL | Tolerable Upper Intake Level |
| WD | Wilson Disease |

TABLE OF CONTENTS

Page

ABSTRACT ..... ii

DEDICATION ..... iv

ACKNOWLEDGEMENTS ..... v

CONTRIBUTORS AND FUNDING SOURCES ..... vi

NOMENCLATURE ..... viii

TABLE OF CONTENTS ..... xi

LIST OF FIGURES ..... xiv

LIST OF TABLES ..... xvi

1. INTRODUCTION ..... 18

1.1. Copper—An Essential Micronutrient ..... 18
1.1.1. Nutritional Aspects of Copper ..... 19
1.1.2. Dietary Copper Deficiency ..... 22
1.1.3. Dietary Copper Toxicity ..... 26
1.2. Normal Physiology ..... 28
1.2.1. Absorption ..... 28
1.2.2. Distribution ..... 32
1.2.3. Elimination ..... 34
1.3. Major Cuproenzymes and Function ..... 37
1.3.1. Cytochrome *c* Oxidase ..... 39
1.3.2. Superoxide Dismutase ..... 40
1.3.3. Dopamine-β-Hydroxylase ..... 42
1.3.4. Lysyl Oxidase ..... 43
1.3.5. Tyrosinase ..... 44
1.3.6. Ceruloplasmin ..... 46
1.3.7. Sulfhydryl Oxidase ..... 46
1.4. Pathophysiology of Wilsons and Menkes Diseases ..... 48
1.4.1. Wilsons Disease ..... 49
1.4.2. Menkes Disease ..... 51
1.5. Pathogenic *ATP7A* Variant Clinical Case Reports ..... 55

1.6. Elesclomol as a Small Molecular Ionophore Therapeutic ..... 59
1.7. References ..... 63

2. PROPOSAL & PRELIMINARY DATA ..... 85

2.1. AIMS ..... 85
2.1.1. Specific Aim 1: To evaluate tolerability and pharmacokinetics ..... 86
2.1.2. Specific Aim 2: Pilot Study and Interventional Optimization ..... 86
2.1.3. Specific Aim 3: To evaluate biomarkers of intervention ..... 87
2.2. Approach ..... 88
*2.2.1.* Approach to AIM 1 ..... 89
*2.2.2.* Approach to AIM 2 ..... 98
*2.2.3.* Approach to AIM 3 ..... 103
2.3. Use of Vertebrate Animals ..... 105
2.4. Vertebrate Animal General Methods ..... 107

3. *SCIENCE* PUBLICATION ..... 111

3.1. Abstract ..... 111
3.2. Main Text ..... 112
3.3. ES Restores Mitochondrial Function in *Ctr1* Knockout H9c2 Cells and Mice ..... 113
3.4. ES Alone Does Not Rescue *mottled-brindled* Mice ..... 124
3.5. ES-$Cu^{2+}$ Complex Rescues *mottled-brindled* Mice ..... 124
3.6. Neuromotor Assessment of ES-$Cu^{2+}$ Rescue ..... 139
3.7. Brain Histology ..... 142
3.8. Biochemical Markers of ES-$Cu^{2+}$ Therapy ..... 148
3.9. Discussion ..... 157
3.10. Materials & Methods ..... 160
3.10.1. Reagents ..... 160
3.10.2. Synthesis of Elesclomol-$Cu^{2+}$ Complex ..... 161
3.10.3. Synthesis of Copper Histidine Complex ..... 161
3.10.4. *In vivo* Pharmacokinetics and Toxicological ..... 162
3.10.5. Brain Elesclomol-$Cu^{2+}$ Exposure ..... 164
3.10.6. LC-MS Quantification in Plasma and Brain ..... 164
3.10.7. Cardiac *CTR1* Knockout Mice ..... 166
3.10.8. *Mottled-brindled* Mice ..... 166
3.10.9. Administration of Elesclomol to Cardiac *Ctr1* Knockout Mice ..... 167
3.10.10. Administration of substances to *mo-br* Mice ..... 168
3.10.11. Growth Curves and Kaplan-Meier Survival Plot ..... 169
3.10.12. Locomotor Function ..... 170
3.10.13. Necropsy & Histology ..... 172
3.10.14. Biochemistry ..... 173
3.10.15. *ATP7A* Knockout B16 Melanoma Cells ..... 174
3.10.16. *CTR1* Knockout H9c2 Cells ..... 175

3.10.17. Statistical analysis and software ..... 177
3.11. Acknowledgments ..... 178
3.12. References ..... 180

4. CONCLUSIONS ..... 185

4.1. Future Works ..... 185
4.2. ES-$Cu^{2+}$ Clinical Trial Design ..... 188

LIST OF FIGURES

Page

Figure 1-1 Copper Transport within Cells .....31

Figure 1-2: Structure of ES and its $Cu^{2+}$ Complex.....60

Figure 1-3: Schematic Diagram of Proposed ES-Mediated Mitochondrial Release of Copper in the Brain.....62

Figure 2-1: Phase Solubility of ES-$Cu^{2+}$ in Captisol Aqueous Vehicle .....92

Figure 2-2: Subcutaneous PK Nonlinear 2-Compartment Models and Parameters.....95

Figure 2-3: Quantification of ES/ES-$Cu^{2+}$ in Brain Tissue.....97

Figure 2-4: Wildtype and *mo-br* Males at Postnatal Day 5.....98

Figure 2-5: Survival of *mo-br* Males in Intervention Pilot Study .....100

Figure 3-1: Effects of ES treatment on OCR and relative ATP levels in *Ctr1* KO H9c2 cardiac cells.....114

Figure 3-2: ES 0.5% Methocel pharmacokinetics (PK).....118

Figure 3-3: Effects of ES treatment in cardiac *Ctr1* KO mice.....120

Figure 3-4: Effects of ES treatment in cardiac *Ctr1* KO mice. Supplemental Data.....122

Figure 3-5: Effects of ES treatment on SOD1 levels in cardiac *Ctr1* KO mice.....123

Figure 3-6: Brain ES exposure.....125

Figure 3-7: Captisol ES-$Cu^{2+}$ phase solubility.....127

Figure 3-8: ES-$Cu^{2+}$ 20% Captisol® pharmacokinetics.....130

Figure 3-9: Effects of ES-$Cu^{2+}$ treatment in *mo-br* mice.....133

Figure 3-10: Effects of ES-$Cu^{2+}$ treatment in *mo-br* mice. Supplemental Data.....135

Figure 3-11: Histological examination of 2 and 10 week livers.....136

Figure 3-12: Neuromotor tests of 10 week old mice.....140

Figure 3-13: Neuropathology of 2 and 10 week old mice.....144

Figure 3-14: Additional neuropathology in 2 week old mice. .....146

Figure 3-15: Additional neuropathology in 10 week old mice. .....147

Figure 3-16: ES-$Cu^{2+}$ rescues biochemical phenotypes in 2 and 10 week old *mo-br* mice.....151

Figure 3-17: Heart biochemistry *mo-br* mice.....153

Figure 3-18: Effects of ES treatment on SOD1 levels in *mo-br* mice.....154

LIST OF TABLES

Page

Table 1-1 United States Institute of Medicine Panel on Micronutrients 2002: Dietary Copper 19

Table 1-2 Copper Content of Common Foodstuffs 21

Table 1-3 Medical Conditions Altering Copper Metabolism 24

Table 1-4 ASPEN Recommendations for Parenteral Nutrition: Copper 25

Table 1-5 Select Cuproenzymes, Metallochaperones, Site of Metalation, and Function. 38

Table 2-1: Retention Time and MS Parameters of Analysis 91

Table 2-2: Acute Tolerability of ES-$Cu^2$ in Adult C57BL/6 Mice 93

Table 2-3: Optimized Treatment Protocol 101

Table 3-1: Elesclomol tolerability in adult C57BL/6 females. 117

Table 3-2: Elesclomol-$Cu^{2+}$ tolerability in adult C57BL/6 females. 128

Table 3-3: Treatment Regime and 10 week survival in the mottled-brindled mouse. 129

Table 3-4: CBC of 10 week old C57BL/6 and *mo-br* mice. 137

Table 3-5: Serum chemistries of 10 week old C57BL/6 and *mo-br* mice. 138

Table 3-6: Gait parameters at 10 week assessment in WT and *mo-br* males. 141

Table 3-7: Body, brain, and heart weights at 2 & 10 week necropsy. 155

Table 3-8: Thymus, lungs, kidney, liver, and spleen weights at 2 & 10 week necropsy 156

# Chapter 1

# Introduction and Literature Review

# 1. INTRODUCTION

## 1.1. Copper—An Essential Micronutrient

Copper is a transition metal utilized by a number of essential enzymes as an oxidative cofactor. Cuproenzymes, oxidoreductases requiring copper for functional activity, contribute to a diverse range of biological processes within the body including mitochondrial energy generation, connective tissue maturation, catecholamine metabolism, free radical scavenging, and hematopoiesis.

Though a required trace mineral, free copper possesses toxic properties in the reductive environments of cells and tissues. Homeostatic control of copper absorption, elimination, and distribution to copper-binding proteins is tightly controlled in order to minimize reactive oxygen species generation by free copper. Excess or deficiency of copper results in severe human disease impacting multiple organ systems. Though dietary perturbations of copper balance are rare, several genetic disorders linked to pathogenic mutations in copper membrane transporters highlight the importance of physiological copper regulation.

### 1.1.1. Nutritional Aspects of Copper

According to the United States Institute of Medicine Panel on Micronutrients (2002), the recommended dietary allowance (RDA) for copper in both adult men and women is 900 µg with an increased requirement to 1,000 µg·day$^{-1}$ in pregnant women. Lactating women require the highest dietary copper intake at 1,300 µg·day$^{-1}$. RDA guidelines in children vary depending upon age. *(1)* See Table 1-1.

**Table 1-1 United States Institute of Medicine Panel on Micronutrients 2002: Dietary Copper**

| Age | Estimated Average Requirement (EAR) | Recommended Dietary Allowance (RDA) | Tolerable Upper Intake Level (UL) |
|---|---|---|---|
| Children | | | |
| **0 – 6 months** | 200 µg | N/A¤ | N/A¤ |
| **7 – 12 months** | 220 µg | N/A¤ | N/A¤ |
| **1 – 3 years** | 260 µg | 340 µg | 1,000 µg |
| **4 – 8 years** | 340 µg | 440 µg | 3,000 µg |
| **9 – 13 years** | 540 µg | 700 µg | 5,000 µg |
| **14 – 18 years** | 685 µg | 890 µg | 8,000 µg |
| Adults | | | |
| **19 – 70+ years** | 700 µg | 900 µg | 10,000 µg |
| ***Pregnancy** | 800 µg | 1,000 µg | 10,000 µg |
| ***Lactation** | 1,000 µg | 1,300 µg | 10,000 µg |

* Special Populations: Women Age 18+.
¤ Value not determined.

RDA is calculated via the following formula where the estimated average requirement (EAR) serves as the minimum daily intake needed to avoid nutrient deficiency. RDA approximates the intake required to avoid deficiency in 95% of individuals within a population. *(2)*

$$RDA = EAR + 2 \cdot (SD)$$

Analysis of diet indicates most adults from the United States consume between 1,200 to 1,600 µg of copper daily with an average intake of approximately 1,560 µg. *(3, 4)* Sources of dietary copper include meats, dairy, nuts, whole grains, seeds, and shellfish. *(4, 5)* See Table 1-2. Western diets include an abundance of these foodstuffs and generally provide an excess of daily dietary copper though some debate remains for special populations including pediatric, geriatric, and the chronically ill regarding micronutrient recommendations. *(6)*

The average human adult possesses a total body copper content of 100 mg with the majority of copper bound to proteins in skeletal muscle, blood plasma, hepatic tissue, and the central nervous system. *(4)* Copper from uncontaminated drinking water, cooking instruments, or from transcutaneous sources contributes little to overall body copper status as compared to food content. *(1, 4)* Chronic, intensive exposure from occupational or domestic sources, however, may induce toxicity in children and adults in a dose and route-dependent manner. *(1, 4-6)*

**Table 1-2 Copper Content of Common Foodstuffs**

| Food Type | Foodstuff | Copper Content ($\mu g \cdot g^{-1}$) |
|---|---|---|
| Meats | Beef – Striated Muscle | 0.1 – 1.8 |
| | Pork – Striated Muscle | 0.1 – 9.1 |
| | Beef – Liver | 157 |
| | Beef – Kidney | 2.1 – 4.3 |
| Fish | Tuna | 0.1 – 1.2 |
| | Salmon | 0.5 – 0.8 |
| Shellfish | Oysters | 0.3 – 16.0 |
| | Shrimp | 2.0 – 2.9 |
| Dairy | Bovine Milk | 0.1 – 0.9 |
| | Cheese | < 0.03 |
| Grains | Corn | 0.6 – 16.6 |
| | Wheat Bread | 2.9 – 3.4 |
| | Pasta | 0.1 – 0.5 |
| Vegetables | Lettuce | 0.1 – 2.9 |
| | Cabbage | 0.1 – 7.7 |
| | Peas | 1.9 – 2.4 |
| | Potato | 0.5 – 16 |
| | Tomato | 0.1 – 3.4 |
| Nuts | Tree Nut[#] | 14.4 |
| | Peanut[*] | 7.1 |

[#] Average of almond, cashew, hazelnut, macadamia, pecan, pistachio, and walnuts.
[*] Peanut phylogenetically a legume but considered by general populace as a nut.

### 1.1.2. Dietary Copper Deficiency

Overt copper deficiency from diet alone is extremely rare in healthy adults and older children consuming solid foods. *(4, 6, 7)* Dietary copper deficiency can develop in patients suffering enteric malabsorption syndromes or undergoing long-term total parenteral nutrition (TPN) with inadequate trace mineral compensation. *(8, 9)*

Adult cases of copper deficiency involve an underlying defect in copper absorption in the gastrointestinal tract. Gastric bypass surgery in obese patients provides the most common example of malabsorption-induced copper deficiency in adults followed by celiac disease, short bowel syndrome of any etiology, and absorption interference by mega doses of zinc or iron. *(8, 10)* Symptomatic manifestations of copper deficiency in adults and older children appear gradually due to comparatively large body copper reserves and slow rate of copper turnover.

Unlike adults and children consuming solid foods, infants are at an elevated risk of symptomatic copper deficiency. *(8, 11)* Newborn infants possess stores of copper located primarily in the liver. Copper accumulation in fetal hepatic tissue during the third trimester of pregnancy serves as an important initial reservoir that is depleted during rapid postnatal development. *(12, 13)* Neonates have elevated copper requirements as compared to adults and are more sensitive to the effects of dietary copper deficiency though overt manifestations are often nonspecific.

Studies assessing the copper content of human breastmilk indicate initial copper milk content ranging from around 500 to 600 $\mu g \cdot L^{-1}$ which decreases with lactation stage to

less than 200 $\mu g \cdot L^{-1}$ by 6 months postpartum. Decreased maternal copper milk content corresponds with the introduction of solid foods to an infant's diet typically around 6 to 8 months of age. *(14)*

Infant hepatic copper reserves in conjunction with copper content in breastmilk or formula provide adequate dietary copper until weaning for most infants. Preterm infants are at the highest risk of developing systemic copper deficiency due to impaired copper stores sequestered in the liver during the third trimester of gestation, increased metabolic demand, and lack of appropriate dietary supplementation in some formula preparations. *(8, 11-14)*

Diagnosis of nutritional copper deficiency in adult and pediatric populations includes detailed patient history with risk factors for impaired absorption. Clinical evaluation is key due to the lack of sensitive biomarkers specific for copper deficiency. *(4)* Serological values indicating hematological abnormalities, including hypocupremia, hypoceruloplasminemia, neutropenia, and anemia, provide clinical as well as laboratory evidence of impaired cuproenzyme function. Clinical suspicion in conjunction with serum copper concentrations less than 0.45 $mg \cdot L^{-1}$ and ceruloplasmin levels below 20 $mg \cdot L^{-1}$ with corresponding decrease in hematocrit and neutropenia indicates high probability of copper deficiency. *(15, 16)* See Table 1-4.

## Table 1-3 Medical Conditions Altering Copper Metabolism

| | Condition | Mechanism | Status |
|---|---|---|---|
| Age | Prematurity | Impaired fetal hepatic reserves.<br>Increased metabolic demand.<br>Low dietary content. | Acquired Copper Deficiency |
| | Neonates | Increased metabolic demand.<br>Low dietary content. | Acquired Copper Deficiency |
| | Geriatric | Poor nutrition.<br>Sequestration in protein aggregates.<br>ROS generation.* | Acquired Copper Deficiency or Toxicosis |
| Surgical | Gastric Bypass | Reduced absorption via gastric dumping; Roux-en-Y anastomosis. | Acquired Copper Deficiency - Iatrogenic |
| Malabsorption | Short Bowel Syndrome | Reduced absorption via loss of small bowel length. | Acquired Copper Deficiency |
| | Crohn's Disease | | |
| | Celiac Disease | Reduced absorption via loss of small bowel surface area. | Acquired Copper Deficiency |
| Inborn Errors of Metabolism | Occipital Horn Syndrome | Moderate impairment of ATP7A transport. | Primary Copper Deficiency |
| | Menkes Disease | Severe impairment of ATP7A transport. | Primary Copper Deficiency - Profound |
| | Wilson's Disease | Moderate to severe impairment of ATP7B transport. | Primary Copper Toxicosis |
| Supplementation | Zinc | Increased metallothionein synthesis.<br>Competition with apical enterocyte transporters. | Acquired Copper Deficiency |
| Environmental Exposure | Copper Salts | Chronic or massive ingestion.<br>Inhalation.<br>Secondary zinc deficiency. | Acquired Copper Toxicosis |

*The exact mechanism of copper dysregulation in several neurodegenerative conditions, including Parkinson's disease, Alzheimer dementia, and multiple sclerosis remains to be fully elucidated. Protein aggregates, including α-synuclein Lewy bodies in Parkinson's disease and polymorphous β-amyloid deposits of Alzheimer dementia are theorized to generate ROS by chelating copper while others have argued sequestration results in deficient metalation of cuproenzymes involved in ROS neutralization, catecholamine synthesis, and ATP generation.

Treatment of both adult and pediatric nutritional copper deficiency involves administration of oral copper ($CuSO_4$) 3 to 8 $mg \cdot day^{-1}$. *(8-10)* For most adult patients, 0.3 to 0.5 $mg \cdot day^{-1}$ for enteral or parenteral feeds is sufficient per the 2021 American Society for Parenteral and Enteral Nutrition (ASPEN) guidelines. *(17)*

Treatment of any concurrent underlying medical conditions or polypharmacy that may be affecting normal absorption of copper in the small intestines should be evaluated. Resolution of common symptoms, such as anemia, bone mineralization changes, and serological abnormalities occurs quickly in adults. See Table 1-4. *(15, 16, 18)*

In neonates, failure to thrive (FTT) and bone changes, including osteopenia, long bone fractures, and boney malformations, appear at approximately 8 to 10 weeks of age. Premature and low birthweight for gestational age (LBGA) infants should be monitored closely and provided with prophylactic copper supplementation. *(8, 13-15)* Per the 2021 ASPEN guidelines, enteral and parenteral feeds should include supplementation of 20 $\mu g \cdot kg^{-1} \cdot day^{-1}$ for children under 40 kg. See Table 1-4. *(19)*

**Table 1-4 ASPEN Recommendations for Parenteral Nutrition: Copper**

| | Weight | Parenteral | Enteral |
|---|---|---|---|
| Children* | | | |
| **Preterm Neonates** | < 3 kg | 20 $\mu g \cdot kg^{-1} \cdot day^{-1}$ | N/A |
| **Term Neonates** | 3-10 kg | 20 $\mu g \cdot kg^{-1} \cdot day^{-1}$ | N/A |
| **Children** | 10-40 kg | 20 $\mu g \cdot kg^{-1} \cdot day^{-1}$<br>Maximum: 500 $\mu g \cdot day^{-1}$ | N/A |
| **Adolescents** | > 40 kg | 200 – 500 $\mu g \cdot day^{-1}$ | 3-5 $mg \cdot day^{-1}$ |
| Adults* | | | |
| **Adults 18+** | > 40 kg | 0.3 – 0.5 $mg \cdot day^{-1}$ | 3-8 $mg \cdot day^{-1}$ |

*ASPEN 2019 Recommendations on Appropriate Parenteral Nutritional Dosing for Adult, Neonatal, and Pediatric Patients.

### 1.1.3. Dietary Copper Toxicity

Copper toxicosis from excess dietary copper is rare and toxic exposure typically involves acute ingestion or chronic inhalation of common copper salts, such as $CuSO_4$, used for agricultural or industrial purposes. *(20, 21)* Leaching of copper from pipes may contribute significant quantities through drinking water following chronic exposure. The Environmental Protection Agency limits inorganic copper content in potable water to not exceed 1,300 $\mu g \cdot L^{-1}$. *(22, 23)*

Acute copper intoxication causes a wide range of symptoms depending upon route of administration. Oral copper intoxication following massive dose consumption induces diarrhea and other gastrointestinal complaints which progress to hepatic dysfunction, renal failure, rhabdomyolysis, and death in severe cases. *(24, 25)* Small children are at higher risk of intoxication from household sources such as copper salts used as gardening fungicides, desiccants, and blue refrigerator cold packs. *(21)*

Inhalation of copper salts causes “vineyard sprayer’s lung disease”; a fibrotic interstitial pulmonary disorder first described in French vineyard works with silicosis-like lesions following repeated exposure to aerosolized $CuSO_4$ solutions used to prevent mildew growth on grape vines. *(20, 21)*

For dietary copper, the tolerable upper intake level (UL) varies in regard to age with no ill effects observed at daily intakes up to 10,000 µg in adults. In children, UL ranges from 1,000 µg to 8,000 µg per day. See Table 1-1. *(1)* Healthy adults and children, unless

exposed to high levels of inorganic copper contaminants, do not develop copper toxicity from normal dietary sources.

Diets high in copper-containing foods or exposure to copper contaminates result in compensatory changes in absorption and elimination which maintain stable total body copper levels. While variation in copper absorption from the gastrointestinal tract contributes to maintaining stable copper levels, excretion of copper in the form of bile acid complexes in feces serves as the most important homeostatic mechanism. *(26, 27)*

Diagnosis of oral copper intoxication involves patient history with a focus on deducing the mechanism of exposure and duration. Acute intoxication primarily involves gastrointestinal symptoms including diarrhea, vomiting, abdominal pain, and dehydration. The presence of blue-green material in feces is highly indicative of acute oral intoxication. Laboratory abnormalities may include elevated serum copper levels, elevated liver enzymes, and elevated urine copper. *(21, 24, 25)* Children and young adults with unexplained hypercupremia, central nervous system involvement, hepatomegaly, or Kayser-Fleischer rings of the cornea should be evaluated for Wilson's disease.

Treatment of copper intoxication begins with identifying and eliminating the mode of exposure with or without chelation therapy. Trientine (Syprine®) and D-penicillamine (Cuprimine®) are two agents used clinically which irreversibly bind copper and facilitate elimination via uresis. *(24, 25)* High doses of zinc, which competes with copper for absorption, are also used to reduce systemic copper absorption. In the most severe cases, plasmapheresis, dialysis, and/or liver transplant may be indicated.

## 1.2. Normal Physiology

### 1.2.1. Absorption

Copper absorption occurs in the gastrointestinal tract primarily in the small intestines of mammals. The bioavailability of dietary copper varies with age and current copper nutritional status, but studies indicate approximately 30-40% of ingested copper is absorbed through the intestines in healthy adults. *(26)* Critical to maintaining systemic copper balance is the enterohepatic cycling of copper from gastrointestinal secretions, such as saliva and bile, which may account for upwards of 50% of copper reaching the small intestines. *(27)*

Copper absorption varies inversely with long-term dietary consumption patterns and systemic copper nutritional status. In situations involving high dietary or body copper levels, absorption decreases to as little as 12% while copper depletion increases absorption to upwards of 63%. *(27)* Control of absorption, however, plays a secondary role in regulating global copper levels with compensatory changes in biliary elimination serving as the primary mode of copper homeostasis. *(26, 27)*

Transport across the polarized enterocyte lining of the small intestines involves the action of two principle ion transporters. CTR1 facilitates influx of $Cu^{+}$ from the alimentary canal whereas ATP7A accomplishes basolateral transport from enterocyte cytosol to hepatic portal circulation. DMT1, a divalent cation transporter responsible primarily for

iron influx, may also play a role in copper transport though its significance under normal physiological conditions is an area of debate. See Figure 1-1 *(28-30)*

In the generalized cell, CTR1 and ATP7A serve a similar function in terms of facilitating cellular copper influx and efflux. A notable exception is in hepatic tissue where an ATP7A paralog, ATP7B, fulfills the role of egress transporter of copper.

The high-affinity copper transporter 1 (CTR1) is the principal importer of copper from the alimentary canal to enterocyte cytoplasm. *(31)* Regulation of CTR1 expression and localization to the apical enterocyte membrane plays a crucial role in the modulation of copper influx from the gastrointestinal tract as well as in the generalized cell. Under conditions of high intracellular copper content, CTR1 rapidly internalizes to sub-plasma membrane vesicles to decrease copper influx. *(32)*

CTR1 is encoded by the *SLC31A1* gene on the long arm of chromosome 9 at band 9q32. To date, no human disease phenotypes have been definitively associated with pathological mutations in *SLC31A1*. *(33, 34)* Recent research implicates tissue-specific deficiencies of CTR1 may play a role in the development of cardiac myopathies and idiopathic hepatic cirrhotic disease. Mutations impairing the transport activity of the Ctr1 rodent homolog result in embryonic lethality owing to severe copper deficiency and impaired fetal connective tissue development in rodent models. *(33, 34)*

Copper-transporting ATPase α (ATP7A) is a P-type ATPase responsible for copper egress from the intestinal lining. *(30)* ATP7A is located in membrane vesicles of the Trans-Golgi Network (TGN) and facilitates the import of copper from cytosol to the Golgi. *(35, 36)* Under conditions of high cytoplasmic copper content, ATP7A re-localizes

to the basolateral aspect of the enterocytes. In the generalized cell, relocation occurs to the plasma membrane. In both enterocytes and the non-hepatic cells, ATP7A then facilitates the active efflux of $Cu^{+}$ ions from the cytosol. *(36)*

ATP7A is encoded by the *ATP7A* gene located on the long arm of chromosome X at band Xq21. Pathogenic mutations impairing the transport activity of ATP7A result in several human diseases including Menkes Disease (MD) and Occipital Horn Syndrome (OHS). Hallmarks of ATP7A-related pathology include systemic copper deficiency with severe connective tissue and/or neurodegenerative characteristics. *(37, 38)*

The combined actions of CTR1 and ATP7A result in directional transport of dietary copper from the gastrointestinal tract to hepatic portal circulation. The concerted action of these two transporters also plays a key role in directional copper exchange across several other biologically important polarized epithelial structures including the blood-brain-barrier (BBB) and blood-cerebral spinal fluid-barrier (BCSFB). *(30)*

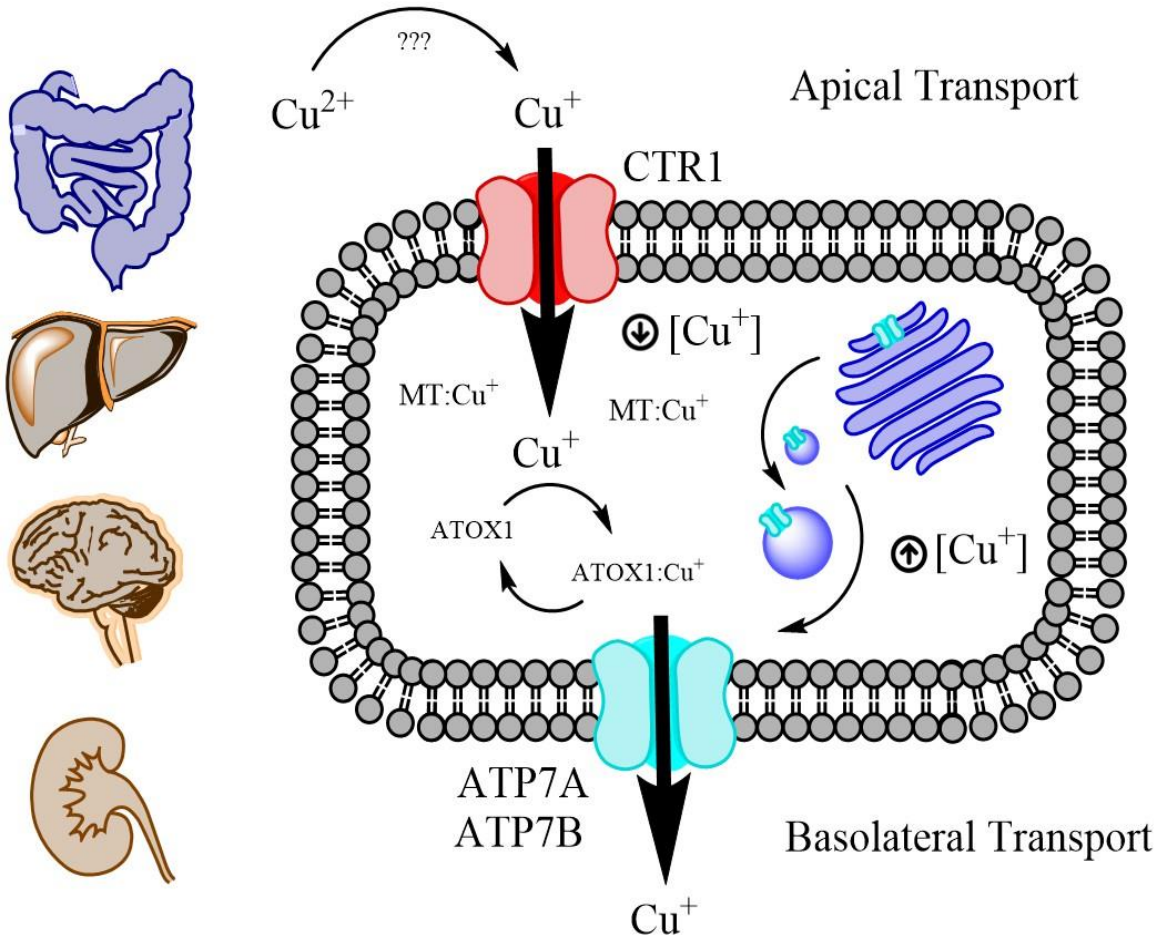


**Figure 1-1 Copper Transport within Cells**

Reduction of $Cu^{2+}$ to $Cu^{+}$ occurs before CTR1-mediated influx by an unknown reductase. Within the cytoplasm, $Cu^{+}$ is escorted to ATP7A or ATP7B by ATOX1. Metallothionein serves as an intracellular storage and buffering molecule. ATP7A mediates basolateral transport in the enterocyte lining of the intestines, BBB endothelium, and renal epithelium. Transport across the enterocyte lining to portal circulation results in absorption of dietary copper. Transport across hepatocytes to the biliary interface results in elimination of copper through fecal bile acid coordination. Impaired ATP7A transport results in systemic copper deficiency caused by lack of intestinal absorption (Menkes). Loss of ATP7B results in toxic accumulation due to lack of hepatic elimination (Wilson's).

### 1.2.2. Distribution

Once copper enters hepatic portal circulation, copper binds rapidly to serum albumin and transcuprein. *(30, 36)* Under physiological conditions, copper may bind with most amino acids through glycine-like complexation. *(32)* Radiotracer studies indicate amino acid complexation does not contribute significantly to bulk copper distribution through blood. *(39, 40)*

Virtually no free copper exists in biological systems owning to copper's propensity to redox cycle and generate toxic reactive oxygen species. *(20)* To date, little is known regarding the precise mechanism of copper delivery to mammalian cells. Copper bound to albumin and transcuprein comprises the "exchangeable copper pool" capable of distribution to hepatocytes and other cell types within the body. *(39-42)*

L-histidine is the primary amino acid capable of physiologically relevant complexation with copper. Histidine may form either glycine-like or histamine-like complexes with a 2:1 stoichiometric ratio with the $Cu^{2+}$ cupric ion. L-histidine may play a role in copper binding within the gastrointestinal tract, but current data indicates the role of free amino acids is limited in biological fluids. *(42)* The copper (II)-histidinate complex rapidly donates $Cu^{2+}$ to albumin, which possesses a tripeptide binding region and is the most abundant copper chelator and transporter of copper in both blood and cerebrospinal fluid with a reported $K_a$ value of $10^{11}$ to $10^{22}$ $M^{-1}$. *(43, 44)*

Albumin possesses a high-affinity binding site at the N-terminus; involving the asparagine-$NH_2$, histidine $N_1$ imidazole, two deprotonated peptide nitrogens from alanine and histidine, and the aspartate $COO^-$ functional groups. This tripeptide segment is responsible for divalent transport of both copper and nickel and is a highly conserved metal binding motif. *(45)* The high abundance of albumin in various biological fluids provides an extracellular mechanism for sequestering free copper in the event of copper overload. Serum albumin may bind and sequester an estimated 40 $\mu g \cdot mL^{-1}$of copper yet normal total serum copper is only 1 $\mu g \cdot mL^{-1}$. *(46)*

Transcuprein, or $\alpha_2$-macroglobulin, is approximately 270 kDa and transports copper in a similar, high-affinity mechanism to albumin. Despite its lower abundance, transcuprein successfully competes with albumin. Whereas binding to albumin does not directionally traffic copper within the cardiovascular system, evidence indicates transcuprein preferentially targets bound copper to hepatocytes in portal circulation and renal epithelial cells in the kidneys. *(47, 48)*

Transcuprein, as revealed by radioisotope studies using $^{67}Cu$, freely exchanges copper with albumin. *(40)* In portal and renal circulation, radiolabeled transcuprein rapidly loses signal as copper is distributed by an as of yet unknown mechanism to tissue. *(48)* Once transiting hepatic tissue, radiolabeled copper again appears but bound to ceruloplasmin, the most abundant copper-containing protein in blood, interstitial fluid, and cerebrospinal fluid.

### 1.2.3. Elimination

Hepatocytes control excretion of body copper through complexation and export of bile acid copper complexes utilizing ATP7B as the primary TGN import transporter and efflux actuator. *(36)* ATP7B mediates loading of copper to secretory vesicles for metalation of hepatic cuproenzymes. Ceruloplasmin, a copper-requiring ferroxidase essential for iron metabolism and hematopoiesis, contains 60-95% of copper found within blood. Studies using radiolabeled copper reveal that the six copper atoms bound to ceruloplasmin are not exchangeable and do not contribute to the labile copper pool for tissue exchange. *(40)*

The liver stores excess body copper in hepatocytes bound to intracellular metallothioneins. *(49)* Metallothioneins (MT) are a family of cysteine-rich, low molecular weight proteins found ubiquitously expressed in mammalian cells. Metallothioneins play a vital role in the prevention of heavy metal toxicity by binding a diverse range of bioactive metals including copper, zinc, and iron. Two isoforms, MT-1 and MT-2 play essential roles in the storage of copper in hepatic and non-hepatic tissues. *(50)* In response to high metal loads, MT-1 and MT-2 expression levels increase and serve as intracellular binders of excess metal ions. *(51)*

Excretion of excess hepatic copper involves ATP7B-mediated export of copper. Bile acid conjugates represent the main mode of elimination for many divalent trace metals, including manganese, lead, selenium, and zinc. The precise mechanism of conjugate formation is currently unknown. Elimination of copper involves efflux of $Cu^{2+}$ into secretory vesicles of the hepatocyte TGN followed by fusion and exocytosis to canalicular

membranes of the biliary system. Bile acid conjugates exhibit reduced reabsorption of copper. *(49)*

Excretion through feces is the principal mode of copper elimination from the body. An estimated 80-90% of copper elimination occurs through biliary excretion with trace quantities eliminated through sweat and urine under normal physiological conditions. *(35, 49)* Remaining copper elimination occurs in the sequestering of copper in keratinized structures such as stratum cornea of skin and hair. *(26)* Secondary elimination mechanisms remain, to this date, relatively unstudied. Slow progression of hereditary copper accumulation disorders hint to auxiliary mechanisms of elimination but remain controversial.

When systemic copper levels are elevated, increased biliary secretion and migration of ATP7B to the canalicular interface in rodent models results in enhanced elimination of copper. *(50)* Winge and Mehra demonstrated enhanced fecal elimination in men exposed to high levels of copper with concurrent decrease in copper absorption via retention in enterocytes. *(26)* Enterocyte shedding, occurring on average every 3-4 days, represents an additional mechanism protecting the body from toxic levels of copper exposure. Diarrhea and gastrointestinal symptoms during the course of acute copper toxicosis via oral exposure may reflect enterocyte toxicity and enhanced shedding—resulting in a non-biliary fecal excretion mechanism.

Impairment of copper efflux from liver parenchyma results in systemic accumulation of copper. Genetic mutations involving decreased function of ATP7B result in Wilson's

disease (WD). Prolonged exposure to increased hepatic copper levels results in systemic accumulation of copper with progressive liver injury resulting in cirrhosis. *(53, 54)*

Wilson disease protein or ATP7B is encoded by the *ATP7B* gene located on the long arm of chromosome 13 at band 13q14.3. It shares 57% structural homology and function with ATP7A but exhibits a restricted tissue expression pattern. ATP7B exhibits high levels of expression in hepatocytes with limited expression in neurovascular structures and mammary glands. ATP7B can also be found expressed in syncytial placental tissue. *(55)*

Defects in ATP7B-mediated transport results in systemic accumulation of copper through impaired biliary excretion of copper. Manifestations of WD occur in childhood and early adulthood. Chronic copper toxicosis manifests primarily as liver dysfunction, cirrhosis, and neurodegenerative changes following toxic copper accumulation in the brain. *(20, 21, 53, 54)*

Unlike Menkes disease, WD responds favorably to copper chelation therapy if identified before irreversible end-organ damage occurs. WD is inherited in an autosomal recessive fashion. Heterozygote insufficiency is not observed, and most carriers of ATP7B defects remain unidentified with minimal increases in biological markers of copper hyper-accumulation. *(54)*

### 1.3. Major Cuproenzymes and Function

Cuproenzymes are classified primarily as oxidoreductases and catalyze the oxidation of various substrates. In mammals, cuproenzymes are involved in antioxidant scavenging, iron transport, iron metabolism, energy generation by mitochondrial electron transport, connective tissue maturation, pigment synthesis, activation of neuroendocrine peptides, and the metabolism of various amino acids and biogenic amines including catecholamines, neurotransmitters, and histamine. See Table 1-5. Given the diverse biological activities of cuproenzymes, copper deficiency or genetic perturbations in normal copper homeostasis results in a wide range of pathologies.

Table 1-5 Select Cuproenzymes, Metallochaperones, Site of Metalation, and Function.

| Enzyme | Chaperone | Site of Metalation | Function |
|---|---|---|---|
| **Cytochrome *c* Oxidase (CcO)** | COX17, Mito. Cu Shuttle | Mitochondria | Terminal Electron Transport (Complex IV) - ATP Generation |
| **Cu/Zn Superoxide Dismutase (SOD1)** | CCS | Cytoplasm, Mitochondria | ROS Scavenging |
| **Dopamine-β-Hydroxylase (DBH)** | ATOX1 | Golgi | Catecholamine Synthesis |
| **Lysyl Oxidase (LOX)** | ATOX1 | Golgi | Elastin/Collagen Crosslinking (ECM Maturation) |
| **Tyrosinase (TYR)** | ATOX1 | Golgi | Melanin Synthesis |
| **Keratin Sulfhydralase** | ATOX1 | Golgi | Keratin Crosslinking |
| **Metallothionein (MT1/2)** | GSH? | Cytoplasm | Storage of Divalent Cations, Liver Primary Systemic Storage |
| **Ceruloplasmin (Cp)** | ATOX1 | Golgi, Hepatocytes | Ferroxidase - Fe Metabolism |

### 1.3.1. Cytochrome *c* Oxidase

Cytochrome *c* oxidase (CcO) is an integral multimeric protein complex located in the inner mitochondrial membrane. CcO, also known as Complex IV, catalyzes the terminal step of the electron transport chain responsible for generation of adenosine triphosphate (ATP) by cellular respiration. *(56, 57)* The CcO complex consists of 14 subunits of which two subunits, COX1 and COX2, contain copper prosthetic sites forming $Cu_B$ and $Cu_A$ centers, respectively. *(58)* The complex contains two heme centers, heme a and heme $a_3$, which form binuclear centers with $Cu_A$ and $Cu_B$. These two binuclear centers are essential for CcO bioactivity.

To achieve terminal electron transfer, four molecules of cytochrome *c* previously reduced by Complex III dock sequentially near the heme a-$Cu_A$ binuclear center of COX2 resulting in the reduction of heme a-$Cu_A$. Four electrons are then passed to the heme $a_3$-$Cu_B$ center of COX1. Heme $a_3$-$Cu_B$ catalyzes the reduction of $O_2$ to $H_2O$ resulting in the net transport of 4 $H^+$ to the intermembrane space (IMS). The combined actions of CcO restore the oxidation state of four molecules of cytochrome *c* for the continuance of the electron transport cycle and functions as an electron-driven $H^+$ pump to generate the proton-motive gradient used by ATP synthase, Complex V, for the synthesis of ATP. *(59)*

The assembly of CcO is a complex, multistep process closely linked to copper transport systems within the mitochondria. Though both CcO assembly and mitochondrial copper transport have yet to be fully elucidated, basic transport and assembly networks have been established in the mitochondria.

Copper import to the mitochondria involves binding of copper to an as yet unidentified ligand in the cytosol. Once bound, the Cu-ligand complex enters the matrix through an as yet unidentified membrane transporter. The matrix serves as the primary storage site for copper within the mitochondria. For metalation of COX1 and COX2, a series of intermediate metallochaperones play an essential role in copper incorporation and assembly. *(59, 60)*

COX1 contains the $Cu_B$ metalation site. Incorporation of copper involves the passage of $Cu^+$ ion from the metallochaperone COX17 within the IMS. COX17 then passes copper to the inner membrane-associated protein COX11 which accomplishes COX1 metalation by an unknown mechanism. *(61)*

COX2 contains the $Cu_A$ metalation site. Incorporation of copper, as with COX1, involves COX17; however, assembly appears to involve several additional proteins including soluble metallochaperones COX19 and COX23 as well as membrane-associated SCO1 and SCO2. *(60, 61, 62)* Proper assembly and bioactivity of CcO require both adequate copper stores, functional mitochondrial copper transport, and assembly networks.

### 1.3.2. Superoxide Dismutase

Superoxide dismutase (SOD) catalyzes the conversion of superoxide radicals to molecular oxygen and hydrogen peroxide which is subsequently degraded by catalase. In

humans, three isoforms of SOD contribute to ROS defense. *SOD1*, *SOD2*, and *SOD3* genes are located on chromosomes 21q22.11, 6q25.3, and 4p15.2. *(63)*

SOD1 and SOD3 are copper/zinc prosthetic group-containing dismutases whereas SOD2 utilizes a manganese/iron oxidoreductant group. *(64, 65)* Both SOD2 and SOD3 are homotetramers whereas SOD1 is a homodimer. SOD2 localizes to the mitochondrial matrix whereas SOD1 can be found in the cytoplasm and IMS of mitochondria. SOD3 localizes to the extracellular matrix via Golgi-mediated secretory pathway. *(66)*

Metalation of SOD1 occurs by a soluble 54 kDa metallochaperone appropriately named copper chaperone for superoxide dismutase (CCS). CCS acquires copper in the cytoplasm and directly metalates SOD1 in both the cytosol and IMS of the mitochondria. *(67)*

Intense research evaluating the effects of SOD1 dysfunction on neurodegenerative diseases, such as familial amyotrophic lateral sclerosis (ALS) and dementia, continues though limited consensus on pathogenic mechanisms remains. *(65, 68)* Toxic gain-of-function mutations involving deficiency in zinc binding with subsequent generation of ROS by impaired copper/zinc prosthetic groups provide a leading mechanistic explanation of SOD1-mediated effects in familial ALS. SOD2-related dysfunction seems to be implicated in diverse pathological processes affecting the liver, heart, lungs, and brain but will not be discussed in further detail owning to the presence of a manganese/iron center rather than copper-utilizing domain. *(64)*

SOD1 and SOD3 isoforms remain exquisitely resistant to copper deficiency and exhibit slow rates of protein turnover. In MD rodent models, SOD1 and SOD3 levels

remain statistically equivalent to wild-type mice in both quantity and bioactivity. *(69)* SOD1-related dysfunction does not appear to contribute significantly to neurodegeneration or connective tissue abnormalities observed in MD.

### 1.3.3. Dopamine-β-Hydroxylase

Dopamine-β-hydroxylase (DBH) is a 290 kDa homotetramer which catalyzes the hydroxylation of the neurotransmitter dopamine to norepinephrine. DBH requires ascorbic acid and molecular oxygen and shares mechanistic similarity with peptidylglycine-α-monooxygenase. DBH subunits contain a N-terminal coupled copper binuclear site located within a conserved DOMON domain. Each DOMON domain contains a cysteine-rich region with one $Cu_H$ and one $Cu_M$ copper-binding sites. *(70)* $Cu_M$ participates in substrate hydroxylation whereas $Cu_H$ functions in electron transfer from ascorbic acid. *(71)*

DBH is encoded by the *DBH* gene on chromosome 9 located at band 9q34.2. DBH expression in noradrenergic neurons located in the locus coeruleus of the central nervous system and sympathetic ganglia of the peripheral nervous system provides a vital biosynthetic step in catecholamine metabolism. *(72)* Expression in chromaffin cells of the adrenal medulla plays a role in catecholamine endocrine function. *(73)*

Metalation of DBH occurs within TGN vesicles. *(74)* Delivery of copper to ATP7A involves the soluble cytosolic chaperone ATOX1 in mammalian cells. *(75)* DBH exhibits high sensitivity to copper depletion characterized by elevated levels of dopamine and absence of norepinephrine and epinephrine. *(74, 76)*

In the central nervous system (CNS), excess dopamine contributes to both structural and functional abnormalities. Peripheral loss of catecholamine biosynthesis causes dysautonomia—characterized by cardiac arrhythmia, neurogenic bladder, anhydrosis, hypotension, hypothermia, constipation, and weakness.

Autosomal recessive DBH deficiency, a rare cause of idiopathic dysautonomia, and research involving schizophrenia, addiction, and anxiety reveal the importance of neurotransmitter regulation. *(76)* Secondary DBH deficiency may be caused by chronic alcoholism, malnutrition, dietary copper deficiency, infection, amyloidosis, autoimmune disorders, diabetes, paraneoplastic syndrome, or drug toxicity. MD patients, characterized by profound systemic copper deficiency, are profoundly deficient in DBH activity with prominent dysautonomic symptoms.

### 1.3.4. Lysyl Oxidase

Lysyl oxidase (LOX) is a quinone-containing copper amine oxidase responsible for maturation of extracellular matrix proteins. Lysyl oxidase, also known as protein-lysine 6-oxidase, is encoded by the *LOX* gene located on chromosome 5 at band 5q23.3. *(77)*

Structurally, LOX exists as an extracellular matrix soluble homodimer of 32 kDa. The human crystallographic structure of LOX has yet to be determined due to a high degree of intrinsic disorder. *(78)* The C-terminal of LOX contains an active site consisting of copper, tyrosine, cysteine, and lysine. Function of LOX requires lysyl tyrosylquinone cofactor. Molecular oxygen and active site copper mechanistically restore the redox state of the lysyl

tyrosylquinone cofactor followed by hydrolysis and release of hydrogen peroxide and ammonia. *(79)*

LOX facilitates the conversion of lysine residues of collagen and elastin to bioactive allysines. These allysine aldehydes form pyridinolines in collagen and desmosines in elastin which coordinate with three and four allysine derivatives to form stable collagen fibrils and mature elastin. *(80)*

LOX metalation occurs in the secretory pathway vesicles of the TGN. LOX metalation requires ATOX1 chaperone and functional ATP7A for maturation. Metalation is required for secretion of mature, functional LOX. LOX exhibits high sensitivity to systemic copper state *(81)*.

LOX insufficiency, secondary to copper deficiency, may manifest due to dietary deficiency or genetic lesion in infants. *(11, 12, 13)* Lung development in the early postnatal period seems profoundly sensitive to LOX deficiency owning to the high content of elastin and collagen in lung parenchymal matrix. OHS and MD present with multiple connective tissue and skeletal muscle abnormalities within 3-6 months postnatally.

### 1.3.5. Tyrosinase

Tyrosinase (TYR) catalyzes the rate-limiting steps in the biosynthetic pathway of melanin known as the Raper-Mason pathway. *(82)* Tyrosinase participates in two reactions including the conversion of L-tyrosine to dopamine and tyramine to dopamine-*o*-quinone.

Tyrosinase is encoded by *TYR* gene located on chromosome 11 at band 11q14.3. TYR possess a $Cu_A$ and $Cu_B$-containing binuclear center responsible for catalyzing the oxidative hydroxylation of L-tyrosine and tyramine. *(83)*

Autosomal recessive deficiency in TYR results in type 1 oculocutaneous albinism. Expression of TYR is limited to melanocytes and is responsible for eumelanin production. *(84)* Metalation of TYR occurs in the TGN and is dependent on ATOX1 and ATP7A. *(75)*

TYR exhibits resistance to systemic copper deficiency and hypopigmentation is not observed in diet-acquired copper-deficient infants. Interestingly, hypopigmentation manifests in severe ATP7A lesions yet is often absent or variable in OHS. Even among those affected with MD, variable quantities of pigment production results in ocular coloration and steely-grey hair and skin. *(85)*

Pigmentation deficiency predisposes those affected to retinopathy, blindness, and development of melanoma, squamous cell carcinoma, and basal cell carcinoma of the skin and eyes. In murine models of MD, excluding the *mottled-brindled* mouse, administration of exogenous copper salts and copper histidine results in rapid pigment production which can be used as a phenotypic measure of copper repletion. *(86)*

### 1.3.6. Ceruloplasmin

Ceruloplasmin (Cp) is a ferroxidase encoded by *CP2* gene located on chromosome 3, band 3q24. Ceruloplasmin irreversibly binds 60-95% of all copper found in blood and other biologically relevant fluids including cerebrospinal fluid. *(40, 49)*

Cp is a soluble monomeric peptide of approximately 132 kDa. CP binds both cupric and cuprous ions and is primarily synthesized by the liver. Metalation of Cp occurs in hepatocyte trans-Golgi vesicles in an ATP7B-dependent metalation mechanism. Each Cp peptide binds six copper ions which stabilizes its tertiary structure. Apoceruloplasmin undergoes rapid degradation and lacks ferroxidase activity. *(87)*

Aceruloplasminemia, an autosomal recessive disorder of Cp deficiency, results in hyper-accumulation of iron due to impaired $Fe^{2+}/Fe^{3+}$ cycling. Symptoms of aceruloplasminemia include iron overload, ataxia, early-onset dementia, cirrhosis, and retinopathy with paradoxical microcytic anemia. *(88)*

### 1.3.7. Sulfhydryl Oxidase

The proposed copper-dependent keratin sulfhydryl oxidase catalyzes disulfide linkages in hair shafts. Though hypothesized as enzymes necessary for proper keratin structural maturation to date no definitive enzyme has been identified in mammals specific to the skin or hair follicle. *(89)* Though the specific enzyme has yet to be identified, keratin

abnormality in patients diagnosed with MD indicates an as of yet unidentified role for copper in hair maturation.

In severe hereditary copper deficiency, kinky, brittle hair shafts provide a pathognomonic trait ascribed to MD. *(90)* Keratinized structures contain the highest concentration of copper within the human body. Deficiency results in profound changes in keratin superstructures resulting in full strand compromised integrity unique among trichopathies. *(91)*

### 1.4. Pathophysiology of Wilsons and Menkes Diseases

Genetic lesions impairing the copper membrane transporting functions of ATP7A and ATP7B result in Menkes and Wilson diseases. Both disorders involve abnormal copper transport with subsequent accumulation of copper in sink tissues. In WD, impaired directional transport of copper from hepatic parenchyma to the biliary tree results in copper accumulation with potentially debilitating and fatal end-organ damage in the central nervous system and liver.

MD involves systemic copper deficiency due to copper trapping in gut enterocytes, renal tubular epithelium, and cells comprising the BBB and BCSFB. Multiple copper-requiring physiological processes become impaired with perturbations of brain development and connective tissue abnormalities contributing to rapid clinical deterioration and death.

Unlike Menkes disease, FDA-approved chelation therapy results in good clinical outcomes in Wilson's disease patients if diagnosed before onset of CNS symptoms or irreversible hepatic failure. No current effective therapy exists for treatment of children affected by MD or its less severe variant, OHS.

### 1.4.1. Wilsons Disease

As previously described, ATP7B functions as the primary hepatocyte copper efflux transporter. Impaired fecal elimination through bile acid conjugates causes an insidious accumulation of copper across various organ systems. Albumin, metallothioneins, and extracellular deposits of copper comprise a robust system of copper sequestration. WD progresses slowly over the course of years to decades depending upon dietary practices of individual patients and the severity of specific genetic lesion in the *ATP7B* gene. *(52-54)*

Liver manifestations of WD typically appear before CNS involvement. *(92)* Symptoms of chronic copper-induced hepatitis include fatigue, jaundice, swelling, and pruritus. Clinical findings include hepatomegaly, splenomegaly, ascites, coagulopathy, edema, and spider telangiectasias—indicative of severe hepatic dysfunction and fulminant hepatic failure. Portal hypertension develops as cirrhotic changes impede circulation resulting in potentially fatal esophageal varices, internal hemorrhoids, and caput medusa.

Approximately 5% of WD diagnoses present with hepatic failure requiring liver transplantation. *(93)* Patient prognosis depends upon extent of hepatic impairment and accumulation of secondary end-organ damage including cardiomyopathy, renal tubular acidosis, and CNS involvement.

Neurologic symptoms of WD tend to manifest in patients of older age at time of diagnosis. Pyramidal symptoms tend to be nonspecific and resemble Parkinsonian dysfunction characterized by bradykinesia, ataxia, tremor, and rigidity due to damage

accumulated in the substantia nigra and pyramidal tracts of the brain stem and spinal cord. *(94)*

Cognition and executive function represent irreversible changes due to copper toxicity induced damage to cortical neurons of the frontal lobe. Subcortical dementia, mood disorders, impulsivity, apathy, and a psychosis present with insidious onset and may delay diagnosis if metabolic causes of psychiatric illness are not thoroughly evaluated. *(95)*

Kayser-Fleischer rings, a deposition of copper around the edge of the cornea, present in greater than 90% of patients exhibiting neurologic symptoms and greater than 50% of those who present with liver manifestations only. Kayser-Fleischer rings are pathognomonic for WD. Corneal copper deposits can predate end-organ damage and severe as a key clinical finding for diagnosing suspected WD. Definitive diagnosis includes elevated total serum copper level, low ceruloplasmin, and elevated 24-hour urinary copper excretion. *(92)*

Treatment of WD involves long-term chelation therapy with dietary modifications. A low copper diet in conjunction with trientine or D-penicillamine chelation efficaciously depletes copper overload by forming irreversible copper-drug complexes. *(96, 97)* As serum copper depletes, copper sequestered in tissues slowly normalize over the course of weeks to months. Copper-drug complexes undergo urinary excretion—effectively bypassing defective fecal elimination. Though life-long chelation therapy is required, WD patients have a generally favorable prognosis barring severe liver disease or irreversible neurocognitive impairment.

### 1.4.2. Menkes Disease

Loss or reduction in ATP7A activity profoundly affects the body's ability to transport copper across biological membranes. Systemic copper deficiency develops due to the inability to transport copper across the basolateral aspect of enterocytes to portal circulation. As a result, body copper levels are exceedingly low with certain tissues, such as the brain and kidney, experiencing profound deficiency or accumulation owing to impaired serum-tissue copper exchange. *(98, 99)*

Enterocytes and renal epithelia experience hyper-accumulation of copper due to the continued activity of CTR1. In the intestines, this phenomenon is benign due to the rapid cellular turnover and shedding of enterocytes through the alimentary canal. Kidneys experience toxic accumulation of copper with marked signs of tubulointerstitial damage resulting in severe kidney dysfunction. *(100)*

In the brain, defective copper transport across the BBB and BCSFB exacerbates copper deficiency compared to circulating systemic levels. Defective BBB transport of copper renders the brain minimally responsive to parenteral copper supplementation by copper salts or amino acid complexes. *(101, 102)*

Pathology of allelic ATP7A defects can be classified into two groups of associated symptoms: CNS degenerative changes and connective tissue abnormalities. Brain and connective tissue pathology results from specific cuproenzyme deficiencies secondary to primary copper deficiency. *(103)*

In the CNS, primary copper deficiency impairs the function of three key cuproenzymes: CcO, SOD1, and DBH. *(104, 105)* CcO, or complex IV of the electron transport chain, is a large multimeric complex containing two copper-binding subunits COX1 and COX2 required for cytochrome *c* oxidation. COX1/2 are metalated by a complex relay shuttle of mitochondrial metallochaperones including COA6, SCO1, SCO2, COX11, and COX17. *(59, 61-63, 106)* Lack of copper prevents COX1/2 metalation and subsequent CcO assembly resulting in defective energy production. CcO dysfunction is indicated as the primary mode of progressive neurological injury seen in MD. *(107, 108)*

SOD1 and DBH dysfunction result in enhanced ROS sensitivity and abnormal neurotransmitter function also implicated in neuronal injury. *(69, 76, 107)* SOD1 is found in both the cytoplasm and mitochondrial intermembrane space and is metalated by CCS in both locations. *(61)* DBH is a TGN secretory pathway cuproenzyme. The combined effects of CcO, SOD1, and DBH dysfunction result in severe neurological injury and death as seen in MD. *(107)*

Connective tissue abnormalities result from impaired elastin and collagen crosslinking mediated by lysyl oxidase (LOX). Impaired matrix maturation causes marfanoid characteristics including vascular abnormalities, hyper-flexible joints, loose skin, lens subluxation, and epiphyseal elongation. Bony malformations are common particularly those of the occipital bone of the skull and long bones along with noted deficiencies in skeletal muscle development.

Hypopigmentation and kinky hair arise from TYR and keratin sulfhydralase dysfunction—resulting in pathognomonic silvery, kinky hair. *(110, 111)* Connective tissue abnormalities, though pronounced, marginally contribute to early death. *(113, 114)*

Neurological sparing seen in some variants of *ATP7A* mutation indicates the CNS, and thus CcO function, is more resistant to copper deficiency as compared to connective tissue defects. Low turnover rate of CcO compared to LOX, tyrosinase, etc., may explain this observation.

Mutations in *ATP7A* are diverse and result in a spectrum of copper deficiency disorders that range in severity depending upon the degree of residual function spared by the specific genetic abnormality. *(114)* These disorders include MD, OHS, and newly characterized subtype of X-linked distal hereditary motor neuropathy (HMN).

Of the fifty genetic disorders included in newborn "heel-stick" testing, Menkes and associated conditions are not included in any state-mandated screens. Diagnosis involves clinical examination, serological testing, and confirmatory exome sequencing. Development of a catecholamine-based blood test for use in neonatal screening purposes is ongoing and essential given that some *ATP7A* mutations may respond to copper supplementation within < 28 days postpartum. *(115)*

Suspected MD patients exhibiting characteristic hair morphology, connective tissue abnormalities, and low copper levels despite adequate oral intake or supplementation warrant genetic testing for definitive diagnosis.

Commercially available tests for MD, OHS, and HMN are available as part of the GeneDx (OPKO Health Company) and Invitae screening panels, for both diagnostic and maternal genetic counseling purposes.

ATP7A retains approximately 20-30% functionality in OHS patients. OHS presents with pronounced defects in connective tissue with or without mild cognitive impairment. Though lifespan is reduced, OHS patients survive to adulthood. *(112)*

HMN presents with progressive muscle weakness and wasting. The precise pathophysiology of HMN is not currently known. HMN missense mutations in *ATP7A* result in defective ATP7A trafficking with corresponding impairment of copper homeostasis in peripheral neurons without overt signs, symptoms, or laboratory findings of copper deficiency. *(116)*

ATP7A activity levels in Menkes range from total absence to upwards of 15% residual functionality. *(118, 119)* Menkes patients exhibit both connective tissue defects and neurodegeneration. MD is further subdivided into classical and atypical disease. Atypical cases are characterized by less severe neurological manifestations, higher residual ATP7A activity, and show greater response to early supplementation therapy utilizing copper histidine. Classical Menkes patients possess the most deleterious mutations that result in a near or complete loss of ATP7A function. *(120)* These patients show minimal response to copper histidine therapy even when initiated early before maturation of the BBB. *(101, 102)*

No FDA-approved therapy exists for MD, OHS, or *ATP7A*-related X-linked HMN. Supplementation with copper histidine by infusion has shown mixed results with positive

outcomes correlating strongly with degree of residual ATP7A activity and age of therapy initiation. OHS and atypical Menkes benefit from enhanced free copper levels but difficulties still exist in distributing copper within the CNS while avoiding renal impairment. Prognosis for MD and OHS, even with early copper therapy, remains poor with emphasis on symptom management and palliative care.

To date, three clinical trials exploring the utility of early copper histidine supplementation conducted by Kaler, et al. demonstrate little benefit in classical Menkes—representing the most severe allelic variants. Two Phase III studies, NCT00811785 "Molecular Bases of Response to Copper Treatment in Menkes disease, Related Phenotypes, and Unexplained Copper Deficiency" and NCT04337684 "Long Term Follow-up on Menkes Disease Patients" remain ongoing at the NIH Clinical Center with conclusion scheduled in December 2021.

### 1.5. Pathogenic *ATP7A* Variant Clinical Case Reports

Medical literature contains numerous patient case reports involving pathogenic *ATP7A* variants. Given the rarity of MD and OSH, diagnosis may not be readily apparent to the general practioner despite the striking phenotypic features of MD. The importance of a multidisciplinary approach to address the numerous organ system manifestations of MD and OSH are discussed in detail by Ojha and Prasad in their 2016 review article in *Journal of Multidisciplinary Healthcare*. *(121)* Their findings underscore the importance of early coordination of care between medical genetics, neurology, GI/nutrition,

developmental pediatrics, urology, nephrology, and physical/occupational therapy in improving diagnosis, care, and clinical outcomes for patients with hereditary copper deficiency disorders.

The following is a review of two case reports highlighting presentation, description of genetic changes, supplementation therapy, and implications for the development of therapeutics for MD.

### Case Report 1: Thailand, Panichsillaphakit et al. 2022 *(122)*

A 4-month old male infant of Southeastern Asian descent presented with generalized tonic seizure and nystagmus refractory to phenobarbital therapy since 6-weeks of age. He was initially followed by neurology for evaluation of seizure disorder. He was referred for genetic consultation due to hypopigmented skin and kinky hair.

At the time of his exam, he exhibited marked truncal hypotonia, spastic limbs, and myclonus. His physical exam was otherwise unremarkable. His labs revealed profound hypocuperemia and hypoceruloplasminemia. Imagining studies included MRI and magnetic resonance angiography which revealed severe cerebellar atrophy, cortical atrophy, ventriculomegaly, skeletal defects, and tortuosity of intracranial arteries. EEG revealed multifocal epilepsy with parieto-occipital focus. All other finding from his extensive workup were unremarkable.

Singleton whole exome sequencing revealed a splice-site mutation c.2172+1 G>T in *ATP7A*. The variant was subsequently categorized as pathogenic according to the American College of Medical Genetics and Genomics Classification. The patient's mutation represented a severe loss-of-function mutation resulting in a complete lack of ATP7A functionality. The patient was immediately started on 250 mg His-$Cu^{2+}$ via subcutaneous injection twice daily per current experimental treatment guidance.

The patient saw initial improvement in serum copper, ceruloplasmin, and hair texture. He remained hypopigmented as compared to his parents. His osteopenia progressed with marked formation of wormian bone and he declined neurologically with progression to status epilepticus. He became ventilator dependent and died at 9.5-months of age.

This patient presented with classic MD refractory to copper supplementation. His specific mutation resulted in a lack of ATP7A expression with marked neurodegenerative features superimposed upon severe connective tissue defects.

Since 1993, five other cases with similar presentations have been described in Thai medical literature. Even with early copper supplementation, no child diagnosed with MD of this cohort lived to 3-years of age. Without a lipophilic carrier, these patients received no therapeutic benefit from subcutaneous copper injection. Despite improvement in serum copper levels, the CNS lacks the ability to import supplemented copper to the brain across the BBB and BCSFB.

Case Report 2: Spain, Leon-Garcia et al. 2012 *(123)*

An 11-month old infant of Caucasian descent presented with seizure and global developmental delay. On physical exam he exhibited hypotonia, ataxia, myoclonic seizure, and phenotypic markers of MD. His initial laboratory workup was unremarkable except for marked hypocuperemia and hypoceruloplasminemia. No imaging studies were reported. His EEG reveal multifocal myoclonic epilepsy.

At 18-months, a pathogenic variant c.3288 C > T was confirmed by sequencing in *ATP7A.* This missense mutation resulted in the substitution of threonine with isoleucine (p.T1048I) in the P-domain involved in ATP binding with a resultant partial loss-of-function in ATP7A-mediated copper transport. The patient was started on copper supplementation with 100 $\mu g \cdot kg^{-1} \cdot day^{-1}$ HIS-$Cu^{2+}$. He maintained this therapeutic regime for 6.5 years until discontinued due to concerns for renal toxicity.

With supplementation, the patient saw normalization of serum copper and ceruloplasmin levels. His neuromotor function improved with regards to tone and ataxia. His seizure frequency decreased with noted improvements in cognitive and psychosocial function though he remained non-verbal with significant intellectual disability. The patient still demonstrated profound osseous and connective tissue deformity—a feature shared with OHS. OHS rarely presents with neurologic symptoms and is managed primarily as a connective tissue disorder.

The patient's presentation illustrates a case of atypical MD in which residual ATP7A activity resulted in relative neurologic sparing and allowed survival to adulthood. Residual ATP7A activity both protected the child from infantile neurological devastation and facilitated partial resolution of symptoms once supplementation started. Though the patient demonstrated clinical improvement, therapy was not started until the relatively late age of 18-months which likely blunted the positive effects of His-$Cu^{2+}$.

Atypical MD and OHS cases indicate that the clinical progression of pathogenic allelic *ATP7A* variants are highly dependent upon the nature of the underlying genetic lesion—a fact that has been well-described by Dr. Stephen Kaler in multiple publications. *(38, 115, 116, 120, 124, 125)* Atypical MD with 5-15% and OHS with < 30% function supports the argument that relatively small improvments in CNS copper levels prevent the most deleterious neurodegenerative effects seen in classic MD and do not alter underlying connective tissue symptoms.

### 1.6. Elesclomol as a Small Molecular Ionophore Therapeutic

Elesclomol (ES) is a small molecule originally developed by Synta Pharmaceuticals as a chemotherapeutic adjuvant agent to be used in combination with other standard of care cancer therapeutics. After failing several Phase III clinical trials, development of ES was halted due to lack of superiority.

Chemically, ES is a lipophilic, substituted bis(thio-hydrazide) amide derivative with a molecular weight of 400.5 $g \cdot mol^{-1}$. ES strongly and specifically coordinates $Cu^{2+}$ in a 1:1 stoichiometric ratio with a KES-Cu β of 1024.2 M but not $Cu^{+}$. *(126)* Within the central core of the molecule, $Cu^{2+}$ coordinates with four atoms of ES forming two S – Cu and N – Cu interactions that result in an approximately square planar configuration following deprotonation of two amide groups. See Figure 1-2. *(126, 127)*

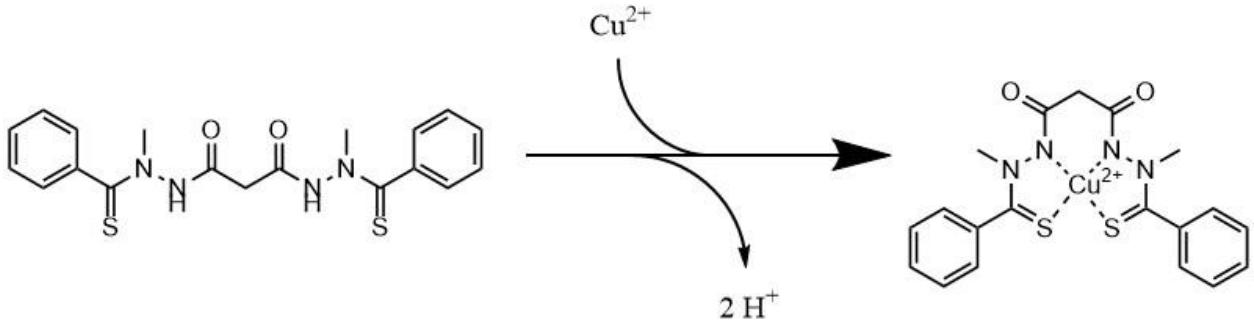


**Figure 1-2: Structure of ES and its $Cu^{2+}$ Complex.**

Cancer cell killing is thought to be achieved by a combination of free copper ROS generation and/or a unique copper-mediate mode of cell death in conjunction with other chemotherapeutic agents. Precise modes of ES-induced cell death are unknown. *(126-129)* Cancer cell killing requires increased cellular ROS sensitivity, adequate copper for mitochondrial overload, and FDX1 activity for reduction of the ES-$Cu^{2+}$ complex and subsequent release of $Cu^{+}$. *(129)* ES is relatively nontoxic in non-cancer cell lines and monotherapy is well tolerated up to 50 $mg \cdot kg^{-1} \cdot day^{-1}$ in mice. ES exhibits favorable pharmacokinetic and metabolic properties.

Mechanistically, ES escorts copper through lipid bilayer membranes to the inner mitochondrial matrix (IMM) where it functions as both a competitive inhibitor and neosubstrate for the small Fe-S protein ferredoxin 1 (FDX1) involved in the mitochondrial cytochrome P450 system. FDX1 reduces $Cu^{2+}$ to $Cu^{+}$ and releases ES and $Cu^{+}$. *(129)* ES is a p-glycoprotein substrate and is rapidly effluxes from the cell where it is free to coordinate a new $Cu^{2+}$ ion. Repeated cycling results in increased intracellular and mitochondrial levels of copper. See Figure 1-3.

In a publication by Soma et al., several diverse small molecules that bind copper were screened for their ability to rescue a *Saccharomyces cerevisiae* strain deficient in electron transport due to deletion of *coa6* (*coa6Δ*). Coa6 is an assembly factor for CcO and a component of the mitochondrial copper relay system utilized to metalate the CcO subunit Cox2 in *Saccharomyces cerevisiae. (130)*

ES restored near-wildtype growth, oxygen consumption rate, and CcO function with an $ED_{50}$ of 0.8 nM; representing the most potent molecule identified in by Soma et al.'s *coa6Δ* functional complementation assay. The results of this initial publication by Soma et al. served as an in vitro groundwork and justification for the transition to vertebrate animal models of hereditary copper deficiency disorders.

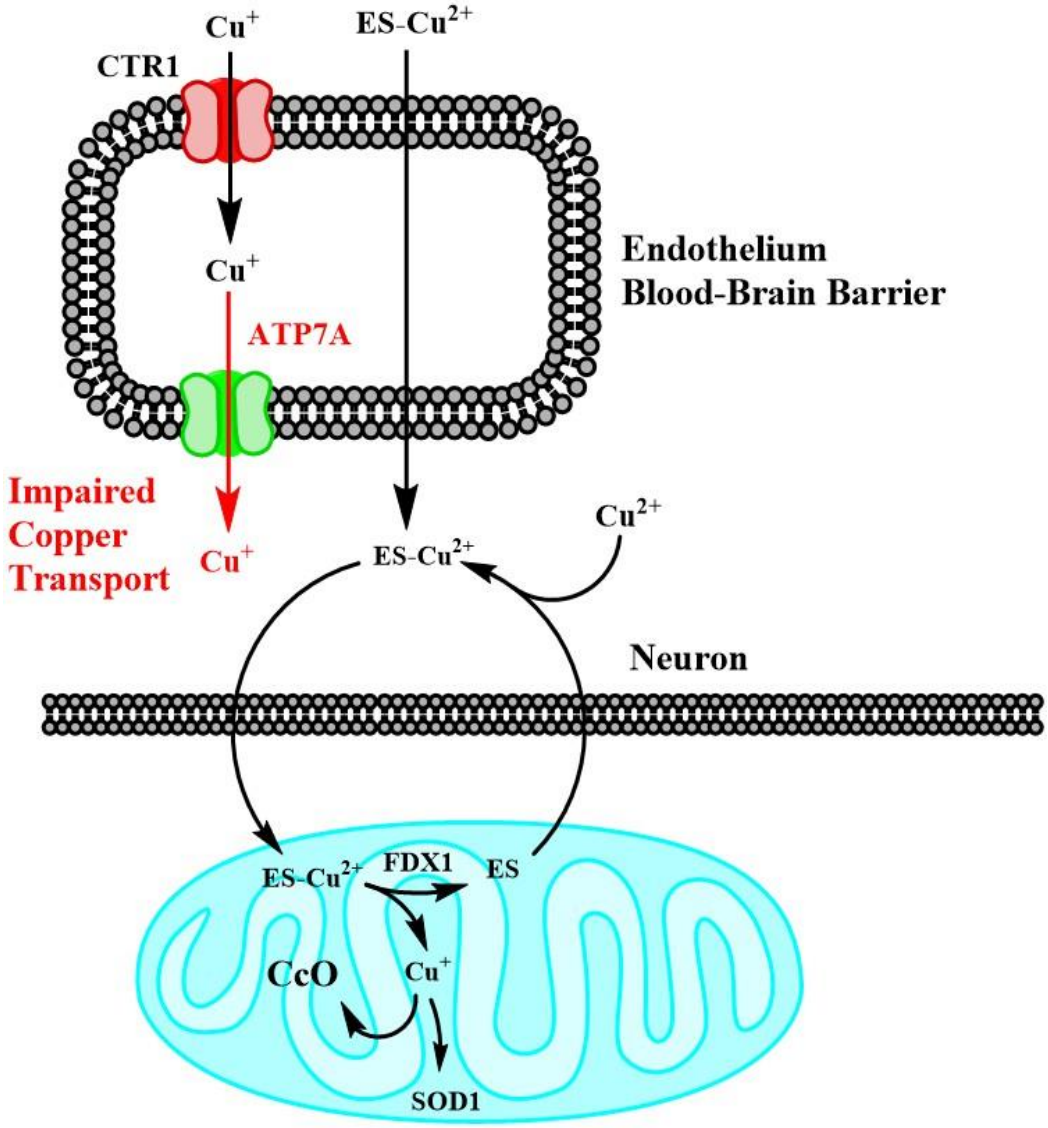


**Figure 1-3: Schematic Diagram of Proposed ES-Mediated Mitochondrial Release of Copper in the Brain**

The BBB renders parenteral copper supplementation via salts or amino acid coordinate complexes ineffective as a treatment modality. Use of a lipophilic carrier is required to bypass ATP7A-mediated basolateral transport of copper across endothelium of the BBB. The ES-$Cu^{2+}$ complex is theorized to cross the BBB. In neuronal mitochondria, copper release is mediated by the reduction of coordinated $Cu^{2+}$ to $Cu^{+}$ by the actions of ferredoxin 1 (FDX1). Metallochaperones of the mitochondrial copper relay system use $Cu^{+}$ to metalate CcO subunits COX1 and COX2—restoring energy production by electron transport. SOD1, located in the intermembrane space, is metalated by its chaperone CCS—restoring free radical scavenging.

## 1.7. References


1) Institute of Medicine. (2002). *Dietary Reference Intakes for Vitamin A, Vitamin K, Arsenic, Boron, Chromium, Copper, Iodine, Iron, Manganese, Molybdenum, Nickel, Silicon, Vanadium, and Zinc*. National Academies Press. 224-257.
2) Institute of Medicine. (1998). *Dietary Reference Intakes: A Risk Assessment Model for Establishing Upper Intake Levels for Nutrients.* National Academies Press. 4-6.
3) US Department of Agriculture ARS. Total nutrient intakes: percent reporting and mean amounts of selected vitamins and minerals from food and dietary supplements, by gender and age – What we eat in America – NHANES, 2009–2010, 2012.
4) Bost, M., Houdart, S., Oberli, M., Kalonji, E., Huneau, J.-F., & Margaritis, I. (2016). Dietary copper and human health: Current evidence and unresolved issues. *Journal of Trace Elements in Medicine and Biology*, *35*, 107–115. https://doi.org/10.1016/j.jtemb.2016.02.006
5) King, J. C., Blumberg, J., Ingwersen L., Jenab, M., Tucker, K. L. (2008). Tree Nuts and Peanuts as Components of a Healthy Diet. Nuts and Health Symposium. *The Journal of Nutrition. 138(9):*1736S-1740S. https://doi.org/10.1093/jn/138.9.1736S
6) Klevay, L.M. (2011). Is the Western diet adequate in copper? *Journal of Trace Elements in Medicine and Biology, 25,* 204-212. https://doi.org/10.1016/j.jtemb.2011.08.146

7) Collins, J. F. Chapter 24: Copper. Erdeman J. W., Macdonald I. A. Zeisel S.H. eds. *Present Knowledge in Nutrition*. 11th Ed. Vol. 1: Basic Nutrition and Metabolism. Washington, DC: Wiley-Blackwell; 2020: pgs. 409-427.

8) Beshgetoor, D., & Hambidge, M. (1998). Clinical conditions altering copper metabolism in humans. *The American Journal of Clinical Nutrition*, *67*(5), 1017S-1021S. https://doi.org/10.1093/ajcn/67.5.1017s

9) Jin, J., Mulesa, L., Rouillet, M. C. (2017). Trace Elements in Parenteral Nutrition: Considerations for the Prescribing Clinician. *Nutrients, 9(5):*440 https://doi.org10.3390/nu9050440

10) Griffith, D. P., Liff, D. A., Ziegler, T. R., Esper, G. J., & Winton, E. F. (2009). Acquired Copper Deficiency: A Potentially Serious and Preventable Complication Following Gastric Bypass Surgery. *Obesity*, *17*(4), 827–831. https://doi.org/10.1038/oby.2008.614

11) Lönnerdal, B. (1998). Copper nutrition during infancy and childhood. *The American Journal of Clinical Nutrition*, *67*(5), 1046S-1053S. https://doi.org/10.1093/ajcn/67.5.1046s

12) L. Shaw, J. C. (1980). Trace Elements in the Fetus and Young Infant. *American Journal of Diseases of Children*, *134*(1), 74. https://doi.org/10.1001/archpedi.1980.02130130056017

13) Widdowson, E. M., Dauncey, J., & Shaw, J. C. L. (1974). Trace elements in foetal and early postnatal development. *Proceedings of the Nutrition Society*, *33*(3), 275–284. https://doi.org/10.1079/pns19740050

14) Vuori, E., & Kuitunen, P. (1979). The Concentrations of copper and zinc in human milk: A Longitudinal Study. *Acta Paediatrica*, *68*(1), 33–37. https://doi.org/10.1111/j.1651-2227.1979.tb04426.x

15) Kumar, N., Butz, J. A., Burritt, M. F. (2007). Clinical significance of the laboratory determination of low serum copper in adults. *Clinical Chemistry and Laboratory Medicine, 45(10):*1402-1410. https://doi.org/10.1515/CCLM.2007.292

16) Wazir, S. M., Ghobrial, I. (2017). Copper deficiency, a new triad: anemia, leucopenia, and myeloneuropathy. *Journal of community hospital internal medicine perspectives*, *7*(4), 265–268. https://doi.org/10.1080/20009666.2017.1351289

17) Mueller C.M. The A.S.P.E.N. Adult Nutrition Support Core Curriculum, 3rd Ed. Silver Spring, MD: ASPEN; 2017.

18) Johnson, L. E. (2021, February 22). *Copper deficiency - nutritional disorders*. Merck Manuals Professional Edition. Retrieved March 2, 2021, from https://www.merckmanuals.com/professional/nutritional-disorders/mineral-deficiency-and-toxicity/copper-deficiency

19) Corkins M.R. The A.S.P.E.N. Pediatric Nutrition Support Core Curriculum, 2nd Ed. Silver Spring, MD: ASPEN; 2015.

20) Gaetke, L. M., Chow-Johnson, H. S., Chow, C. K. (2014) Copper: Toxicological relevance and mechanisms. *Archives of Toxicology*. 2014 Nov; 88(11): 1929–1938. doi: 10.1007/s00204-014-1355-y

21) Toxicological Profile for Copper. CDC Agency for Toxic Substances and Disease Registry (ATSDR). 2022. Pgs. 21-103. https://www.atsdr.cdc.gov/ToxProfiles/tp132.pdf

22) National Research Council. (2000). *Copper in Drinking Water* (1st ed.) [E-book]. National Academies Press. https://www.ncbi.nlm.nih.gov/books/NBK225402/

23) National Primary Drinking Water Regulations. Inorganic Chemicals. United States Environmental Protection Agency. (2019). https://www.epa.gov/ground-water-and-drinking-water/national-primary-drinking-water-regulations#Inorganic

24) Royer, A. Sharman, T. (2021). Copper Toxicity. *StatPearls*. Treasure Island, FL. https://www.ncbi.nlm.nih.gov/books/NBK557456/

25) Johnson, L. E. (2021, December 22). *Copper Toxicity*. Merck Manuals Professional Edition. Retrieved March 2, 2021, from https://www.merckmanuals.com/professional/nutritional-disorders/mineral-deficiency-and-toxicity/copper-toxicity

26) Winge, D. R., & Mehra, R. K. (1990). Host defenses against copper toxicity. *International Review of Experimental Pathology*, *31*, 47–83. https://doi.org/10.1016/b978-0-12-364931-7.50007-0

27) Turnlund, J. R., Keyes, W. R., Anderson, H. L., & Acord, L. L. (1989). Copper absorption and retention in young men at three levels of dietary copper by use of the stable isotope 65Cu. *The American Journal of Clinical Nutrition*, *49*(5), 870–878. https://doi.org/10.1093/ajcn/49.5.870

28) Wang, T., Xiang, P., Ha, J. H., Wang, X., Doguer, C., Flores, S. R. L., Kang, Y. J., & Collins, J. F. (2018). Copper supplementation reverses dietary iron overload-induced pathologies in mice. *The Journal of Nutritional Biochemistry*, *59*, 56–63. https://doi.org/10.1016/j.jnutbio.2018.05.006

29) Jiang, L., Garrick, M. D., Garrick, L. M., Zhao, L., & Collins, J. F. (2013). Divalent metal transporter 1 (Dmt1) Mediates Copper Transport in the Duodenum of Iron-Deficient Rats and When Overexpressed in Iron-Deprived HEK-293 Cells. *The Journal of Nutrition*, *143*(12), 1927–1933. https://doi.org/10.3945/jn.113.181867

30) Gupta, A., & Lutsenko, S. (2009). Human copper transporters: mechanism, role in human diseases and therapeutic potential. *Future Medicinal Chemistry*, *1*(6), 1125–1142. https://doi.org/10.4155/fmc.09.84

31) Nose, Y., Kim, B. E., & Thiele, D. J. (2006). Ctr1 drives intestinal copper absorption and is essential for growth, iron metabolism, and neonatal cardiac function. *Cell Metabolism*, *4*(3), 235–244. https://doi.org/10.1016/j.cmet.2006.08.009

32) Clifford, R. J., Maryon, E. B., & Kaplan, J. H. (2016). Dynamic internalization and recycling of a metal ion transporter: Cu homeostasis and CTR1, the human $Cu^{+}$ uptake system. *Journal of Cell Science*, *129*(8), 1711–1721. https://doi.org/10.1242/jcs.173351

33) Lee, J., Prohaska, J. R., & Thiele, D. J. (2001). Essential role for mammalian copper transporter Ctr1 in copper homeostasis and embryonic development.

*Proceedings of the National Academy of Sciences*, *98*(12), 6842–6847. https://doi.org/10.1073/pnas.111058698

34) Kuo, Y.M., Zhou, B., Cosco, D., & Gitschier, J. (2001). The copper transporter CTR1 provides an essential function in mammalian embryonic development. *Proceedings of the National Academy of Sciences*, *98*(12), 6836–6841. https://doi.org/10.1073/pnas.111057298

35) Linder M. C., Hazegh-Azam M. (1996) Copper biochemistry and molecular biology. *American Journal of Clinical Nutrition*. 1996;63(5):797S-811S. DOI: 10.1093/ajcn/63.5.797

36) E. D. Harris, Cellular copper transport and metabolism. *Annual Review of Nutrition.* ***20(1)***, 291-310 (2000). DOI: 10.1146/annurev.nutr.20.1.291

37) L. B. Møller, Z. Tümer, C. Lund, C. Petersen, T. Cole, R Hanusch, N. Horn, Similar splice-site mutations of the ATP7A gene lead to different phenotypes: classical Menkes disease or occipital horn syndrome. *American Journal of Human Genetics*. 66(4), 1211-1220 (2000).

38) J. Tang, S. Robertson, K. E. Lem, S. C. Godwin, S. G. Kaler, Functional copper transport explains neurologic sparing in occipital horn syndrome. *Genet Med.* ***8(11)***, 711-718 (2006).

39) Matte JJ, Girard CL, Guay F. Intestinal fate of dietary zinc and copper: postprandial net fluxes of these trace elements in portal vein of pigs. J Trace Elements Med Biol. 2017;44:65–70.

https://doi.org/10.1016/j.jtemb.2017.06.003.

40) Marceau N, Aspin N. Distribution of ceruloplasmin- ceruloplasmin-bound 67 Cu in the rat. Am J Phys. 1972;222:106–10. https://doi.org/10.1152/ajplegacy.1972.222.1.106.

41) Boal, A. K., & Rosenzweig, A. C. (2009). Structural biology of copper trafficking. *Chemical reviews*, *109*(10), 4760–4779. https://doi.org/10.1021/cr900104z

42) Kirsipuu, T., Zadorožnaja, A., Smirnova, J. *et al.* Copper(II)-binding equilibria in human blood. *Sci Rep* **10,** 5686 (2020). https://doi.org/10.1038/s41598-020-62560-4

43) Neumann, P. Z. & Sass-Kortsak, A. The state of copper in human serum: evidence for an amino acid-bound fraction. *J. Clin. Invest.* **46**, 646-658 https://doi.org/10.1172/JCI105566 (1967).

44) Deschamps, P., Kulkarni, P. P., Gautam-Basak, M. & Sarkar, B. The saga of copper(II)-L-histidine. *Coord. Chem. Rev.* **249**, 895-909 https://doi.org/10.1016/j.ccr.2005.09.013 (2005).

45) Bal, W., Sokolowska, M., Kurowska, E. & Faller, P. Binding of transition metal ions to albumin: sites, affinities and rates. *Biochim. Biophys. Acta* **1830**, 5444–5455, https://doi.org/10.1016/j.bbagen.2013.06.018 (2013).

46) Fasano, M. *et al*. The extraordinary ligand binding properties of human serum albumin. *IUBMB Life* **57**, 787–796, https://doi.org/10.1080/15216540500404093 (2005).

47) Moriya, M. *et al*. Copper is taken up efficiently from albumin and alpha2-macroglobulin by cultured human cells by more than one mechanism. *Am. J. Physiol. Cell Physiol* **295**, C708–721, https://doi.org/10.1152/ajpcell.00029.2008 (2008).

48) Marrero, A. *et al*. The crystal structure of human alpha2-macroglobulin reveals a unique molecular cage. *Angew. Chem. Int. Ed. Engl.* **51**, 3340–3344, https://doi.org/10.1002/anie.201108015 (2012).

49) Cousins RJ. Absorption, transport, and hepatic metabolism of copper and zinc: special reference to metallothionein and ceruloplasmin. Physiol Rev. 1985;65:238–309. https://doi.org/10.1152/physrev.1985.65.2.238.

50) Thirumoorthy, N., Manisenthil Kumar, K. T., Shyam Sundar, A., Panayappan, L., & Chatterjee, M. (2007). Metallothionein: an overview. *World journal of gastroenterology*, *13*(7), 993–996. https://doi.org/10.3748/wjg.v13.i7.993

51) Tapia, L., González-Agüero, M., Cisternas, M. F., Suazo, M., Cambiazo, V., Uauy, R., & González, M. (2004). Metallothionein is crucial for safe intracellular copper storage and cell survival at normal and supra-physiological exposure levels. *The Biochemical journal*, *378*(Pt 2), 617–624. https://doi.org/10.1042/BJ20031174

52) Weiss, K. H., Lozoya, J. C., Tuma, S., Gotthardt, D., Reichert, J., Ehehalt, R., Stremmel, W., & Füllekrug, J. (2008). Copper-induced translocation of the Wilson disease protein ATP7B independent of Murr1/COMMD1 and Rab7. *The*

*American journal of pathology*, *173*(6), 1783–1794. https://doi.org/10.2353/ajpath.2008.071134

53) Członkowska, A., Litwin, T., Dusek, P. *et al.* Wilson disease. *Nat Rev Dis Primers* **4,** 21 (2018). https://doi.org/10.1038/s41572-018-0018-3

54) Wu F, Wang J, Pu C, Qiao L, Jiang C. Wilson's disease: a comprehensive review of the molecular mechanisms. Int J Mol Sci. 2015 Mar 20;16(3):6419-31. doi: 10.3390/ijms16036419

55) Lenartowicz M, Krzeptowski W. Budowa. Structure and function of ATP7A and ATP7B proteins--Cu-transporting ATPases. *Postepy Biochem*. 2010;56(3):317-27.

56) Capaldi, R. A. Structure and function of cytochrome c oxidase. *Annu. Rev. Biochem.* **59**, 569–596 (1990).

57) Malatesta, F., Antonini, G., Sarti, P. & Brunori, M. Structure and function of a molecular machine: cytochrome c oxidase. *Biophys. Chem.* **54**, 1–33 (1995).

58) Zong, S., Wu, M., Gu, J. *et al.* Structure of the intact 14-subunit human cytochrome *c* oxidase. *Cell Res* **28,** 1026–1034 (2018). https://doi.org/10.1038/s41422-018-0071-1

59) Horn, D., & Barrientos, A. (2008). Mitochondrial copper metabolism and delivery to cytochrome c oxidase. *IUBMB life*, *60*(7), 421–429. https://doi.org/10.1002/iub.50

60) Baker, Z. N., Cobine, P. A., & Leary, S. C. (2017). The mitochondrion: a central architect of copper homeostasis. *Metallomics : integrated biometal science*, *9*(11), 1501–1512. https://doi.org/10.1039/c7mt00221a

61) Palumaa, P., Kangur, L., Voronova, A., & Sillard, R. (2004). Metal-binding mechanism of Cox17, a copper chaperone for cytochrome c oxidase. *The Biochemical journal*, *382*(Pt 1), 307–314. https://doi.org/10.1042/BJ20040360

62) Soma S, Morgada MN, Naik MT, Boulet A, Roesler AA, Dziuba N, Ghosh A, Yu Q, Lindahl PA, Ames JB, Leary SC, Vila AJ, Gohil VM. COA6 Is Structurally Tuned to Function as a Thiol-Disulfide Oxidoreductase in Copper Delivery to Mitochondrial Cytochrome c Oxidase. Cell Rep. 2019 Dec 17;29(12):4114-4126.e5. doi: 10.1016/j.celrep.2019.11.054.

63) O.M. Ighodaro, O.A. Akinloye. First line defence antioxidants-superoxide dismutase (SOD), catalase (CAT) and glutathione peroxidase (GPX): Their fundamental role in the entire antioxidant defence grid, Alexandria Journal of Medicine,Volume 54, Issue 4, 2018, Pages 287-293, https://doi.org/10.1016/j.ajme.2017.09.001.

64) Azadmanesh, J., & Borgstahl, G. (2018). A Review of the Catalytic Mechanism of Human Manganese Superoxide Dismutase. *Antioxidants (Basel, Switzerland)*, *7*(2), 25. https://doi.org/10.3390/antiox7020025

65) Rakhit R, Chakrabartty A. Structure, folding, and misfolding of Cu,Zn superoxide dismutase in amyotrophic lateral sclerosis. Biochim Biophys Acta. 2006 Nov-Dec;1762(11-12):1025-37. doi: 10.1016/j.bbadis.2006.05.004.

66) Zelko IN, Mariani TJ, Folz RJ. Superoxide dismutase multigene family: a comparison of the CuZn-SOD (SOD1), Mn-SOD (SOD2), and EC-SOD (SOD3) gene structures, evolution, and expression. Free Radic Biol Med. 2002 Aug 1;33(3):337-49. doi: 10.1016/s0891-5849(02)00905-x.

67) Boyd, S. D., Ullrich, M. S., Skopp, A., & Winkler, D. D. (2020). Copper Sources for Sod1 Activation. *Antioxidants (Basel, Switzerland)*, *9*(6), 500. https://doi.org/10.3390/antiox9060500

68) Trist BG, Hare DJ, Double KL. A Proposed Mechanism for Neurodegeneration in Movement Disorders Characterized by Metal Dyshomeostasis and Oxidative Stress. Cell Chem Biol. 2018 Jul 19;25(7):807-816. doi: 10.1016/j.chembiol.2018.05.004.

69) Hodgkinson, V. L., Zhu, S., Wang Y., Ladomersky, E. Nickelson, K. Weisman, G. A., Lee, J. Gitlin, J. D. & Petris, M. J. (2015). Autonomous requirements of the Menkes disease protein in the nervous system. *American Journal of Physiology-Cell Physiology* 2015 309:10, C660-C668

70) Vendelboe TV, Harris P, Zhao Y, Walter TS, Harlos K, El Omari K, Christensen HE. The crystal structure of human dopamine β-hydroxylase at 2.9 Å resolution. Sci Adv. 2016 Apr 8;2(4):e1500980. doi: 10.1126/sciadv.1500980.

71) Francisco WA, Wille G, Smith AJ, Merkler DJ, Klinman JP. Investigation of the pathway for inter-copper electron transfer in peptidylglycine alpha-amidating monooxygenase. J Am Chem Soc. 2004 Oct 20;126(41):13168-9. doi: 10.1021/ja046888z.

72) Moore RY, Gustafson EL. The distribution of dopamine-beta-hydroxylase, neuropeptide Y and galanin in locus coeruleus neurons. J Chem Neuroanat. 1989 Mar-Apr;2(2):95-106.

73) Berends, A., Eisenhofer, G., Fishbein, L., Horst-Schrivers, A., Kema, I. P., Links, T. P., Lenders, J., & Kerstens, M. N. (2019). Intricacies of the Molecular Machinery of Catecholamine Biosynthesis and Secretion by Chromaffin Cells of the Normal Adrenal Medulla and in Pheochromocytoma and Paraganglioma. *Cancers*, *11*(8), 1121. https://doi.org/10.3390/cancers11081121

74) Katsuyama M, Kimura E, Ibi M, Iwata K, Matsumoto M, Asaoka N, Yabe-Nishimura C. Clioquinol inhibits dopamine-β-hydroxylase secretion and noradrenaline synthesis by affecting the redox status of ATOX1 and copper transport in human neuroblastoma SH-SY5Y cells. Arch Toxicol. 2021 Jan;95(1):135-148. doi: 10.1007/s00204-020-02894-0.

75) Hatori, Y., & Lutsenko, S. (2016). The Role of Copper Chaperone Atox1 in Coupling Redox Homeostasis to Intracellular Copper Distribution. *Antioxidants (Basel, Switzerland)*, *5*(3), 25. https://doi.org/10.3390/antiox5030025

76) Jepma M, Deinum J, Asplund CL, Rombouts SA, Tamsma JT, Tjeerdema N, Spapé MM, Garland EM, Robertson D, Lenders JW, Nieuwenhuis S. Neurocognitive function in dopamine-β-hydroxylase deficiency. Neuropsychopharmacology. 2011 Jul;36(8):1608-19. doi: 10.1038/npp.2011.42. Epub 2011 Apr 6.

77) Gacheru SN, Trackman PC, Shah MA, O'Gara CY, Spacciapoli P, Greenaway FT, Kagan HM (Nov 1990). "Structural and catalytic properties of copper in lysyl oxidase". *The Journal of Biological Chemistry*. **265** (31): 19022–7. doi:10.1016/0162-0134(89)84532-5.

78) Vallet, S.D., Miele, A.E., Uciechowska-Kaczmarzyk, U. *et al.* Insights into the structure and dynamics of lysyl oxidase propeptide, a flexible protein with numerous partners. *Sci Rep* **8,** 11768 (2018). https://doi.org/10.1038/s41598-018-30190-6

79) Csiszar K. Lysyl oxidases: a novel multifunctional amine oxidase family. Prog Nucleic Acid Res Mol Biol. 2001;70:1-32. doi: 10.1016/s0079-6603(01)70012-8.

80) Csiszar K. Lysyl oxidases: a novel multifunctional amine oxidase family. Prog Nucleic Acid Res Mol Biol. 2001;70:1-32. doi: 10.1016/s0079-6603(01)70012-8.

81) Hamza, I., Faisst, A., Prohaska, J., Chen, J., Gruss, P., and Gitlin, J. D. (2001). The metallochaperone Atox1 plays a critical role in perinatal copper homeostasis. *Proc. Natl. Acad. Sci. U.S.A.* 98, 6848–6852. doi: 10.1073/pnas.111058498

82) Ni, Q. Z., Sierra, B. N., La Clair, J. J., & Burkart, M. D. (2020). Chemoenzymatic elaboration of the Raper-Mason pathway unravels the structural diversity within eumelanin pigments. *Chemical science*, *11*(30), 7836–7841. https://doi.org/10.1039/d0sc02262d

83) Olivares, C., & Solano, F. (2009). New insights into the active site structure and catalytic mechanism of tyrosinase and its related proteins. *Pigment cell &*

*melanoma research*, *22*(6), 750–760. https://doi.org/10.1111/j.1755-148X.2009.00636.x

84) Dolinska, M. B., Kus, N. J., Farney, S. K., Wingfield, P. T., Brooks, B. P., & Sergeev, Y. V. (2017). Oculocutaneous albinism type 1: link between mutations, tyrosinase conformational stability, and enzymatic activity. *Pigment cell & melanoma research*, *30*(1), 41–52. https://doi.org/10.1111/pcmr.12546

85) Petris, M. J., Strausak, D., & Mercer, J. F. (2000). The Menkes copper transporter is required for the activation of tyrosinase. *Human molecular genetics*, *9*(19), 2845–2851. https://doi.org/10.1093/hmg/9.19.2845

86) Lenartowicz, M., Krzeptowski, W., Lipiński, P., Grzmil, P., Starzyński, R., Pierzchała, O., & Møller, L. B. (2015). Mottled Mice and Non-Mammalian Models of Menkes Disease. *Frontiers in molecular neuroscience*, *8*, 72. https://doi.org/10.3389/fnmol.2015.00072

87) Bento, I., Peixoto, C., Zaitsev, V. N., & Lindley, P. F. (2007). Ceruloplasmin revisited: structural and functional roles of various metal cation-binding sites. *Acta crystallographica. Section D, Biological crystallography*, *63*(Pt 2), 240–248. https://doi.org/10.1107/S090744490604947X

88) Marchi, G., Busti, F., Lira Zidanes, A., Castagna, A., & Girelli, D. (2019). Aceruloplasminemia: A Severe Neurodegenerative Disorder Deserving an Early Diagnosis. *Frontiers in neuroscience*, *13*, 325. https://doi.org/10.3389/fnins.2019.00325

89) Mercer J. F. (2001). The molecular basis of copper-transport diseases. *Trends in molecular medicine*, *7*(2), 64–69. https://doi.org/10.1016/s1471-4914(01)01920-

90) Yamada, H., Taneda, A., Takamori, K. and Ogawa, H. (1996), Menkes' kinky hair disease: Report of a case and distribution of sulfhydryl residues and disulfide bonds in kinky hair. Journal of the European Academy of Dermatology and Venereology, 6: 240-245. https://doi.org/10.1111/j.1468-3083.1996.tb00177.x

91) Singh S, Bresnan MJ. Menkes Kinky-Hair Syndrome (Trichopoliodystrophy): Low Copper Levels in the Blood, Hair, and Urine. *Am J Dis Child.* 1973;125(4):572–578. doi:10.1001/archpedi.1973.04160040072015

92) Mulligan, C., & Bronstein, J. M. (2020). Wilson Disease: An Overview and Approach to Management. *Neurologic clinics*, *38*(2), 417–432. https://doi.org/10.1016/j.ncl.2020.01.005

93) Catana, A. M., & Medici, V. (2012). Liver transplantation for Wilson disease. *World journal of hepatology*, *4*(1), 5–10. https://doi.org/10.4254/wjh.v4.i1.5

94) Dusek, P., Litwin, T., & Członkowska, A. (2019). Neurologic impairment in Wilson disease. *Annals of translational medicine*, *7*(Suppl 2), S64. https://doi.org/10.21037/atm.2019.02.43

95) Litwin, T., Dusek, P., Szafrański, T., Dzieżyc, K., Członkowska, A., & Rybakowski, J. K. (2018). Psychiatric manifestations in Wilson's disease: possibilities and difficulties for treatment. *Therapeutic advances in psychopharmacology*, *8*(7), 199–211. https://doi.org/10.1177/2045125318759461

96) Peisach, J.; Blumberg, W. E. (1969). "A mechanism for the action of penicillamine in the treatment of Wilson's disease". *Molecular Pharmacology*. **5** (2): 200–209

97) Mohr, I., & Weiss, K. H. (2019). Current anti-copper therapies in management of Wilson disease. *Annals of translational medicine*, *7*(Suppl 2), S69. https://doi.org/10.21037/atm.2019.02.48

98) Camakaris J, Voskoboinik I, Mercer JF. (1999). Molecular mechanisms of copper homeostasis. *Biochemical Biophysical Research Communications,* 261(2):225-232. doi: 10.1006/bbrc.1999.1073

99) Ramos D, Mar D, Ishida M, Vargas R, Gaite M, Montgomery A, Linder MC. (2016). Mechanism of Copper Uptake from Blood Plasma Ceruloplasmin by Mammalian Cells. *PloS one, 11*(3), e0149516. doi:10.1371/journal.pone.0149516

100) Kim MY, Kim JH, Cho MH, Choi YH, Kim SH, Im YJ, Cheong HI. (2018). Urological Problems in Patients with Menkes Disease. *Journal of Korean medical science*, *34*(1), e4. doi:10.3346/jkms.2019.34.e4

101) Fu X, Zhang Y, Jiang W, Monnot AD, Bates CA, Zheng W. (2014). Regulation of copper transport crossing brain barrier systems by Cu-ATPases: effect of manganese exposure. *Toxicological Sciences 139*(2), 432–451. doi:10.1093/toxsci/kfu048

102) Choi BS, Zheng W. (2009). Copper transport to the brain by the blood-brain barrier and blood-CSF barrier. *Brain research, 1248*, 14–21. doi:10.1016/j.brainres.2008.10.056

103) Kodama, H. and Murata, Y. (1999), Molecular genetics and pathophysiology of Menkes disease. Pediatrics International, 41: 430-435. https://doi.org/10.1046/j.1442-200x.1999.01091.x

104) Meguro Y, Kodama H, Abe T, Kobayashi S, Kodama Y, Nishimura M. (1991). Changes of copper level and cytochrome c oxidase activity in the macular mouse with age. *Brain Development,* 13(3): 184-186

105) Hodgkinson VL, Zhu S, Ladomersky E, Nickelson K, Weisman GA, Petris MJ. (2015). Autonomous requirements of the Menkes disease protein in the nervous system. *American journal of physiology. Cell physiology*, 309(10), C660–C668. doi:10.1152/ajpcell.00130.2015

106) Cobine PA, Pierrel F, Winge DR. Copper trafficking to the mitochondrion and assembly of copper metalloenzymes. *Biochimica et. Biophysica Acta.* 1763(7):759-72. doi: 10.1016/j.bbamcr.2006.03.002

107) Zlatic S, Comstra HS, Gokhale A, Petris MJ, Faundez V. (2015). Molecular basis of neurodegeneration and neurodevelopmental defects in Menkes disease. *Neurobiology of Disease,* 81: 154–161. doi:10.1016/j.nbd.2014.12.024.

108) Bhattacharjee A, Yang H., Duffy M, Robinson E, Conrad-Antoville A, Lu YW, Ralle M. (2016). The Activity of Menkes Disease Protein ATP7A Is Essential for Redox Balance in Mitochondria. *The Journal of biological chemistry*, *291*(32), 16644–16658. doi:10.1074/jbc.M116.727248

109) Shanbhag V, Jasmer-McDonald K, Zhu S, Martin AL, Gudekar N, Khan A, Ladomersky E, Singh K, Weisman GA, Petris MJ. (2019). ATP7A delivers

copper to the lysyl oxidase family of enzymes and promotes tumorigenesis and metastasis. Proceedings of the National Academy of Sciences Apr 2019, 116 (14) 6836-6841; DOI: 10.1073/pnas.1817473116

110) Gillespie JM. (1973). Keratin structure and changes with copper deficiency. Australas J Dermatol. 1973 Dec; 14(3): 127–131.

111) Setty SR, Tenza D, Sviderskaya EV, Bennett DC, Raposo G, Marks MS. (2008). Cell-specific ATP7A transport sustains copper-dependent tyrosinase activity in melanosomes. *Nature,* 454(7208), 1142–1146. doi:10.1038/nature07163

112) Beyens A, van Meensel K, Pottie L, de Rycke R, de Bruyne M, Baeke F, Callewaert B. (2019). Defining the Clinical, Molecular and Ultrastructural Characteristics in Occipital Horn Syndrome: Two New Cases and Review of the Literature. *Genes*, 10(7): 528. doi:10.3390/genes10070528.

113) Møller LB, Tümer Z, Lund C, Petersen C, Cole T, Hanusch R, Horn N. (2000). Similar splice-site mutations of the ATP7A gene lead to different phenotypes: Classical Menkes disease or occipital horn syndrome. *American Journal of Human Genetics*, 66(4): 1211–1220. doi:10.1086/302857.

114) Ambrosini L, Mercer JF. (1999). Defective copper-induced trafficking and localization of the Menkes protein in patients with mild and copper-treated classical Menkes disease. Hum Mol Genet. 1999 Aug; 8(8): 1547–1555.

115) Kaler, S. G., Holmes, C. S., Goldstein, D. S., Tang, J., Godwin, S. C., Donsante, A., Liew, C. J., Sato, S., & Patronas, N. (2008). Neonatal diagnosis and treatment

of Menkes disease. *The New England journal of medicine*, *358*(6), 605–614. https://doi.org/10.1056/NEJMoa070613

116) Kennerson ML, Nicholson GA, Kaler SG, Kowalski B, Mercer JF, Tang J, Garbern JY. (2010). Missense mutations in the copper transporter gene ATP7A cause X-linked distal hereditary motor neuropathy. *American journal of human genetics*, 86(3), 343–352. doi:10.1016/j.ajhg.2010.01.027

117) Skjørringe T, Pedersen A, Thorborg S, Nissen P, Gourdon P, Birk Møller L. (2017). Characterization of ATP7A missense mutants suggests a correlation between intracellular trafficking and severity of Menkes disease. *Scientific reports*, *7*(1), 757. doi:10.1038/s41598-017-00618-6

118) Skjørringe T, Pedersen A, Thorborg S, Nissen P, Gourdon P, Birk Møller L. (2017). Characterization of ATP7A missense mutants suggests a correlation between intracellular trafficking and severity of Menkes disease. *Scientific reports*, *7*(1), 757. doi:10.1038/s41598-017-00618-6

119) Tchan MC, Wilcken B, Christodoulou J. (2013). The mild form of Menkes disease: a 34 year progress report on the original case. *JIMD reports*, *9*, 81–84. doi:10.1007/8904_2012_183

120) Tang J, Donsante A, Desai V, Patronas N, Kaler SG. (2008). Clinical outcomes in Menkes disease patients with a copper-responsive ATP7A mutation, G727R. *Molecular genetics and metabolism*, *95*(3), 174–181. doi:10.1016/j.ymgme.2008.06.015

121) Ojha, R., & Prasad, A. N. (2016). Menkes disease: what a multidisciplinary approach can do. *Journal of Multidisciplinary Healthcare*, 9, 371–385. https://doi.org/10.2147/JMDH.S93454

122) Panichsillaphakit, E., Kwanbunbumpen, T., Chomtho, S., & Visuthranukul, C. (2022). Copper-histidine therapy in an infant with novel splice-site variant in the ATP7A gene of Menkes disease: the first experience in South East Asia and literature review. *BMJ Case Reports*, 15(4), e247937.

123) León-García, G., Santana, A., Villegas-Sepúlveda, N., Pérez-González, C., Henrríquez-Esquíroz, J. M., de León-García, C., Wong, C., & Baeza, I. (2012). The T1048I mutation in ATP7A gene causes an unusual Menkes disease presentation. *BMC Pediatrics*, 12, 150. https://doi.org/10.1186/1471-2431-12-150

124) S. G. Kaler, ATP7A-related copper transport diseases: emerging concepts and future trends. Nat Rev Neurol. 7(1), 15-29 (2011).

125) S. G. Kaler, Neurodevelopment and brain growth in classic Menkes disease is influenced by age and symptomatology at initiation of copper treatment. J. Trace Elem Med Biol. 28(4), 427-430 (2014).

126) Yadav AA, Patel D, Wu X, Hasinoff BB. (2013). Molecular mechanisms of the biological activity of the anticancer drug elesclomol and its complexes with Cu(II), Ni(II) and Pt(II). *Journal of Inorganic Biochemistry*, 126:1-6. doi: 10.1016/j.jinorgbio.2013.04.013.

127) Nagai M, Vo NH, Ogawa LS, Chimmanamada D, Inoue T, Chu J, Beaudette-Zlatanova BC, Lu R, Blackman RK, Barsoum J. (2012) The oncology drug

elesclomol selectively transports copper to the mitochondria to induce oxidative stress in cancer cells. *Free Radical Biology and Medicine,* 52(10): 2142-2150. doi: 10.1016/j.freeradbiomed.2012.03.017.

128) Blackman RK, Cheung-Ong K, Gebbia M, Proia DA, He S, Kepros J, Nislow C. (2012). Mitochondrial electron transport is the cellular target of the oncology drug elesclomol. *PloS One, 7*(1), e29798. doi:10.1371/journal.pone.0029798

129) Tsvetkov P, Detappe A, Cai K., Keys HR, Brune Z, Ying W, Thir P, Reidy M, Kugener G, Rossen J, Kocak M, Kory N, Tsherniak A, Santagata S, Whitesell L, Ghobrial IM, Markley JL, Lindquist S, Golub TR. (2019). Mitochondrial metabolism promotes adaptation to proteotoxic stress. *Nature. Chemical Biology.* 15(7):681-689. doi: 10.1038/s41589-019-0291-9

130) Soma S, Latimer AJ, Chun H, Vicary AC, Timbalia SA, Boulet A, Gohil VM. (2018). Elesclomol restores mitochondrial function in genetic models of copper deficiency. *Proceedings of the National Academy of Sciences of the United States of America, 115*(32), 8161–8166. doi:10.1073/pnas.1806296115

# Chapter 2

# Proposal and Preliminary Data

# 2. PROPOSAL & PRELIMINARY DATA

The proposal aims and preliminary data served as an outline and guide prior to conducting experimentation reported in Chapter 3.

## 2.1. AIMS

Preclinical trial studies will be undertaken to assess the efficacy of elesclomol-based copper ionophore replacement therapy in the *mottled-brindled* (*mo-br)* murine model of Menkes disease (MD). The membrane transporter ATP7A is a P-type ATPase responsible for copper import to trans-Golgi vesicles for metalation of cuproenzymes of the secretory pathway as well as cellular copper efflux across polarized biological membrane structures such as the enterocyte lining, blood-brain barrier (BBB), and renal epithelium. Mutations severely reducing ATP7A function result in MD characterized by primary systemic copper deficiency and various cuproenzyme deficiencies secondary to copper depletion.

In the brain, dysfunction of the mitochondrial electron transport chain copper-utilizing enzyme cytochrome *c* oxidase (CcO) triggers severe neurodegeneration; ultimately resulting in death of Menkes patients around three years of age. No FDA-approved therapy exists for MD. Replacement of systemic copper by administration of parenteral copper histidine in human clinical trials shows poor response due to limited BBB penetrance and subsequent lack of brain CcO functional improvement. The discovery that the novel chemotherapeutic adjuvant drug, elesclomol (ES), selectively

releases copper in mitochondria and restores CcO function in yeast and zebrafish models of copper transport deficiency presents a unique opportunity for the repurposing of ES for the treatment of MD.

We propose the preclinical trial efficacy assessment of elesclomol and its copper complex in the *mo-br* C57BL/J mouse. Our preclinical trial will evaluate intervention and efficacy at three levels:

### 2.1.1. Specific Aim 1: To evaluate tolerability and pharmacokinetics

ES exhibits very low intrinsic aqueous solubility and poor oral bioavailability. We will investigate various pharmacological solubilizing systems for use as vehicles for ES delivery via the subcutaneous and intravenous route. Once a suitable vehicle is determined, we will conduct tolerability and pharmacokinetic studies to deduce the therapeutic window and characterize the behavior of ES and its copper complex ($ES\text{-}Cu^{2+}$) within the C57BL/6 mouse. ADMET modeling of BBB partitioning indicates a 90% probability of ES penetrance. We intend to directly quantify brain exposure due to the essentiality of high brain penetrance by ES for our interventional model.

### 2.1.2. Specific Aim 2: Pilot Study and Interventional Optimization

Preliminary data generated using a suboptimal vehicle indicates $ES\text{-}Cu^{2+}$ complex improves survival of *mo-br* males. We intend to optimize formulation and dose in order to conduct a direct superiority trial using copper histidine with long-term survival as the

primary endpoint. Growth patterns and morphological changes, including whisker kinkiness and coat pigmentation, will be assessed as secondary endpoints monitored throughout the course of the trial.

### 2.1.3. Specific Aim 3: To evaluate biomarkers of intervention

Functional, histological, and biochemical markers of brain status will be employed to characterize the effects of ES and ES-$Cu^{2+}$ intervention in *mo-br* brains. Neuromotor and behavioral testing at ten weeks of age will include performance on rotarod, open field, grip strength, and gait treadmill. Histological and biochemical evaluation of tissue samples collected at two and ten weeks of age will provide direct evidence of neurological structure preservation.

Specifically, we will assess the degree of neuronal loss in the cortex and hippocampal formation as well as the preservation of the Purkinje neuron layer of the cerebellum—all of which are susceptible to copper depletion-induced degeneration. In support of our hypothesis that ES-$Cu^{2+}$ halts progressive neurological injury by increasing brain tissue copper and CcO, these biomarkers of brain copper status will be directly measured.

Additional copper biochemical markers, including brain Cu/Zn superoxide dismutase, brain dopamine-β-hydroxylase, serum copper, ceruloplasmin, renal copper, renal metallothionein, and lung lysyl oxidase will be analyzed to better understand copper

distribution and effect on cuproenzymes in various organs affected by primary copper deficiency.

Our studies will provide the basis for development of elesclomol as an investigational agent for the treatment of MD as well as other inherited copper deficiency disorders.

## 2.2. Approach

A preclinical research program will be undertaken to determine the efficacy of ES-based copper supplementation therapy in the *mottled-brindled* mouse model of classical Menkes disease. Based off formulation and pharmacotoxicological data generated by AIM 1, an interventional therapy will be developed utilizing the ES-$Cu^{2+}$ complex in a direct superiority preclinical trial with the current lead investigational agent, copper histidine, in AIM 2. Characterization of behavioral, gross anatomical, histological, and biochemical effects for the four treatment arms vehicle, ES, ES-$Cu^{2+}$ and copper histidine will then be evaluated in AIM 3. All animal work will be conducted in accordance with the *Guide for the Care and Use of Laboratory Animals: 8$^{th}$ Edition.* Animal use protocols #2017-0380 and #2018-0069 were submitted for review and approved by the Texas A&M University System Institutional Animal Care and Use Committee prior to commencement of experimentation.

### *2.2.1.* Approach to AIM 1

Following synthesis of required reagents, we optimized the vehicle, determined tolerability, and characterized pharmacokinetics of ES-$Cu^{2+}$ in C57BL/6 mice in preparation for Aim 2 superiority preclinical trial and Aim 3 evaluation of brain CcO functional, histological, and biochemical parameters.

#### *2.2.1.1.* Synthesis of Materials

Research grade ES (98.6% QC) was purchased from Accel Pharmtech per a custom synthesis agreement. The copper complex of ES was synthesized as described by Yadav et al. Briefly, to a stirred solution of 0.5 mmol ES in ethanol, excess $CuCl_2 \cdot 2H_2O$ was added and incubated at room temperature for one hour to allow complete 1:1 stoichiometric complexation. Crude solid was precipitated by the addition of water and collected by filtration. The solid was dissolved in methylene chloride and filtered. The methylene chloride solution was further washed with two equivalents of water, dried with $Na_2SO_4$, and a solid recovered following solvent removal in a rotary evaporator. Solid was further purified by two rounds of crystallization from acetonitrile followed by a final, 48-hour lyophilization yielding a fine, dark reddish-brown powder. Powder was stored at 4°C for pharmacological formulations. 2 g of ES-$Cu^{2+}$ was synthesized by this method.

The copper complex of histidine was synthesized as described by Gala et al. Briefly, to a stirred solution of 0.2 mmol pharmaceutical grade L-histidine in 100 mM HEPES buffer pH 7.4, $CuCl_2 \cdot 2H_2O$ (17.05 mg) was added and incubated at room temperature for three hours to allow complete 2:1 stoichiometric complexation. The resulting dark blue solution was filtered to remove particulates and stored at 4°C for use as a 50 mM copper histidine stock solution for pharmacological formulations.

#### *2.2.1.2.* Quantification of ES and ES-$Cu^{2+}$ in Analytical Samples

In collaboration with the Integrated Metabolomics Analysis Core (IMAC) at Texas A&M, we developed a high sensitivity LC-MS protocol for detection of ES and ES-$Cu^{2+}$ via negative and positive mode electrospray ionization (ESI) on a triple quadrupole mass spectrometer (Quantiva, Thermo Scientific, Waltham, MA) coupled with a binary pump HPLC (UltiMate 3000, Thermo Scientific). See Table 2-1.

MS parameters were optimized for the target compound under direct infusion to identify the SRM transitions (precursor/product fragment ion pairs) which are listed in Table 2. Chromatographic separation was achieved on a Hypersil Gold 5 µm 50 x 3 mm column (Thermo Scientific) using a solvent gradient method. Sample acquisition and analysis were performed with TraceFinder 3.3 (Thermo Scientific). Lower limit and upper limit of detection for our protocol was 0.78 to 1,000 $ng \cdot mL^{-1}$.

**Table 2-1: Retention Time and MS Parameters of Analysis**

| Compound | Retention Time (min.) | Polarity | Precursor (m/z) | Product (m/z) | Collision Energy (V) |
|---|---|---|---|---|---|
| Fluconazole | 1.5 | Positive | 307.1 | 169.1 | 23.7 |
| | | Positive | 307.1 | 220.1 | 19.0 |
| | | Positive | 307.1 | 238.1 | 16.7 |
| Elesclomol | 2.1 | Negative | 399.0 | 150.0 | 27.5 |
| | | Negative | 399.0 | 165.0 | 24.3 |
| | | Negative | 399.0 | 173.1 | 23.4 |
| ES-$Cu^{2+}$ | 2.5 | Positive | 464.0 | 175.0 | 27.7 |
| | | Positive | 464.0 | 201.0 | 26.6 |
| | | Positive | 464.0 | 430.0 | 16.5 |

#### *2.2.1.3.* Optimization of Formulation

Pilot survival trials utilizing Solutol® HS 15 (polyethylene glycol (15)-hydroxystearate anionic emulsifier) produced unstable solutions with subcutaneous injection site reactions including inflammation and ulceration. We hypothesized that optimization of the solubilizing system could increase bioavailability and reduce adverse reactions attributed to vehicle toxicity and localized suboptimal distribution of ES-$Cu^{2+}$.

Phase solubility assays were conducted to determine the suitability of vehicles for ES and ES-$Cu^{2+}$ complex in Methocel™ A15-LV (carboxyl methylcellulose) and Captisol® (sulfobutylether-β-cyclodextrin) per technical materials. Data collected indicates both systems solubilize ES at > 1.0 mg·$mL^{-1}$. ES-$Cu^{2+}$ exhibits reduced solubility in all tested aqueous media. The Captisol® system proved superior to anionic emulsifiers and CMC and was selected for pharmacotoxicological and preclinical trial studies. 20% Captisol®

possesses an excellent safety profile and achieves a maximum ES-$Cu^{2+}$ concentration of 0.88 mg·$mL^{-1}$ at pH 7.4. See Figure 2-1.

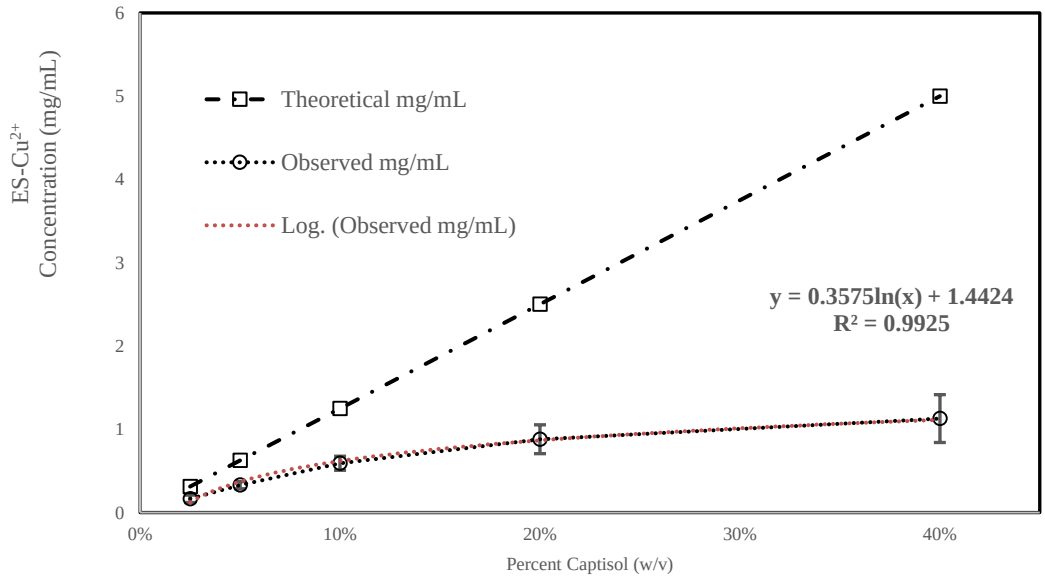


**Figure 2-1: Phase Solubility of ES-$Cu^{2+}$ in Captisol Aqueous Vehicle**

Theoretical concentrations of 5, 2.5, 1.25, 0.625, and 0.3125 mg·$mL^{-1}$ were solvated in 40%, 20%, 10%, 5%, and 2.5% Captisol® (pH 7.4 adjusted) and compared to actual concentrations quantified via LC-MS. A logarithmic regression modeling the maximum stable concentration is listed. Captisol® is isotonic at 24%. Based on this data, a preparation of 20% was selected.

#### *2.2.1.4.* Tolerability

In preliminary toxicity studies, ES-$Cu^{2+}$ is well tolerated as a single bolus dose of 7.25 mg·$kg^{-1}$ in adult mice. Dose escalation starting at 3.625 mg·$kg^{-1}$ indicates significant acute toxicity at doses exceeding 10.875 mg/kg. (3-fold planned individual dose level). Adverse events included grimacing, abnormal behavior, lethargy, and mortality ($n$ = 5,

40%). Single subcutaneous doses of 3.625 and 7.25 mg·kg$^{-1}$ are well tolerated with no significant weight loss observed at five and ten days post administration. See Table 2-2. No injection site reaction was observed using Captisol®.

**Table 2-2: Acute Tolerability of ES-Cu$^{2}$ in Adult C57BL/6 Mice**

| Single SubQ Bolus | | Body Mass (Mean ± SD, ANOVA post hoc Dunnett's 2-Sided Test) | | | | | | | |
|---|---|---|---|---|---|---|---|---|---|
| | | Day 0 | | Day 5 | | | Day 10 | | |
| Dose Level | *n* | Mass | p-value | Mass | % Δ | p-value | Mass | % Δ | p-value |
| Control Vehicle | 4 | 20.6 ± 1.8 | - | 21.2 ± 1.8 | 2.7% | - | 21.7 ± 1.7 | 5.5% | - |
| 3.625 mg·kg$^{-1}$ ES-Cu$^{2+}$ | 5 | 19.8 ± 1.2 | 0.56 | 20.1 ± 1.4 | 1.3% | 0.41 | 20.6± 1.7 | 4.2% | 0.48 |
| 7.25 mg·kg$^{-1}$ ES-Cu$^{2+}$ | 5 | 20.1 ± 1.0 | 0.80 | 19.6 ± 1.0 | -2.8% | 0.19 | 20.1 ± 1.2 | -0.3% | 0.22 |

We propose a 2-fold therapeutic window of safety using 3.625 mg·kg$^{-1}$ per dose equivalent to 0.5 mg·kg$^{-1}$ $Cu^{2+}$ exposure. Acute exposure exceeding 1.0 mg·kg$^{-1}$ $Cu^{2+}$ (7.25 mg·kg$^{-1}$ ES-$Cu^{2+}$) induces signs of acute toxicosis which is considerably lower than the expected 15.5 mg·kg$^{-1}$ $LD_{50}$ in a similar *ATP7A* variant, the *macular* mouse. The $LD_{50}$ of ES is 40 mg·kg$^{-1}$ —indicating toxic synergy of ES/$Cu^{2+}$ co-administration.

Future experiments will include tolerability assessment in wildtype pups focusing on perturbation of normal growth pattern, serum chemistries, necropsy, and histopathology of liver, kidney, heart, etc., run as parallel cohort using the final devised intervention protocol followed in Aim 2.

#### *2.2.1.5.* **Pharmacokinetics**

Concentration versus time plots of ES-$Cu^{2+}$ administered as a single bolus dose by intravenous (3.625 mg·$kg^{-1}$), subcutaneous (7.25 mg·$kg^{-1}$), or oral (10.875 mg·$kg^{-1}$) routes were generated by serial blood sampling followed by LC-Ms quantification with each time point representing a biological triplicate.

Non-compartmental and compartmental analysis was conducted using PKSolver software as described in Zhang et al. Intravenous and subcutaneous PK models and parameters were generated using type 2a 2-compartment model of nonlinear kinetics. See Figure 5. Oral route was not modeled due to poor systemic exposure. Bioavailability ($F_{abs}$) of subcutaneous ES-$Cu^{2+}$ exceeded 66% compared to less than 3% for oral route. Subcutaneous ES-$Cu^{2+}$ exhibits extensive tissue partitioning with a $t_{1/2}\,\beta$ of 18.8 hr, $C_{max}$ of 197.6 ng·$mL^{-1}$, and $AUC_{0\rightarrow\infty}$ 479.6 ng·$mL^{-1}$·$hr^{-1}$. See Figure 2-2.

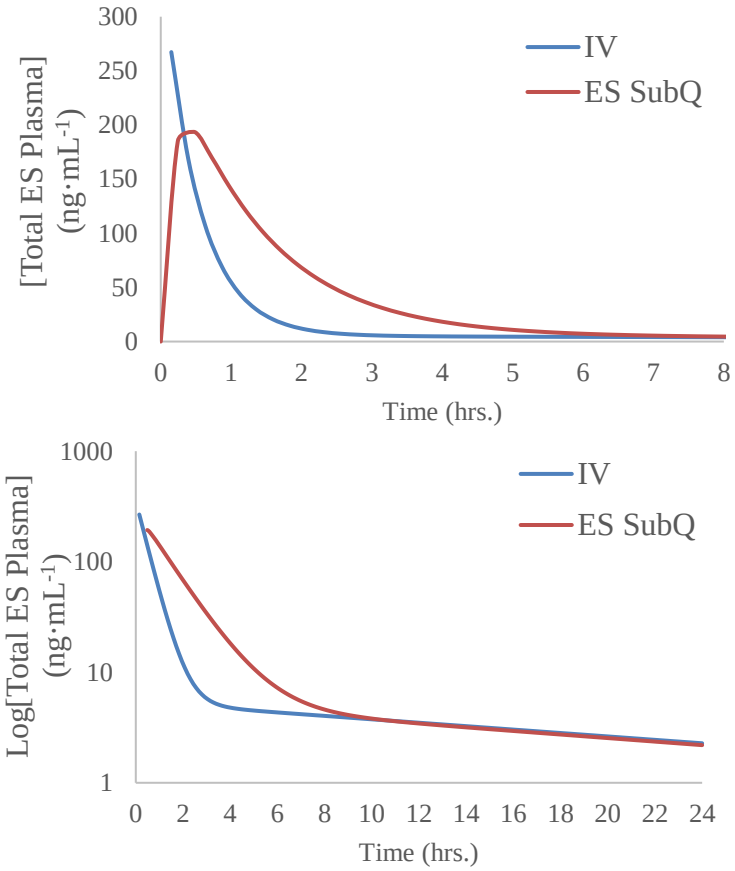


| SubQ PK ES-$Cu^{2+}$ | | |
|---|---|---|
| **Parameter** | **Unit** | **Value** |
| A | ng/ml | 291.77 |
| Alpha | 1/h | 0.76 |
| B | ng/ml | 5.30 |
| Beta | 1/h | 0.04 |
| ka | 1/h | 6.42 |
| k10 | 1/h | 0.55 |
| k12 | 1/h | 0.20 |
| k21 | 1/h | 0.05 |
| t1/2Alpha | h | 0.91 |
| t1/2Beta | h | 18.82 |
| t1/2ka | h | 0.11 |
| V/F | (µg)/(ng/ml) | 0.60 |
| CL/F | (µg)/(ng/ml)/h | 0.33 |
| V2/F | (µg)/(ng/ml) | 2.37 |
| CL2/F | (µg)/(ng/ml)/h | 0.12 |
| Tmax | h | 0.38 |
| Cmax | ng/ml | 197.59 |
| AUC 0-t | ng/ml*h | 420.14 |
| AUC 0-inf | ng/ml*h | 479.63 |
| AUMC | ng/ml*h^2 | 4402.63 |
| MRT | h | 9.18 |

**Figure 2-2: Subcutaneous PK Nonlinear 2-Compartment Models and Parameters**

Plasma concentration vs. time plots indicated nonlinear PK due to extensive tissue partitioning. After initial high $C_{max}$ of 197.6 ng·$mL^{-1}$, ES-$Cu^{2+}$ exhibits rapid tissue distribution. ES is rapidly eliminated from α (vascular) compartment $t_{1/2}$ α 55 min but lingers in β (tissue) compartment $t_{1/2}$ β 18.8 hrs.

### *2.2.1.6.* Brain ES Exposure

High brain exposure of ES represents a central tenant of our hypothesized mechanism of neurological rescue. In order for ES-mediated copper release to neuronal mitochondria for CcO metalation, the ES-$Cu^{2+}$ complex must first penetrate the endothelium of the BBB and enter brain parenchyma.

PK experiments indicate ES partitions to a secondary body compartment. Based off logP (2.81) and high lipophilicity, the ES-$Cu^{2+}$ complex most likely achieves highest levels in fatty tissues such as the brain.

To definitively determine ES brain penetrance, cohorts of juvenile C57BL/6 wildtype mice were dosed with 7.25 $mg \cdot kg^{-1}$ drug in a small pilot study. Mice were euthanized between 30-60 min post treatment, perfused with saline to flush the brain of blood, and brains harvested for quantification of tissue ES/ES-$Cu^{2+}$ concentrations.

Our preliminary data indicates ES achieves high brain concentration following a single subcutaneous bolus dose at a single time point corresponding to the plasma $C_{max}$. Further studies will be conducted to fully characterize brain-ES exposure by examining drug levels in key neurological structures. We will also assess BBB penetrance in adults of varying age as we optimize booster doses in older rescued *mo-br* mice.

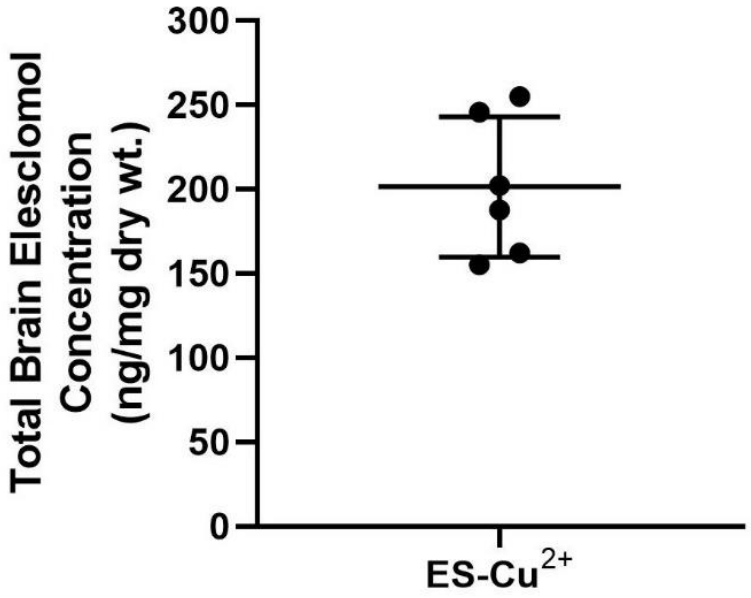


**Figure 2-3: Quantification of ES/ES-$Cu^{2+}$ in Brain Tissue.**

Brains of postnatal day 7 pups ($n$ = 6) were harvested approximately 1 hr after subcutaneous administration of drug. Total ES brain concentration from mechanically pulverized and extracted tissue was quantified by LC-MS. Mean tissue concentration of 201.3 ± 41.7 $ng \cdot mg^{-1}$ was detected—indicating BBB penetrance.

### *2.2.2.* Approach to AIM 2

The *mo-br* mouse is an allelic *Atp7A* variant that models classical Menkes disease due. Affected *mo-br* males present with pigmentation defects, growth retardation, neurodegeneration, connective tissue abnormalities, and death around two weeks of age. Hemizygous males, contrary to some reports, are not rescued by parenteral copper supplementation. We have established a breeding colony of approximately 30 carrier female-wildtype male monogamous pairs as well as an interventional cohort in preparation for *in vivo* studies. See Figure 2-4.

**Figure 2-4: Wildtype and *mo-br* Males at Postnatal Day 5.**

Identification of affected pups due to pigmentation defect allows for easy phenotyping. *Mo-br* mice show small size, tremors, and die around 14 days of age.

#### *2.2.2.1.* Pilot Study

We conducted a small pilot survival study using a suboptimal vehicle, dose, and intervention schedule. The initial results indicate that treatment with ES-$Cu^{2+}$ but not ES results in improved median survival of *mo-br* mice. ES-$Cu^{2+}$ intervention improves growth, pigmentation, and whisker morphology. Other than observation, no other assessment took place. Data from this preliminary study are presented in Figure 2-5.

Median survival is as follows: vehicle – 15 days, ES – 17 days, copper histidine – 19.5 days, and ES-$Cu^{2+}$ – 21 days (log-rank $p = 0.0004$). Pups were dosed with 20% Solutol® formulations on PND 5, 8, 11, 14, 17 and 20 with a total copper dose of 20 µg (2.5 µg of copper per ES-$Cu^{2+}$ or copper histidine subcutaneous injection).

ES-$Cu^{2+}$ appears to have a modest effect however two mice designated ‘Ravi’ and ‘Major’ exhibited > 70 day survival and improved body weight. Poor formulation and/or toxicity at the injection site resulted in severe skin ulceration in the ES-$Cu^{2+}$ cohort. We hypothesize that refinement of formulation, dose, and frequency will mitigate this adverse effect and improve survival.

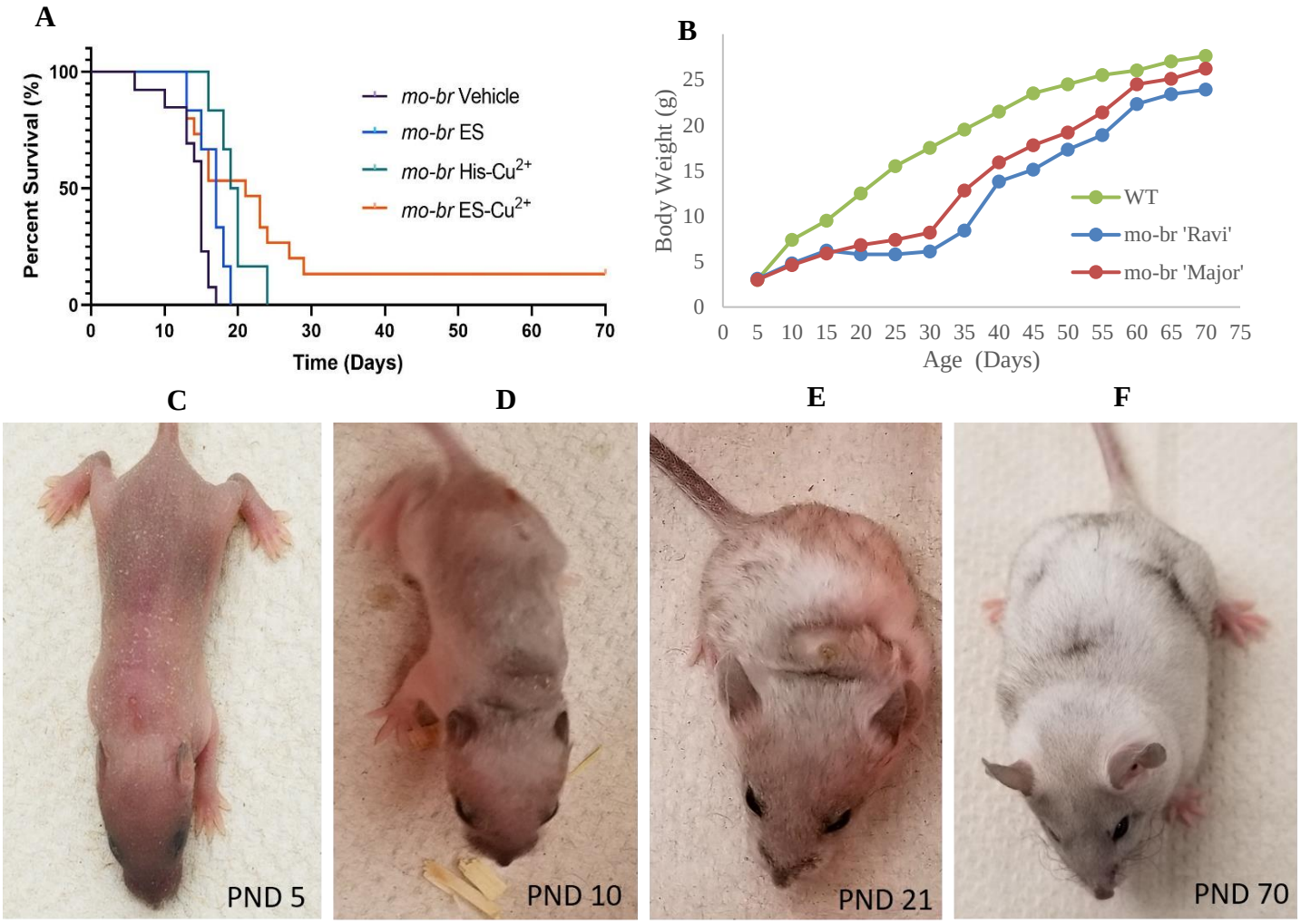


**Figure 2-5: Survival of *mo-br* Males in Intervention Pilot Study**

*Mo-br* males were dosed with vehicle (n =13), ES (6), copper histidine (6), or ES-$Cu^{2+}$ (16). Both copper histidine and ES-$Cu^{2+}$ exhibited minor survival benefit. A) Two mice (12.5%) of the ES-$Cu^{2+}$ cohort survived in excess of 70 days. B) Growth of subjects 'Major' and 'Ravi' approached near wildtype levels near week 10 (70 Days). C-F) Images of subject 'Major' PND 5, 10, 21, and 70. Subject 'Ravi' lived a total of 134 days while 'Major' survived 183 days. Poor survival of the ES-$Cu^{2+}$ cohort could be linked to severe injection site reaction caused by poor vehicle drug distribution in the subcutaneous tissue. Ulceration and necrosis occurred in all ES-$Cu^{2+}$ mice (See Image E). Lesions persisted in subjects 'Ravi' and 'Major' until 7-8 weeks of age.

#### *2.2.2.2.* Optimization of ES-$Cu^{2+}$ Intervention

We have successfully optimized a stable vehicle, adjusted the copper dose within a safe therapeutic window, and simplified an intervention regime as outlined in Aim 1. A healthy pup weighing approximately 4 g possesses around 1 $\mu g \cdot g^{-1}$ of total body copper (4 µg). Our interventional goal is to administer 2 µg of copper coordinated with either ES or histidine on PND 7 and 10 equaling a 4 µg supplementation. See Table 2-3.

**Table 2-3: Optimized Treatment Protocol**

| Treatments (Divide as 2 SubQ Doses PND 7 & 10) | | | | |
|---|---|---|---|---|
| **Cohort** | **Exposure (mg/kg)** | **Total (µg)** | **ES/HIS (µg)** | **$Cu^{2+}$ (µg)** |
| **WT Vehicle** | - | - | - | - |
| **WT ES-$Cu^{2+}$** | 7.25 | 29 | 25.02 | 3.98 |
| ***mo-br* Vehicle** | - | - | - | - |
| ***mo-br* ES** | 6.25 | 25.02 | 25.02 | 3.98 |
| ***mo-br* ES-$Cu^{2+}$** | 7.25 | 29 | 25.02 | 3.98 |
| ***mo-br* His-$Cu^{2+}$** | 5.83 | 23.3 | 19.35 | 3.98 |

#### *2.2.2.3.* Survival Analysis

Mice will be monitored daily beginning on PND 5 until 50% mortality in each *mo-br* cohort is observed in order to calculate median survival. Kaplan-Meier survival analysis with log-rank nonparametric statistical analysis will be employed to deduce the significance of differential survival.

#### *2.2.2.4.* Growth Curves

Growth of cohorts will be tracked daily from PND 5 to PND 70. Improved tissue copper levels should improve body weight in *mo-br* cohorts while toxic effects may manifest as growth delay in treated wild-type male littermates. A subset of adult males will be set aside for longer evaluation and observation depending upon success of initial intervention.

#### *2.2.2.5.* Morphological Features

Our current therapeutic mechanism is not anticipated to significantly improve Golgi copper levels based on known copper transport biology and molecular target location of the ES-$Cu^{2+}$ complex. Changes in pigmentation and whisker characteristics indicate improved tyrosinase and keratin sulfhydralase activity. Based on pilot study observations, some secretory pathway enzymes may also benefit from ES-$Cu^{2+}$ mediated copper redistribution due to leakage from mitochondria. Qualitative observations will be documented as well as follow up *in vitro* experimentation with *ATP7AΔ* B19 melanoma cells. See Figure 2-5 C-F.

### *2.2.3.* Approach to AIM 3

We hypothesize that increased brain tissue and mitochondrial copper levels by ES-mediated escort will improve neurological outcomes in the context of ATP7A primary copper deficiency. Brain ES levels following acute exposure approach levels seen in plasma (Aim 1.6) indicating penetrance and presumed increased $Cu^{2+}$ levels. The next step is to assess the outcomes of increased tissue copper levels in rescued *mo-br* males. Our approach will focus on function, gross anatomical, histological, and biochemical markers of brain status.

#### *2.2.3.1.* Functional Assessment of Brain

Mice at 10 weeks of age will be transferred to the Texas A&M Rodent Preclinical Trial Phenotyping Core for neuromotor evaluation on accelerating rotarod, grip strength apparatus, open field, and gait treadmill. Gross cortical motor, muscle strength, and cerebellar activity will provide a global assessment of brain status in surviving adult *mo-br* males—indicating preservation of neurological function.

#### *2.2.3.2.* Necropsy and Histopathology of Key Brain Structures

Mice at 2 and 10 weeks of age will be sacrificed and necropsied. Multiple organ abnormalities, including reduced brain mass, hypertrophic hearts, and renal fibrosis are well noted in the *mo-br* mouse. Weight and gross appearance of brain, heart, lungs, thymus, liver, spleen, and kidney will be measured and set aside for histological and biochemical analysis.

In the brain, untreated *mo-br* males demonstrate marked degeneration in cortical, hippocampal, and cerebellar neurons. Quantification of necrotic neurons in cortex and hippocampus regions CA1-3 as well as continuity of the Purkinje neuron layer of the cerebellar peduncles will be used in addition to qualitative assessment by a blinded pathologist at the Texas Veterinary Medicine Diagnostic Lab (TVMDL). Digital slide sets and paraffin blocks will be retained for additional sectioning or special staining for future study comparisons.

#### *2.2.3.3.* Biochemical Markers

We will directly quantify brain tissue copper concentration by ICP-MS as described in Aim 1.6 at 2 and 10 weeks. We consider CcO subunit COX1 levels as the definitive biochemical marker of ES-$Cu^{2+}$ therapeutic success in the brain. Improved energy generation in the brain halts neurological injury. We will also quantify levels of two additional cuproenzymes implicated in neurological injury—SOD1 and DBH. Other biomarkers we intend to analyze include serum, heart, kidney, and liver total copper levels, serum ceruloplasmin activity, metallothionein expression level in kidney/liver, and LOX activity in the lungs.

## 2.3. Use of Vertebrate Animals

Justification: Preclinical trial efficacy assessment of a potential human therapeutic for an infantile fatal disorder of copper metabolism. The potential benefit to society outweighs the harm caused to experimental animals. All efforts will be made to reduce suffering and distress of experimental animals.

Use of Animals: All animal work is approved under Animal Use Protocols #2017-0380 and #2018-0069 after review by the Texas A&M University Institutional Animal Care and Use Committee (IACUC). All mice used are sourced from our in-house *mottled-brindled* C57BL/6 in-house breeding program. Live mice will be used as described in Aim 1.4—1.6, Aim 2, and Aim 3.1.

**1)** Aim 1.4—1.6 PK and Tolerability: Adult female mice between 8-12 weeks of age.

**2)** Aim 2 Survival Preclinical Trial: Juvenile male mice beginning postnatal day 5.

**3)** Aim 3.1: Adult male mice of 10—12 weeks of age.

Breeding Program: The *mottled-brindled* colony is maintained by crossing heterozygous carrier females with wildtype C57BL/6 males. Females exhibit reduced fertility and litter size due to their chimeric pattern of random X-inactivation. We estimate each litter will on average produce one *mo-br* affected hemizygous male. All outlined experimentation calls for approximately 150 *mo-br* hemizygous affected males.

For experimental purposes, we will set up 30 breeding pairs requiring five rounds of breeding to yield needed *mo-br* animals. We anticipate each pair to produce 1 *mo-br* affected male every 90 days. Carrier females possess an optimal fertility period of only six months. Breeders are rotated every six months. A maximum of 120 animals will be used for breeding purposes for the outlined experiments. All wild-type animal use will be sourced from littermates in order to reduce animal waste.

Husbandry: Mice are housed in an OptiMice® animal care system with 14/10 hour light-dark cycle in a noise mitigated vivarium. Cage and nutritional enrichment in the form of nestlets, shepherd huts, and Love Mash® (Bio-Serv) reproductive supplement was provided in addition to Teklad 4% fat standard diet (Envigo) and water ad libitum. Cages are changed weekly by Sacchettini Lab staff, and veterinary care provided by Texas A&M Comparative Medicine Program.

Anesthesia: Adult mice are anesthetized using isoflurane before injections and survival bleeds. Animals in acute distress or moribund state are promptly euthanized by $CO_2$ asphyxiation or isoflurane overdose.

Euthanasia**:** Mice are euthanized by $CO_2$ asphyxiation or isoflurane overdose confirmed by either cervical dislocation or bilateral thoracotomy for terminal procedures or conclusion of study.

## 2.4. Vertebrate Animal General Methods

We request a total of 405 mice for vertebrate animal protocols as outlined in Aims 1-3. An accounting of animal utilization, including breeding and colony maintenance is as follows. All animal census and utilization number have been approved under AUP protocols previously listed.

Tolerability and Pharmacokinetics (PK) Aim 1 Studies:

i. Tolerability: Five level dose-escalation study at 0, 3.625, 7.25, 10.875, 14.5, and 18.125 $mg \cdot kg^{-1}$ per day ES-$Cu^{2+}$ will involve subcutaneous injection followed by clinical observation of acute signs of toxicity. Percent weight change per cohort on days 0, 5, and 10 are used to assess tolerability of each dose level. A maximum of 30 adult female mice will be used in this study.

ii. PK: Drug will be given by the intravenous, subcutaneous, and oral route at 3.625, 7.25, and 10.875 $mg \cdot kg^{-1}$ respectively. Each adult female mouse will be have one survival (< 200 µL) and one terminal bleed via isoflurane sedated facial vein or post $CO_2$ euthanized cardiocentesis. Serial bleed times include 0, 5 min, 15 min, 30 min, 1 hr, 2 hr, 4 hr, 8 hr, and 24 hr. Each time point represents a biological triplicate. A maximum of 45 adult female mice will be used in this study.

iii. Brain Penetrance: Drug will be given by subcutaneous injection to 10 postnatal day 7 male pups followed by euthanasia by isoflurane overdose and bilateral thoracotomy. Corpse is exsanguinated, perfused with normal saline, and brain harvested for ES quantification.

Survival Studies Aim 2:

*Mo-br* mice will be administered 2 μg copper (0.5 $mg \cdot kg^{-1}$) as either ES-$Cu^{2+}$ or copper histidine on postnatal days 7 and 10. ES and vehicle will serve as controls. WT male pups will be dosed with vehicle or ES-$Cu^{2+}$ in order to conduct parallel juvenile toxicity studies thus minimizing animal waste. Survival and body weight will be logged beginning postnatal day 5 until death or censure from the study. Cohort size is as follows assuming 50% survival at 70 days (Power – 0.95):

- WT Vehicle n = 15 (Toxicity Study)
- WT ES-$Cu^{2+}$ n = 15 (Toxicity Study)
- *mo-br* Vehicle n = 15
- *mo-br* ES n = 25
- *mo-br* ES-$Cu^{2+}$ n = 25
- *mo-br* His-$Cu^{2+}$ n = 25

A maximum of 120 juvenile mice will be used for this these outlined studies.

Markers of Intervention Therapies Aim 3:

Functional Neuromotor Studies: Behavioral studies will include accelerating rotarod, quantitative forelimb grip strength, open field performance, and gait treadmill. Mice will be sourced from survival studies outlined in Aim 2 General Methodology at 10 weeks of age following censure from survival preclinical trial. We anticipate only WT cohorts and *mo-br* ES-$Cu^{2+}$ cohort will be alive for assessment.

Necropsy and Tissue Harvest: Following completion of function tests, 10-12 week old mice will be euthanized and tissues collected for histology or biochemical analysis. 2 week histology and biochemical samples will be collected from newly treated pups as follows:

- WT n = 5 (Histology) n = 15 (Biochemical Markers) – 20 Total
- *mo-br* Vehicle n = 5 (Histology) n = 15 (Biochemical Markers) – 20 Total
- *mo-br* ES-$Cu^{2+}$ n = 5 (Histology) n = 15 (Biochemical Markers) – 20 Total
- *mo-br* His-$Cu^{2+}$ n = 5 (Histology) n = 15 (Biochemical Markers) – 20 Total

A maximum of 80 juvenile mice will be used for these outlined experiments.

# Chapter 3

## *Science* Publication

## 3. *SCIENCE* PUBLICATION

The following main text, results, and discussion are based on the publication as reported in Guthrie et al., Elesclomol alleviates Menkes pathology and mortality by escorting Cu to cuproenzymes in mice. *Science.* 2020 May 8; 368(6491): 620-625. doi: 10.1126/science.aaz8899.

Publication data and supplementary materials represent Aims 1-3 of the research proposal in addition to experimentation proposed by peer reviewers. Liam M. Guthrie was the primary author of this manuscript and conducted the majority of reported experimentation with detailed contributions located on pages 178-179.

### 3.1. Abstract

Loss of function mutations in the copper transporter *ATP7A* causes Menkes disease. Menkes is an infantile fatal hereditary copper deficiency disorder characterized by progressive neurological injury culminating in death typically by three years of age. Severe copper deficiency leads to multiple pathologies including impaired energy generation caused by cytochrome *c* oxidase dysfunction in the mitochondria. Here we report that the small molecule, elesclomol, escorted copper to mitochondria and increased cytochrome *c* oxidase levels in the brain. Through this mechanism, elesclomol prevented detrimental neurodegenerative changes and improved survival of the *mottled-brindled* mouse; a murine model of severe Menkes disease. Thus, elesclomol holds promise for the treatment of Menkes and associated disorders of hereditary copper deficiency.

### 3.2. Main Text

Copper (Cu) is an essential micronutrient required for numerous critical enzymes including cytochrome *c* oxidase (CcO) of the ATP-generating electron transport pathway found in mitochondria *(1).* Paradoxically, Cu possesses inherent toxicity, in part because of its ability to generate hydroxyl radicals in biological systems *(2).* Organisms have evolved highly complex systems of metallochaperones and transporters to safely distribute Cu *(3, 4).* Mutations impairing the function of any component of Cu transport can impact numerous cellular processes affecting systems as diverse as energy production *(5, 6),* catecholamine biosynthesis, and connective tissue maturation—resulting in debilitating, often fatal human diseases *(7).*

The coordinated efforts of the two major Cu membrane transporters, CTR1 and ATP7A, regulate intracellular Cu levels and directional transport across polarized epithelial layers such as the intestinal enterocyte lining *(8)* and choroid plexus *(9)*. CTR1 affects initial Cu entry while ATP7A facilitates Cu egress from cells.

Mutations in the Cu transporting ATPase, *ATP7A*, results in Menkes disease - a fatal X-linked infantile condition with no FDA-approved treatment *(10)*. Clinical presentations of Menkes include abnormal catecholamine ratios, characteristic kinky hair, hypopigmentation, connective tissue defects, and severe neurodegeneration *(11)*. In the brain, this Cu deficit causes secondary CcO dysfunction leading to progressive neurological injury and death *(12-14).*

Efforts to restore normal Cu levels and enzyme function by means of parenteral Cu supplementation using hydrophilic complexes, such as copper histidine, do not ameliorate severe neurological pathology in Menkes patients because of poor penetrance and low restoration of neuronal CcO function in the brain *(15, 16)*.

We previously reported that elesclomol (ES), a small highly lipophilic $Cu^{2+}$-binding molecule, restores mitochondrial function in the context of defective Cu transport in yeast and mammalian cell lines *(16)*. A membrane traversing drug like ES, capable of Cu delivery to key cuproenzymes, such as CcO in brain mitochondria, could alleviate the neurodegenerative aspects of Menkes disease. This would be similar to hinokitiol, a lipophilic carrier that restores iron levels in the context of defective membrane transport both in vitro and in vivo *(17, 18)*.

### 3.3. ES Restores Mitochondrial Function in *Ctr1* Knockout H9c2 Cells and Mice

We measured oxygen consumption rate (OCR), an indication of electron transport activity, and ATP levels in the Cu importer *Ctr1* knockout (KO) H9c2 rat cardiomyocytes. *Ctr1* KO H9c2 cells exhibited significant reduction in basal OCR and ATP levels. Preincubation with 1 nM ES restored OCR to 103% (+34%) of WT (2.5 vs 3.7 $pM \cdot min^{-1} \cdot \mu g\ protein^{-1}$, $p < 0.001$) (Fig. 3-1A). Similarly, ES treatment increased ATP levels compared to the *Ctr1* KO vehicle (0.74 vs 1.01, $p < 0.001$) (Fig. 3-1B).

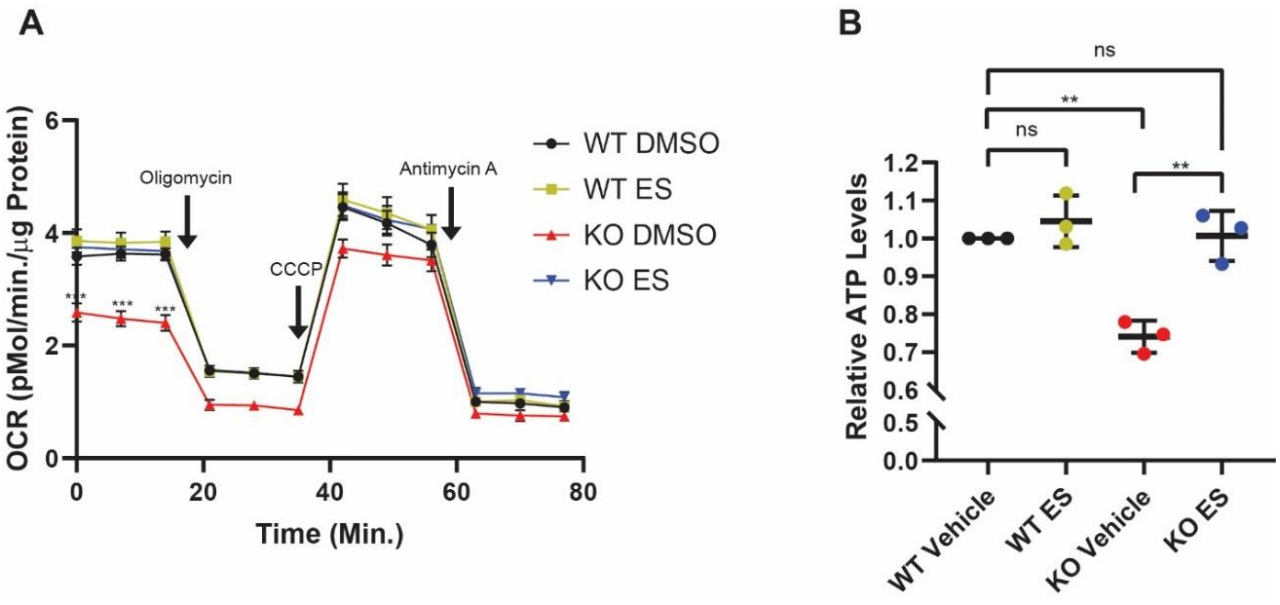


**Figure 3-1: Effects of ES treatment on OCR and relative ATP levels in *Ctr1* KO H9c2 cardiac cells.**

**A)** ES treatment restores mitochondrial respiration in *Ctr1* KO H9c2 cardiac cells ($n$ = 15, three biological replicates each with 5 technical replicates per cohort, *** $p < 0.01$). WT and *Ctr1* KO cells were cultured with and without 1 nM ES for 4 days prior to performing oxygen consumption rate (OCR) measurements. Oligomycin, CCCP, and antimycin A were used to measure ATP-coupled respiration, maximum respiratory capacity, and mitochondria—specific respiration, respectively. OCR data reported as mean ± SEM. **B)** WT and *Ctr1* KO H9c2 cells were cultured with and without 1 nM ES in galactose-containing media for 4 days before ATP measurements. ATP quantification data expressed as mean ± SD, (n=3). Statistical analysis reported as one-way ANOVA with post hoc Tukey's multiple comparisons test.

Loss of CTR1 results in severe cellular Cu deficiency in mice. *Ctr1*$^{-/-}$ mice demonstrate lethality in utero *(19).* The cardiac-specific *Ctr1* knockout (KO) mouse *(20),* exhibits growth retardation, severe hypertrophic cardiomyopathy due to cardiac muscle CcO dysfunction, and death around postnatal day (PND) 12. To assess the ability of ES to escort $Cu^{2+}$ through CTR1-deficient cardiac cellular membranes, we administered subcutaneous ES at 10 $mg \cdot kg^{-1}$.

WT mice tolerated ES injections well with favorable tolerability and pharmacokinetics (Table 3-1) (Fig. 3-2). Adult C57BL/6 mice given ES at 25 $mg \cdot kg^{-1}$ for five consecutive days via the subcutaneous route experienced no signs of acute toxicity or weight loss. ES formulated in 0.5% Methocel™ (w/v) aqueous vehicle performed well as a solvating system (Table 3-1). The pharmacokinetic profile of ES was determined by administering a 10 $mg \cdot kg^{-1}$ subcutaneous (SQ) dose to adult mice followed by serial blood sampling and quantification by LC-MS. We constructed a 1-compartment PK model using PKSolver and determined the total exposure ($AUC_{0-\infty}$) of subcutaneous ES was 300.5 $ng \cdot mL^{-1} \cdot hr^{-1}$ with a $C_{max}$ of 529.7 $ng \cdot mL^{-1}$ and $t_{1/2}$ of 3 min. (Fig 3-2C).

We observed a 100% 26 day survival rate in ES-treated mice whereas those receiving vehicle died between PND 8–12 (Fig. 3-3A, B). Growth of ES mice was restored to WT pattern with no significant deviation from either WT vehicle or WT ES-treated groups (Fig. 3-3A, C) (Fig. 3-4A).

ES mice demonstrated normalization of total body, heart, and spleen weights at PND 10 (Fig. 3-3D, E) (Fig. 3-4B-D). Cardiac histopathology at PND 10 of vehicle treated

KO mice showed pronounced hypertrophy characterized by increased cell area as compared to WT tissue samples (186 vs 87 μm2, $p < 0.01$) (Fig. 3-4F, G).

ES treatment ameliorated severe cardiac pathology with a partial reduction in hypertrophy (119 μm2, $p < 0.01$) (Fig. 3-4F, G). Cardiac [Cu] increased with ES treatment from a vehicle KO baseline of 34% to 55% (1.6 vs 2.6 μg·g-1, $p = 0.04$) (Fig. 3-3F). The 21% increase in cardiac [Cu] resulted in a 28% increase in COX1, the Cu-containing subunit of CcO *(1).* Zn/Cu superoxide dismutase (SOD1), a cuproenzyme highly resistant to depletion *(21),* remained unchanged (Fig. 3-5).

**Table 3-1: Elesclomol tolerability in adult C57BL/6 females.**

| SubQ Bolus | | Body Mass | | | | | | | |
|---|---|---|---|---|---|---|---|---|---|
| | | Day 0 | | Day 5 | | | Day 10 | | |
| Dose Level | *n* | Mass | p-value | Mass | % Δ | p-value | Mass | % Δ | p-value |
| Methocel™ Vehicle | 3 | 18.8 ± 0.7 | 0.39 | 19.5 ± 0.7 | 3.5% | 0.25 | 19.9 ± 0.7 | 5.9% | 0.56 |
| ES 25 mg·kg$^{-1}$ Methocel™ | 5 | 18.3 ± 0.9 | | 18.9 ± 0.6 | 3.3% | | 19.6 ± 0.7 | 7.3% | |
| Captisol® Vehicle | 4 | 18.4 ± 0.7 | 0.73 | 18.9 ± 0.6 | 2.9% | 0.53 | 19.7 ± 0.6 | 7.5% | 0.64 |
| ES 25 mg·kg$^{-1}$ Captisol® | 5 | 18.2 ± 0.8 | | 18.6 ± 0.8 | 2.2% | | 19.5 ± 0.5 | 7.6% | |

Data reported as mean ± SD with statistical significance assessed by one-way ANOVA with post hoc Tukey's HSD test or Welch one-way ANOVA with post hoc Tukey's HSD test.

A

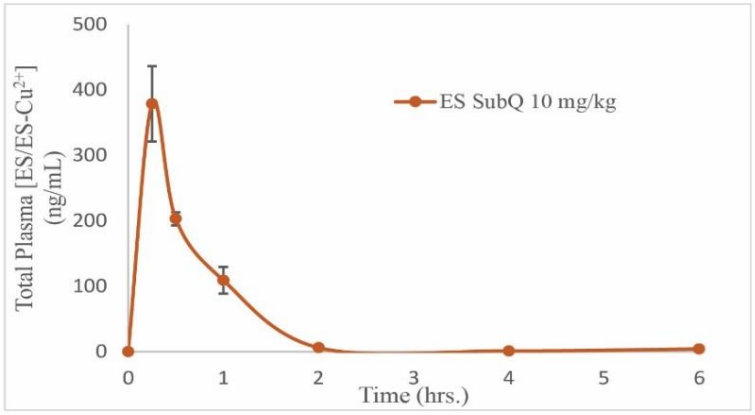


B

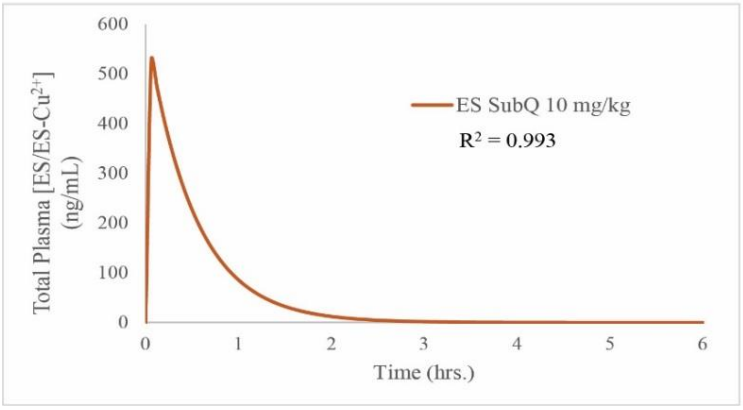


C

| ES Compartmental Analysis | | Route |
|---|---|---|
| Parameter | Units | SubQ |
| Exposure | mg/kg | 10 |
| Dose | µg | 207 |
| A | ng/ml | 601.08 |
| α | 1/h | 0.01 |
| $t_{1/2}$ | h | 0.36 |
| $C_0/C_{max}$ | ng/ml | 529.74 |
| $T_{max}$ | h | 0.05 |
| $AUC_{0-t}$ | ng/ml*h | 300.45 |

**Figure 3-2: ES 0.5% Methocel pharmacokinetics (PK).**

**A)** Non-compartmental analysis (NCA) of plasma vs time plot of subcutaneously administered ES formulated in 0.5% Methocel™ with 2% final DMSO. **B)** PKSolver generated 1-compartment analysis (CA) model. **C)** Calculated PK parameters of subcutaneous ES. NCA data presented as mean ± SD of biological triplicates, analytical duplicates per time point. Methocel™ vehicle was used for cardiac *Ctr1* KO mouse efficacy studies.

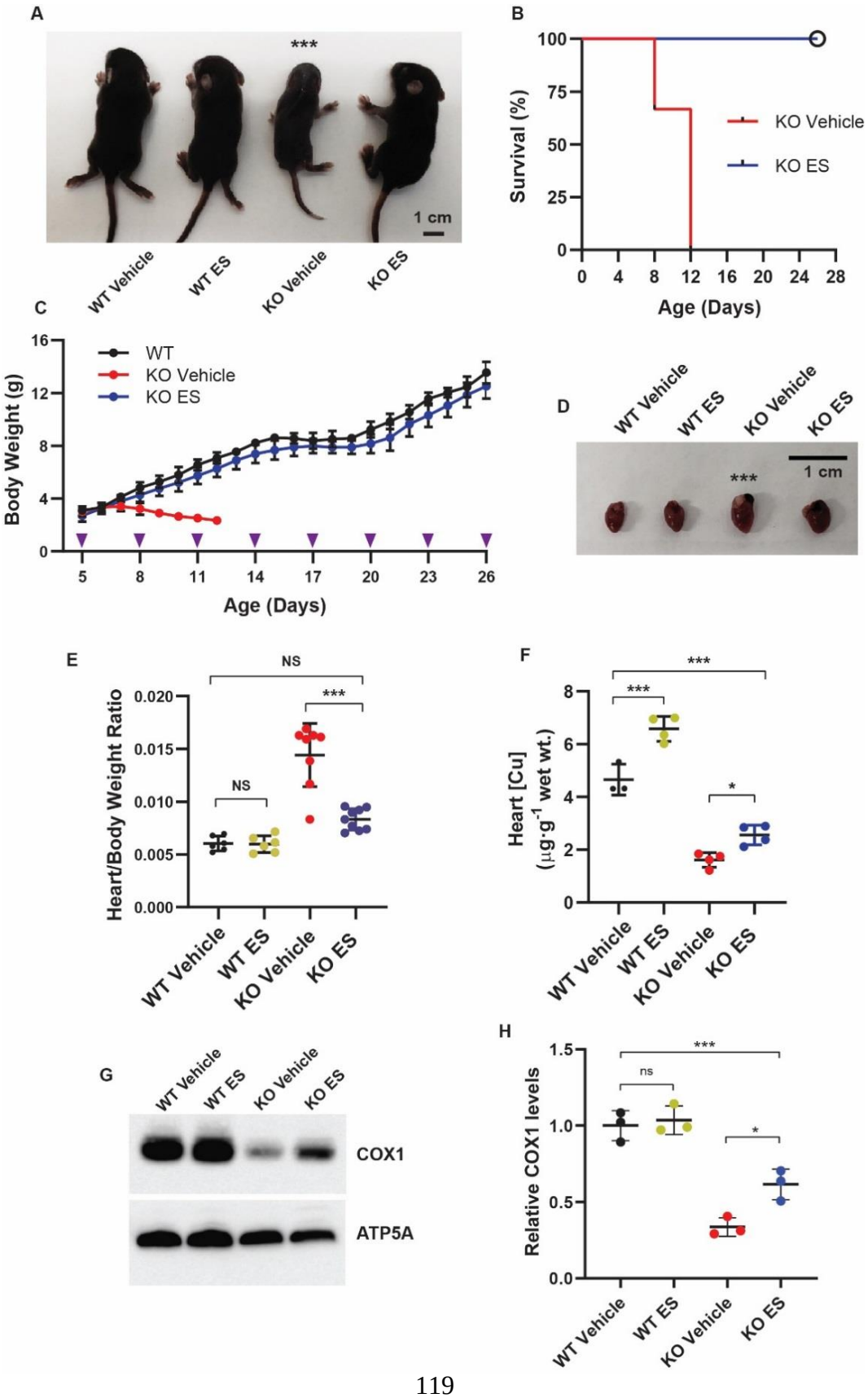
A
***
1 cm
WT Vehicle
WT ES
KO Vehicle
KO ES
B
Survival (%)
100
75
50
25
0
0 4 8 12 16 20 24 28
Age (Days)
KO Vehicle
KO ES
C
Body Weight (g)
16
12
8
4
0
WT
KO Vehicle
KO ES
5 8 11 14 17 20 23 26
Age (Days)
D
WT Vehicle
WT ES
KO Vehicle
KO ES
***
1 cm
E
Heart/Body Weight Ratio
0.020
0.015
0.010
0.005
0.000
NS
***
NS
WT Vehicle
WT ES
KO Vehicle
KO ES
F
Heart [Cu]
(μg·g-1 wet wt.)
8
6
4
2
0
***
***
*
WT Vehicle
WT ES
KO Vehicle
KO ES
G
WT Vehicle
WT ES
KO Vehicle
KO ES
COX1
ATP5A
H
Relative COX1 levels
1.5
1.0
0.5
0.0
***
ns
*
WT Vehicle
WT ES
KO Vehicle
KO ES

**Figure 3-3: Effects of ES treatment in cardiac *Ctr1* KO mice.**

**A)** Gross appearance of mice at PND 10. **B)** Kaplan-Meier survival curve. **C)** Growth Curves. WT and WT ES mice exhibited identical growth curves (WT ES omitted for clarity: see Fig 4A). Cohorts consisted of WT vehicle ($n$ = 3), WT ES ($n$ = 7), KO vehicle ($n$ = 3), and KO ES ($n$ = 9). **D)** Gross appearance of hearts at PND 10. **E)** Heart/body weight ratio. Cohorts consisted of $n$ = 6, 6, 8, & 9 animals respectively. **F)** Heart [Cu] levels. Cohorts consisted of $n$ = 4 per treatment. **G)** Heart COX1 levels. **H)** Quantification of relative COX1 levels. Data reported as mean ± SD with statistical significance assessed by one-way ANOVA with post hoc Tukey's HSD test or Welch one-way ANOVA with post hoc Tukey's HSD test. NS = not significant, *$p < 0.05$, ***$p < 0.001$. Western images analyzed with ImageJ software. Image bars represent 1 cm.

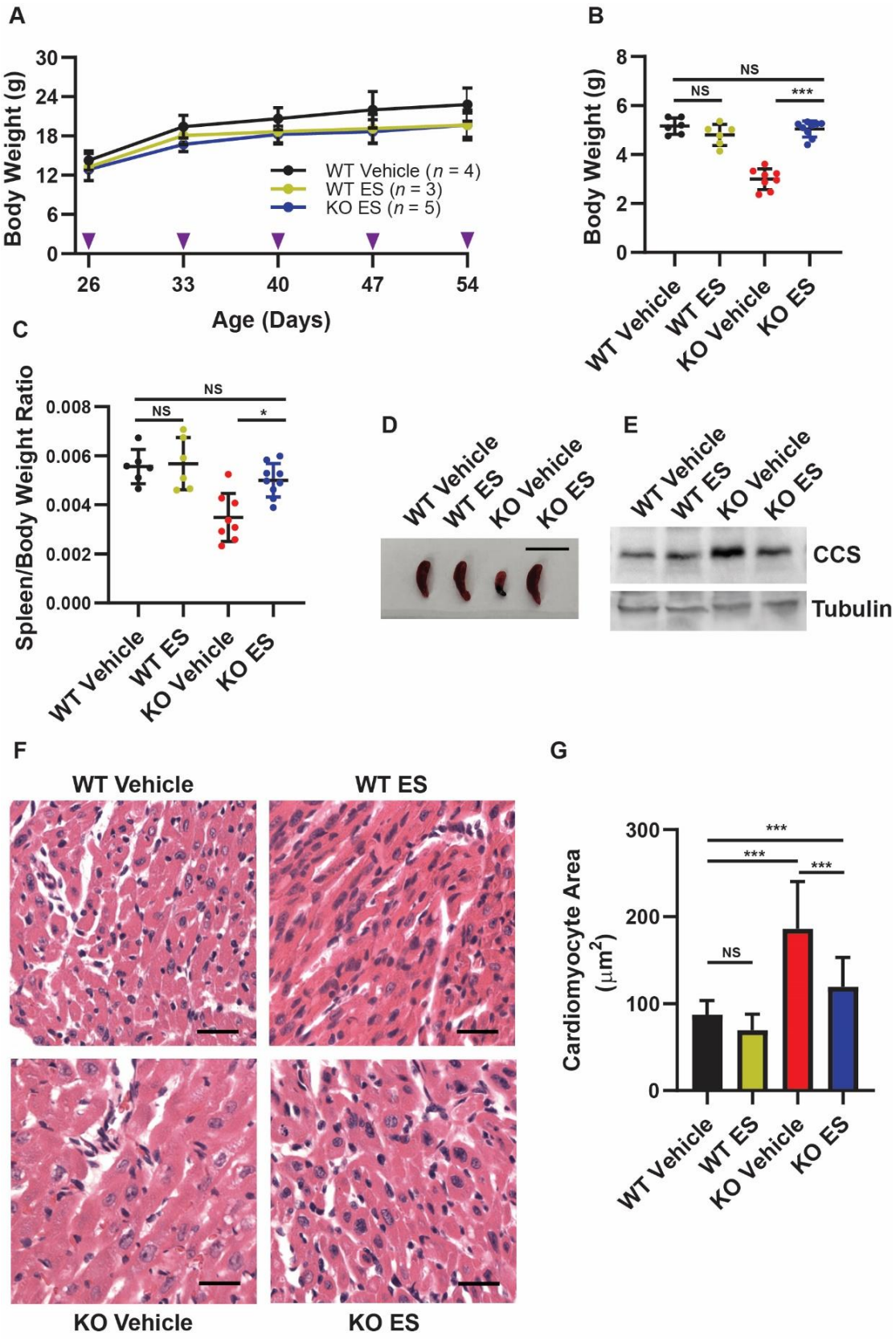
A
Body Weight (g)
30
24
18
12
6
0
26
33
40
47
54
Age (Days)
WT Vehicle (n = 4)
WT ES (n = 3)
KO ES (n = 5)
B
Body Weight (g)
8
6
4
2
0
NS
NS
***
WT Vehicle
WT ES
KO Vehicle
KO ES
C
Spleen/Body Weight Ratio
0.008
0.006
0.004
0.002
0.000
NS
NS
*
WT Vehicle
WT ES
KO Vehicle
KO ES
D
WT Vehicle
WT ES
KO Vehicle
KO ES
E
WT Vehicle
WT ES
KO Vehicle
KO ES
CCS
Tubulin
F
WT Vehicle
WT ES
KO Vehicle
KO ES
G
Cardiomyocyte Area (μm²)
300
200
100
0
***
***
***
NS
WT Vehicle
WT ES
KO Vehicle
KO ES

**Figure 3-4: Effects of ES treatment in cardiac *Ctr1* KO mice. Supplemental Data**

**A)** Extended treatment and monitoring of WT and KO mice to PND 54. **B)** Body weight at PND 10 necropsy: Treatment of KO mice with ES normalized body weight (5.2 g WT vs 5.0 g KO ES, $p = 0.92$) while KO vehicle demonstrates severe growth deficit compared to ES treatment (3.0 g vs 5.0 g, $p < 0.01$). **C)** Spleen/body weight ratio: KO ES treatment normalized spleen/body weight ratio to WT ($p = 0.61$) whereas KO vehicle mice exhibited smaller spleens ($p < 0.01$). Cohorts for B & C consisted of WT vehicle $n = 6$, WT ES $n = 6$, KO vehicle $n = 8$, and KO ES $n = 9$. (NS = not significant, $*p < 0.05$, $***p < 0.001$). **D)** Spleen gross appearance. **E)** Copper chaperone to superoxide dismutase (CCS) expression levels. Partial restoration of tissue/cellular in KO cells qualitatively reduces abundance of CCS with ES treatment. **F/G)** Cardiac histology: KO vehicle mice exhibit pronounced hypertrophic changes characterized by increased cardiomyocyte cell area. All data reported as mean ± SD. Statistical analysis reported as one-way ANOVA with post hoc Tukey's multiple comparisons test unless otherwise noted. Spleen image bar represent 1 cm. Cardiac histology image bars represent 25 μm.

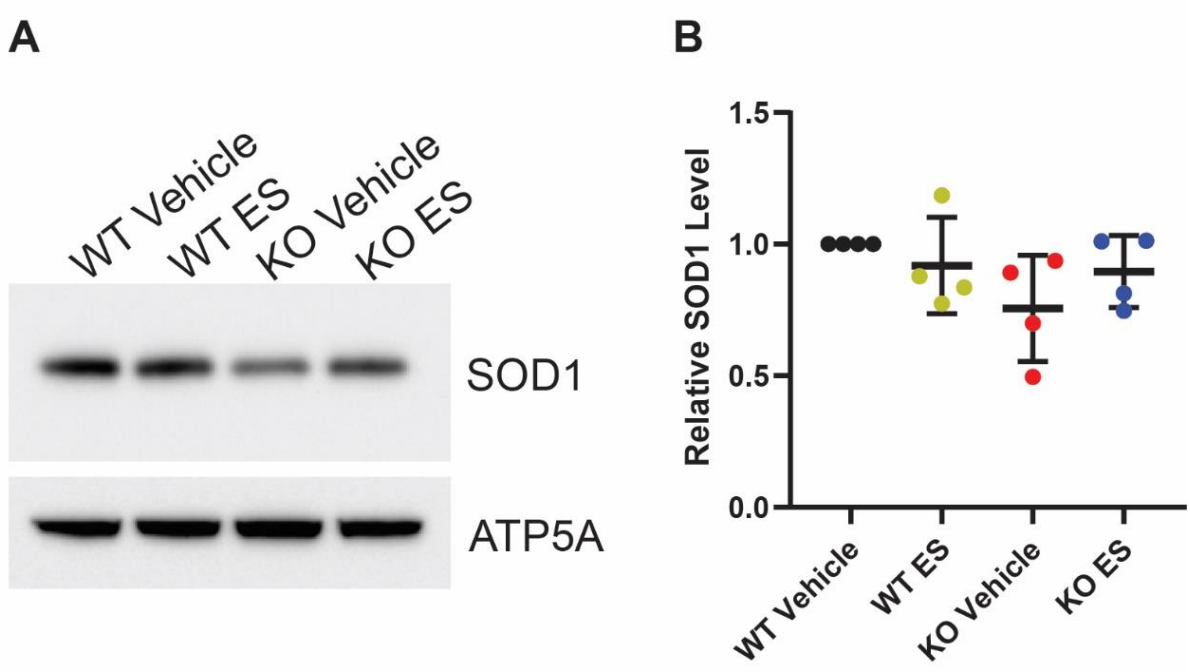


**Figure 3-5: Effects of ES treatment on SOD1 levels in cardiac *Ctr1* KO mice.**

**A)** Representative Western blot depicting SOD1 abundance in cardiac tissue of two-week-old mice. **B)** Quantification of relative abundance ($n = 4$). No significance found between cohorts ($p > 0.01$). All data reported as mean ± SD. Statistical analysis reported as one-way ANOVA with post hoc Tukey's multiple comparisons test. Western images analyzed using ImageJ software.

### 3.4. ES Alone Does Not Rescue *mottled-brindled* Mice

The *mottled-brindled* (*mo-br*) mouse phenotypically recapitulates Menkes disease *(22)*. *Mo-br* mice possess a 6-bp deletion in exon 11 of the mouse homolog *Atp7A* gene resulting in an in-frame deletion of Leu799 and Ala800. This deletion results in little residual Cu transporting function with severe disease phenotypes including hypopigmentation, kinky whiskers, growth delay, neurological abnormalities, seizures, and death at PND 14. As with most Menkes patients, the *mo-br* mouse shows little response to treatment with hydrophilic Cu complexes alone *(23, 24)*.

In preliminary studies, we administered ES at 10 $mg \cdot kg^{-1}$ body weight. Unlike the cardiac *Ctr1* KO mice, this pilot study demonstrated no enhanced survival amongst treated *mo-br* males. This was likely because *mo-br* mice were too deficient in systemic Cu to benefit from ES alone whereas the cardiac *Ctr1* KO mouse possesses an elevated serum Cu pool capable of ES-mediated redistribution to deficient cardiomyocytes *(20)*. We hypothesized that by pre-loading ES with $Cu^{2+}$, we would address the systemic Cu deficiency and ATP7A-mediated defective transport.

### 3.5. ES-$Cu^{2+}$ Complex Rescues *mottled-brindled* Mice

Menkes disease is characterized by severe neurodegeneration, therefore any successful treatment must involve a drug that facilitates Cu delivery across the blood-brain barrier or blood-cerebral spinal fluid barrier *(9, 10, 14)*. Brain pharmacokinetic studies on PND 7 mice demonstrated high levels of ES in the brain at 201.3 ±41.7 $ng \cdot mg^{-1}$ (Fig. 3-6A), whereas adult exposure, though still significant, was about 25-fold lower at 7.8 ± 5.0 $ng \cdot mg^{-1}$ (Fig 3-6B).

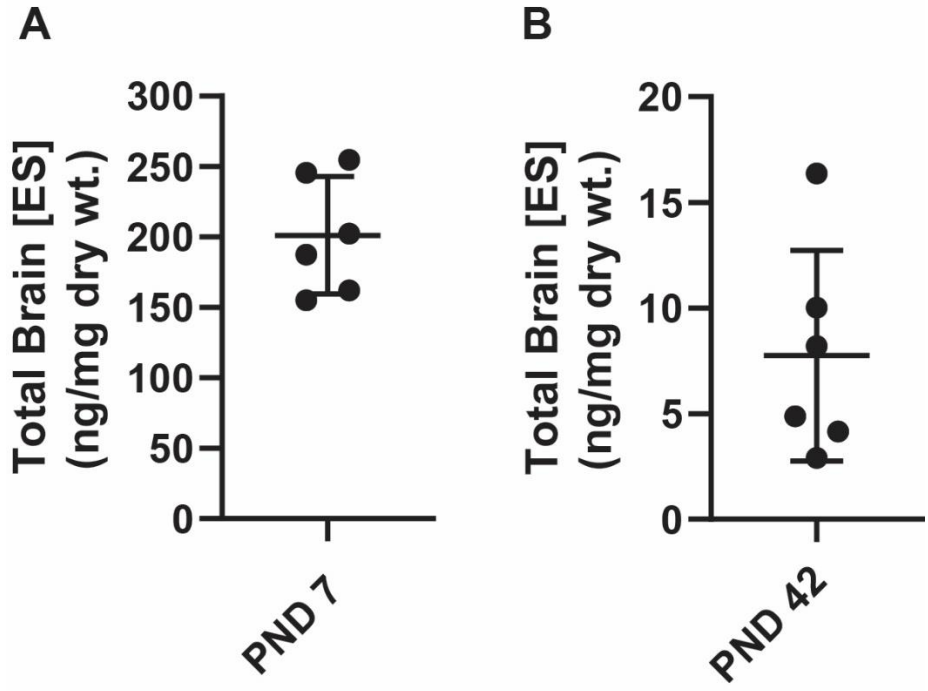


**Figure 3-6: Brain ES exposure.**

WT C57BL/6 mice (*n* = 6) of PND 7 and 42 (6 weeks) of age administered 3.625 mg/kg ES-$Cu^{2+}$ complex were harvested approximately 1 hour after subcutaneous injection. Drug quantification from brain tissue followed euthanasia and saline perfusion. **A)** PND 7 mice: Brain drug exposure 201.3 ± 41.7 ng/mg. **B)** PND 42 mice: Brain drug exposure 7.8 ± 5.0 ng/mg. All data reported as mean ± SD.

In order to solubilize this rather lipophilic complex, we formulated ES-$Cu^{2+}$ in 20% Captisol® aqueous vehicle (Fig. 3-7). Single bolus subcutaneous injections of 7.25 mg·$kg^{-1}$ ES-$Cu^{2+}$ showed no overt signs of acute toxicity. Mice retained body weight as compared to control animals (Table 3-2). Compartmental analysis of the PK profile showed that the ES-$Cu^{2+}$ complex exhibits nonlinear PK (Fig. 3-8A, B). After initial high plasma $C_{max}$ of 197.6 ng·$mL^{-1}$ at 22.8 min, subcutaneous ES-$Cu^{2+}$ exhibits rapid elimination from the central compartment ($t_{1/2}$ α of 54.6 min) and slow elimination from the peripheral compartment ($t_{1/2}$ β of 18.8 hr) (Fig. 3-8C).

Peripheral tissue levels exhibited good ES-$Cu^{2+}$ penetrance (5.3 ng·$mL^{-1}$) indicating tissue partitioning of the metalated complex (Fig. 3-8C). The lipophilic nature of the preformed complex explains the greater tissue penetrance and slower elimination as compared to ES alone. Formation of ES-$Cu^{2+}$ in vivo is rate-limited by the availability of labile copper and provides an explanation for the initial lack of response in *mo-br* mice treated with ES alone. *(31, 32).* Subcutaneous ES-$Cu^{2+}$ complex is 72% bioavailable (Fig. 3-8C).

We next administered ES-$Cu^{2+}$ at 3.625 mg·$kg^{-1}$ per dose by subcutaneous injection on PND 7 and 10. The total dose of Cu approximated the total amount of Cu (4 µg) in a 4 g WT mouse *(26).* Additional *mo-br* cohorts included vehicle, ES only, and copper histidine (HIS-$Cu^{2+}$) formulated with an equivalent dose of Cu as compared to the ES-$Cu^{2+}$ cohort (Table 3-3). We selected HIS-$Cu^{2+}$ as a control because of the drug's investigational status for Menkes disease *(14).* ES-$Cu^{2+}$ was well tolerated and exhibited favorable pharmacokinetics (Table 3-3) (Fig. 3-7, 3-8).

A

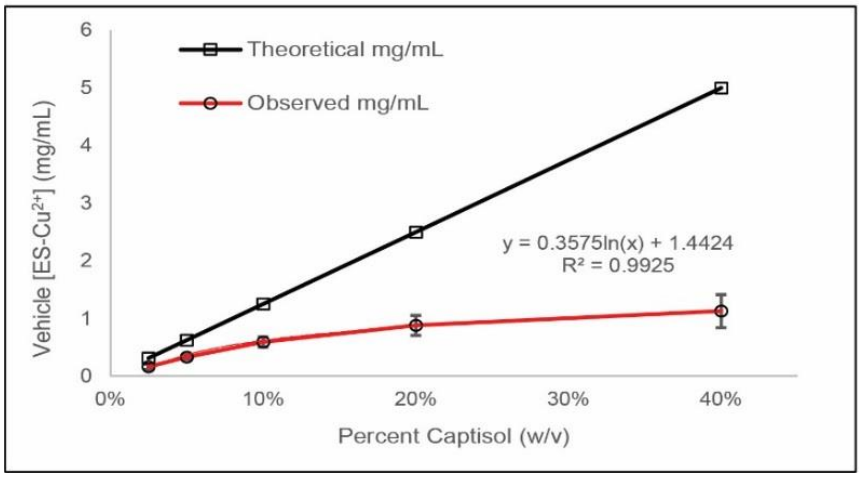


B

| Phase Solubility Assay | | | |
|---|---|---|---|
| Captisol® % (w/v) | Theoretical mg/mL | Observed mg/mL | STDEV mg/mL |
| 2.5% | 0.3125 | 0.17 | 0.04 |
| 5% | 0.625 | 0.33 | 0.04 |
| 10% | 1.25 | 0.59 | 0.08 |
| 20% | 2.5 | 0.88 | 0.17 |
| 40% | 5 | 1.13 | 0.29 |

**Figure 3-7: Captisol ES-$Cu^{2+}$ phase solubility.**

**A)** Theoretical and observed solubility curves of ES-$Cu^{2+}$ complex in 2.5%, 5%, 10%, 20%, and 40% Captisol® vehicle preparations. **B)** Quantified complex by LC-MS demonstrating maximum stable concentrations of drug complex preparations. All data reported as mean ± SD. Individual values represent analytical triplicate

**Table 3-2: Elesclomol-$Cu^{2+}$ tolerability in adult C57BL/6 females.**

| SubQ Bolus | | Body Mass | | | | | | | |
|---|---|---|---|---|---|---|---|---|---|
| | | Day 0 | | Day 5 | | | Day 10 | | |
| Dose Level | *n* | Mass | p-value | Mass | % Δ | p-value | Mass | % Δ | p-value |
| Captisol® Vehicle | 4 | 20.6 ± 1.8 | - | 21.2 ± 1.8 | 2.8% | - | 21.7 ± 1.7 | 5.5% | - |
| 3.625 mg/kg ES-$Cu^{2+}$ | 5 | 19.8 ± 1.2 | 0.56 | 20.1 ± 1.4 | 1.3% | 0.41 | 20.6± 1.7 | 4.2% | 0.48 |
| 7.25 mg/kg ES-$Cu^{2+}$ | 5 | 20.1 ± 1.0 | 0.80 | 19.6 ± 1.0 | -2.8% | 0.19 | 20.1 ± 1.2 | -0.3% | 0.22 |

Data reported as mean ± SD with statistical significance assessed by one-way ANOVA with post hoc Tukey's HSD test or Welch one-way ANOVA with post hoc Tukey's HSD test.

**Table 3-3: Treatment Regime and 10 week survival in the mottled-brindled mouse.**

| | | Treatment | | | | | Survival | |
|---|---|---|---|---|---|---|---|---|
| **Cohort** | ***n*** | **Exposure ($mg \cdot kg^{-1}$)** | **Total (µg)** | **ES/HIS (µg)** | **$Cu^{2+}$ (µg)** | **Median (Days)** | **Viable Mice 10 Weeks** | **Percent (%)** |
| **WT Vehicle** | 15 | - | - | - | - | - | 15 | 100 |
| **WT ES-$Cu^{2+}$** | 13 | 7.25 | 29 | 25.02 | 3.98 | - | 13 | 100 |
| ***mo-br* Vehicle** | 9 | - | - | - | - | 14 | 0 | 0 |
| ***mo-br* ES** | 6 | 6.25 | 25.02 | 25.02 | 3.98 | 16.5 | 0 | 0 |
| ***mo-br* ES-$Cu^{2+}$** | 27 | 7.25 | 29 | 25.02 | 3.98 | **203** | **22** | **81.5** |
| ***mo-br* HIS-$Cu^{2+}$** | 6 | 5.83 | 23.3 | 19.35 | 3.98 | 18 | 0 | 0 |

A

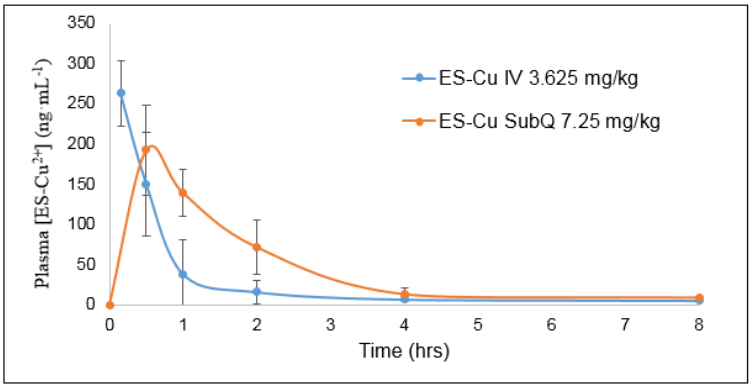


B

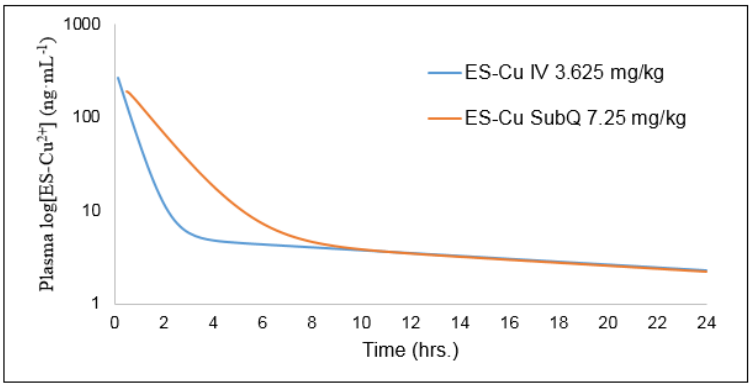


C

| $ES\text{-}Cu^{2+}$ Compartmental Analysis | | Route | | |
|---|---|---|---|---|
| Parameter | Units | IV | SubQ | Oral* |
| Exposure | mg/kg | 3.625 | 7.250 | 10.875 |
| Dose | µg | 72.4 | 158.1 | 232.0 |
| A | ng/ml | 351.53 | 291.77 | 1343.67 |
| α | 1/h | 1.96 | 0.76 | 2.52 |
| $t_{1/2}$ α | h | 0.35 | 0.91 | 0.26 |
| B | ng/ml | 5.36 | 5.30 | N/A |
| β | 1/h | 0.04 | 0.04 | N/A |
| $t_{1/2}$ β | h | 19.42 | 18.82 | N/A |
| $C_0/C_{max}$ | ng/ml | 356.89 | 197.59 | 23.10 |
| $T_{max}$ | h | N/A | 0.38 | 0.39 |
| $AUC_{0-t}$ | ng/ml*h | 265.76 | 420.14 | 24.36 |
| $AUC_{0-inf}$ | ng/ml*h | 329.55 | 479.63 | 24.36 |
| $F_{abs}$ | % | 100.00 | 72.39 | 2.86 |

*Oral NCA/CA data not plotted due to very low bioavailablity ($F_{abs}$). Oral data reported as 1-compartment model.

**Figure 3-8: $ES\text{-}Cu^{2+}$ 20% Captisol® pharmacokinetics.**

**A)** Non-compartmental analysis (NCA) of plasma vs time plot of intravenous and subcutaneously administered $ES\text{-}Cu^{2+}$ formulated in Captisol®. Values at 24 hours were below the lower limit of detection. **B)** PKSolver generated 2-compartment analysis (CA) models. **C)** Calculated PK parameters of intravenous, subcutaneous, and oral $ES\text{-}Cu^{2+}$. NCA data presented as mean ± SD of biological triplicates, analytical duplicates per time point. Captisol® vehicle was used for *mo-br* mouse efficacy studies.

Within 24 hours, we observed pigment production in $ES\text{-}Cu^{2+}$ treated mice in the

immediate vicinity of the injection site (Fig. 3-9A-C) (Fig. 3-10A). Pigment production indicated increased activity of the secretory pathway cuproenzyme tyrosinase. This was in agreement with the in vitro assessment of an *ATP7A* KO B16 melanoma cell line which showed that 1 nM ES was able to partially rescue tyrosinase activity (Fig. 3-10B). Because tyrosinase requires the action of ATP7A for Cu import into the Golgi complex *(27)*, our findings were unexpected and suggest that ES-$Cu^{2+}$ was delivering Cu to cuproenzymes metalated in the Golgi. We also observed that whisker appearance improved from bushy, highly kinked clumps to near-normal by PND 70 in only the ES-$Cu^{2+}$ cohort (Fig. 3-9D, E) (Fig. 3-10C)—indicating improved sulfhydryl oxidase activity *(28)*.

*Mo-br* vehicle, ES only, and HIS-$Cu^{2+}$ cohorts developed seizures beginning around PND 11. Seizures increased in severity, with subsequent death of all individuals in these groups between PND 14-21. We only observed a negligible survival advantage for HIS-$Cu^{2+}$ over vehicle alone (Table 3-3). ES-$Cu^{2+}$ treated *mo-br* adult mice did not have seizures and exhibited similar body size to that of WT siblings (Fig 3-9D, E). ES-$Cu^{2+}$ increased the survival of *mo-br* mice and successfully rescued 82% of animals at 10 weeks of age with a median survival of 203 days ($p < 0.01$, Log-Rank) (Fig. 3-9F) (Fig. 3-10D). After treatment, ES-$Cu^{2+}$ *mo-br* mice experienced accelerated growth and near normal body weight by week 10 (Fig. 3-9G) (Fig. 3-10E). Histological examination of the livers of WT vehicle and both ES-$Cu^{2+}$ treated WT and *mo-br* mice demonstrated no pathological changes associated with drug exposure (Table 3-4, 3-5) (Fig. 3-11).

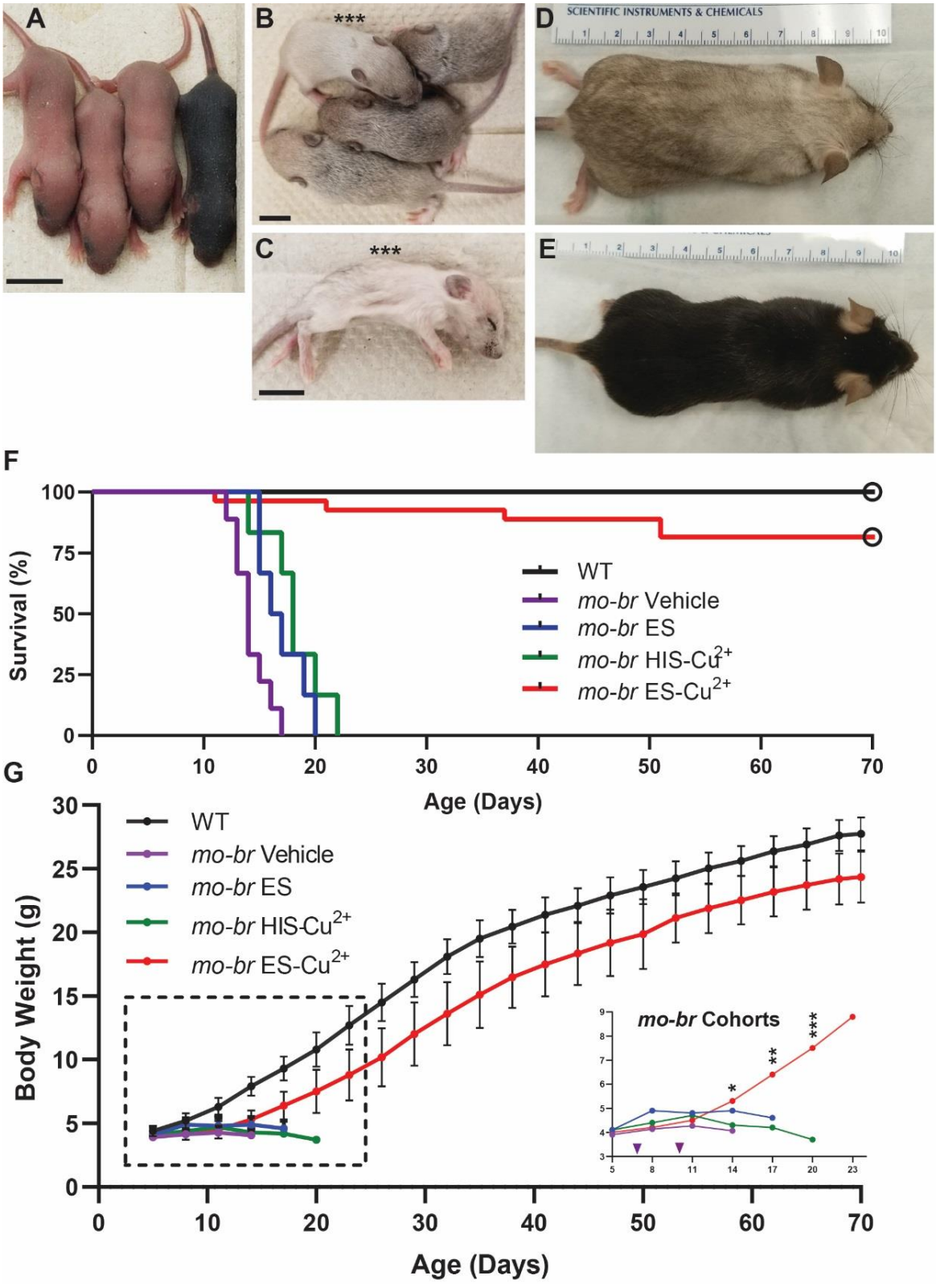
A
B
***
C
***
D
SCIENTIFIC INSTRUMENTS & CHEMICALS
E
F
Survival (%)
100
75
50
25
0
0
10
20
30
40
50
60
70
Age (Days)
WT
mo-br Vehicle
mo-br ES
mo-br HIS-Cu2+
mo-br ES-Cu2+
G
Body Weight (g)
30
25
20
15
10
5
0
0
10
20
30
40
50
60
70
Age (Days)
WT
mo-br Vehicle
mo-br ES
mo-br HIS-Cu2+
mo-br ES-Cu2+
mo-br Cohorts
*
**
***

**Figure 3-9: Effects of ES-$Cu^{2+}$ treatment in *mo-br* mice.**

**A)** *Mo-br* hemizygous males and WT littermate at PND 5 before intervention. **B)** Pigmentation changes in *mo-br* males administered ES-$Cu^{2+}$ compared to vehicle (***) on PND 12. **C)** Moribund *mo-br* vehicle (***) mouse PND 14. **D** & **E)** *mo-br* ES-$Cu^{2+}$ and WT littermate at PND 70. **F)** Kaplan-Meier survival curve. All WT mice survived experimental protocol. **G)** Growth Curves of indicated groups: WT and WT ES- $Cu^{2+}$ mice exhibited near-identical growth curves (WT ES- $Cu^{2+}$ omitted for clarity: see Fig 3-10E). Cohorts consisted of WT vehicle ($n$ = 15), WT ES-$Cu^{2+}$ ($n$ = 13), *mo-br* vehicle ($n$ = 9), *mo-br* ES ($n$ = 6), *mo-br* HIS-$Cu^{2+}$ ($n$ = 6), and *mo-br* ES- $Cu^{2+}$ ($n$ = 27). Data reported as mean ± SD with statistical significance assessed by one-way ANOVA test or Welch one-way ANOVA with post hoc Tukey's HSD test. *$p < 0.05$, **$p < 0.01$, ***$p < 0.001$. Image bars represent 1 cm.

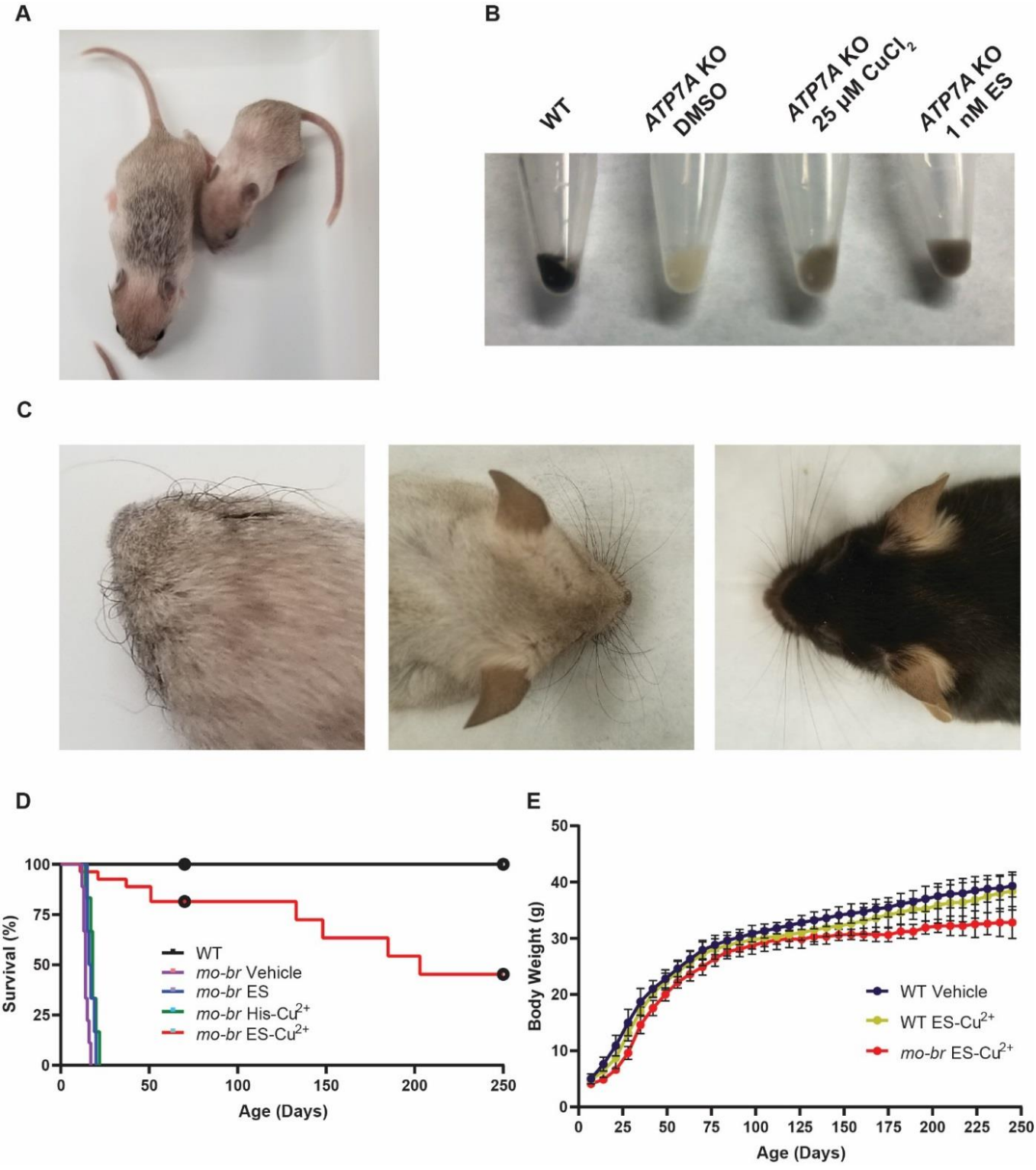
A
B
WT
ATP7A KO DMSO
ATP7A KO 25 μM CuCl2
ATP7A KO 1 nM ES
C
D
Survival (%)
Age (Days)
WT
mo-br Vehicle
mo-br ES
mo-br His-Cu2+
mo-br ES-Cu2+
E
Body Weight (g)
Age (Days)
WT Vehicle
WT ES-Cu2+
mo-br ES-Cu2+

**Figure 3-10: Effects of ES-$Cu^{2+}$ treatment in *mo-br* mice. Supplemental Data.**

**A)** Fur pigmentation: Intense pigmentation changes around the site of injection indicated rescue of the secretory pathway cuproenzyme tyrosinase. **B)** B16 melanoma *ATP7A* KO: ES and treatment improves tyrosinase activity *in vitro*. **C)** Whisker morphology: *mo-br* mice initially presented with highly kinked, bushy clumps of whiskers (left). Whisker appearance normalized at PND 70 (center). WT male at PND 70 (right). **D)** Extended survival study: Subsets of WT ($n$ = 5), WT ES-$Cu^{2+}$ ($n$ = 4), and *mo-br* ES-$Cu^{2+}$ ($n$ = 11) continued on an observation only arm of the initial study until PND 245. All WT mice survived to week 35. *Mo-br* mice reported a median survival of 203 days. ($p < 0.01$, Log-Rank). **E)** Extended growth curve: Weekly weight reveals no difference between WT cohorts. *Mo-br* mice demonstrated gross body weight deficit. All data reported as mean ± SD. Statistical analysis reported as one-way ANOVA with post hoc Tukey's multiple comparisons test unless otherwise noted. Image bars represent 1 cm

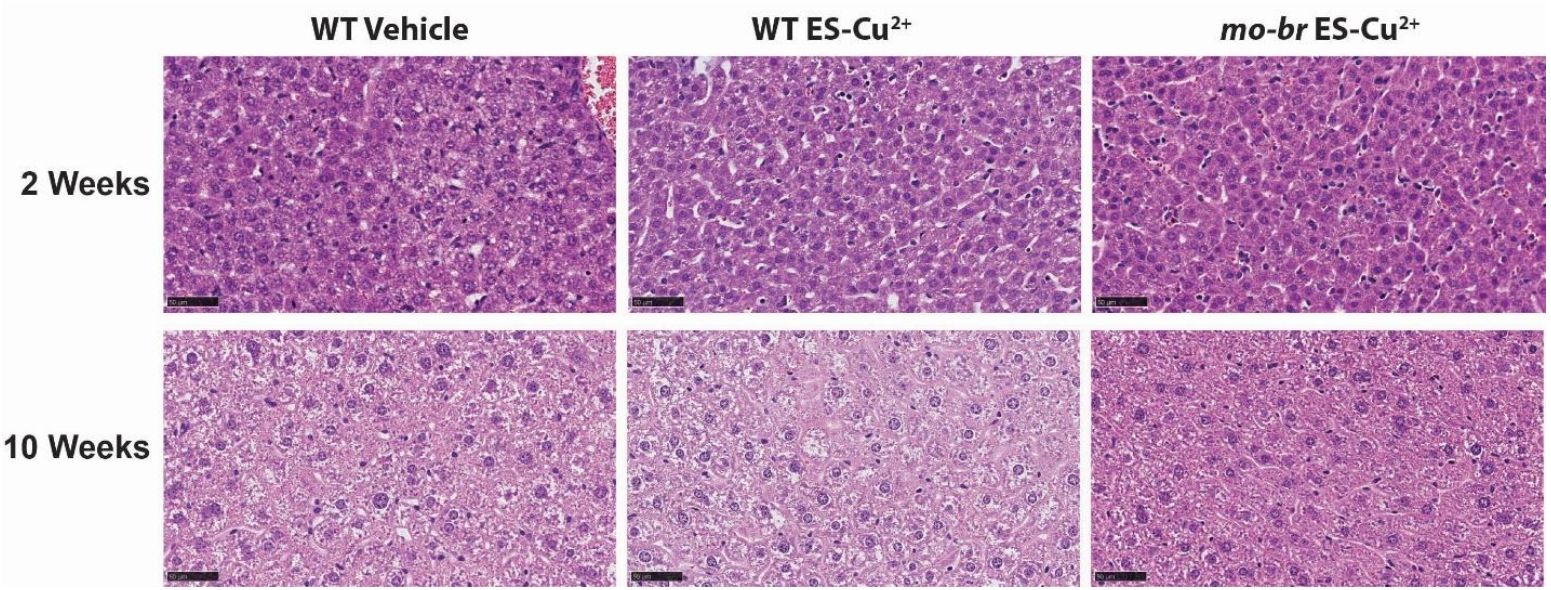


**Figure 3-11: Histological examination of 2 and 10 week livers.**

Livers collected from WT vehicle, WT ES-$Cu^{2+}$, and *mo-br* ES-$Cu^{2+}$ treated mice at 2 and 10 weeks of age revealed no pathological changes following exposure to ES-$Cu^{2+}$ treatment. A blinded pathologist's report indicated minimal, multifocal hepatocellular vacuolization (lipid type) and mild, multifocal extramedullary hematopoiesis in samples collected from 2-week-old mice. Both findings are considered incidental in young animals. No abnormal findings were documented in 10-week-old animals. All samples were fixed in 10% neutral buffered formalin before sectioning and H&E staining. Liver histopathology image bars represent 50 μm.

**Table 3-4: CBC of 10 week old C57BL/6 and *mo-br* mice.**

| CBC | WT Vehicle ($n$ = 5) | WT ES-$Cu^{2+}$ ($n$ = 5) | *mo-br* ES-$Cu^{2+}$ ($n$ = 10) | Ref. Range* |
|---|---|---|---|---|
| WBC $10^9$/l | 6.7 ± 1.5 | 9.1 ± 3.6 | 6.9 ± 2.1 | 6 – 15 |
| LYM $10^9$/l | 5.4 ± 1.1 | 6.7 ± 2.3 | 5.1 ± 2.0 | 3 – 7 |
| MON $10^9$/l | 0.2 ± 0.2 | 0.2 ± 0.2 | 0.1 ± 0.1 | 0.0 – 0.6 |
| NEU $10^9$/l | 1.1 ± 1.0 | 2.2 ± 1.9 | 1.7 ± 1.3 | 0.5 – 3.8 |
| RBC $10^{12}$/l | 11.3 ± 0.4 | 11.2 ± 0.8 | 9.8 ± 0.9 | 7 – 12 |
| HCT % | 52.9 ± 1.2 | 50.3 ± 5.5 | 47.3 ± 3.9 | 35 – 45 |
| HGB g/dl | 16.8 ± 0.9 | 16.4 ± 1.7 | 15.2 ± 1.3 | 12 – 16 |
| MCV fl | 47.0 ± 1.4 | 45.0 ± 2.3 | 48.2 ± 2.1 | 45 – 55 |
| MCH pg | 15.0 ± 1.2 | 14.6 ± 0.7 | 15.5 ± 0.8 | 11 – 13 |
| MCHC g/dl | 31.9 ± 2.0 | 32.6 ± 1.0 | 32.1 ± 0.8 | 22 – 32 |
| PLT $10^9$/l | 463.2 ± 78.2 | 531.2 ± 81.3 | 425.6 ± 156.4 | 200 – 450 |

* Normal hematology ranges as indicated by VetScan HM5 Operator's Manual for mice.

**Table 3-5: Serum chemistries of 10 week old C57BL/6 and *mo-br* mice.**

| Serum Chemistries | WT Vehicle (*n*= 4) | WT ES-$Cu^{2+}$ (*n* = 4) | *mo-br* ES-$Cu^{2+}$ (*n* = 8) | Ref. Range* |
|---|---|---|---|---|
| **ALP (U/l)** | 120.3 ± 11.5 | 155.3 ± 25.5 | 251.1 ± 41.6 | 100 – 184 |
| **ALT (U/l)** | 15.5 ± 4.0 | 14.0 ± 3.5 | 9.3 ± 4.8 | 13 – 56 |
| **BUN (mg/dl)** | 17.0 ± 1.2 | 16.5 ± 1.3 | 11.9 ± 4.6 | 7.8 – 15.5 |
| **CRE (mg/dl)** | 0.3 ± 0.2 | 0.3 ± 0.1 | 2.2 ± 0.8 | 0.3 – 0.4 |
| **TP (g/dl)** | 4.8 ± 0.7 | 4.5 ± 0.8 | 1.7 ± 0.3 | 4.4 – 5.8 |

* Normal ranges as indicated by Clinical Chemistry Reference Intervals for C57BL/6J, C57BL/6N, and C3HeB/FeJ Mice. Otto et al. *J Am Assoc Lab Anim Sci.* 2016; 55(4):375–386. PMID: 27423143

### 3.6. Neuromotor Assessment of ES-$Cu^{2+}$ Rescue

Ten week old *mo-br* mice were evaluated by phenotype and neuromotor functional tests. ES-$Cu^{2+}$ treated *mo-br* mice revealed hypopigmentation but no other gross abnormalities upon observation.

On a forelimb grip strength test using a Chatillon force apparatus, ES-$Cu^{2+}$ treated *mo-br* mice possessed 73% grip strength compared to WT animals (0.94 vs 1.29 N, $p < 0.01$) (Fig 3-12A). On the accelerating rotarod, a test of endurance and motor coordination, ES-$Cu^{2+}$ *mo-br* mice exhibited average latency to fall time of 222 s compared to 379 s ($p < 0.01$) for WT (Fig 3-12B). On the gait treadmill, overall ataxic indices were statistically insignificant for both pelvic and shoulder girdles compared to WT (Fig. 3-12C) (Table 3-6). In the open field, *mo-br* mice demonstrated 24% increased rest time, 35% decreased movement time and traveled 60% of total distance as compared to WT ($p < 0.01$) (Fig. 3-12D-F).

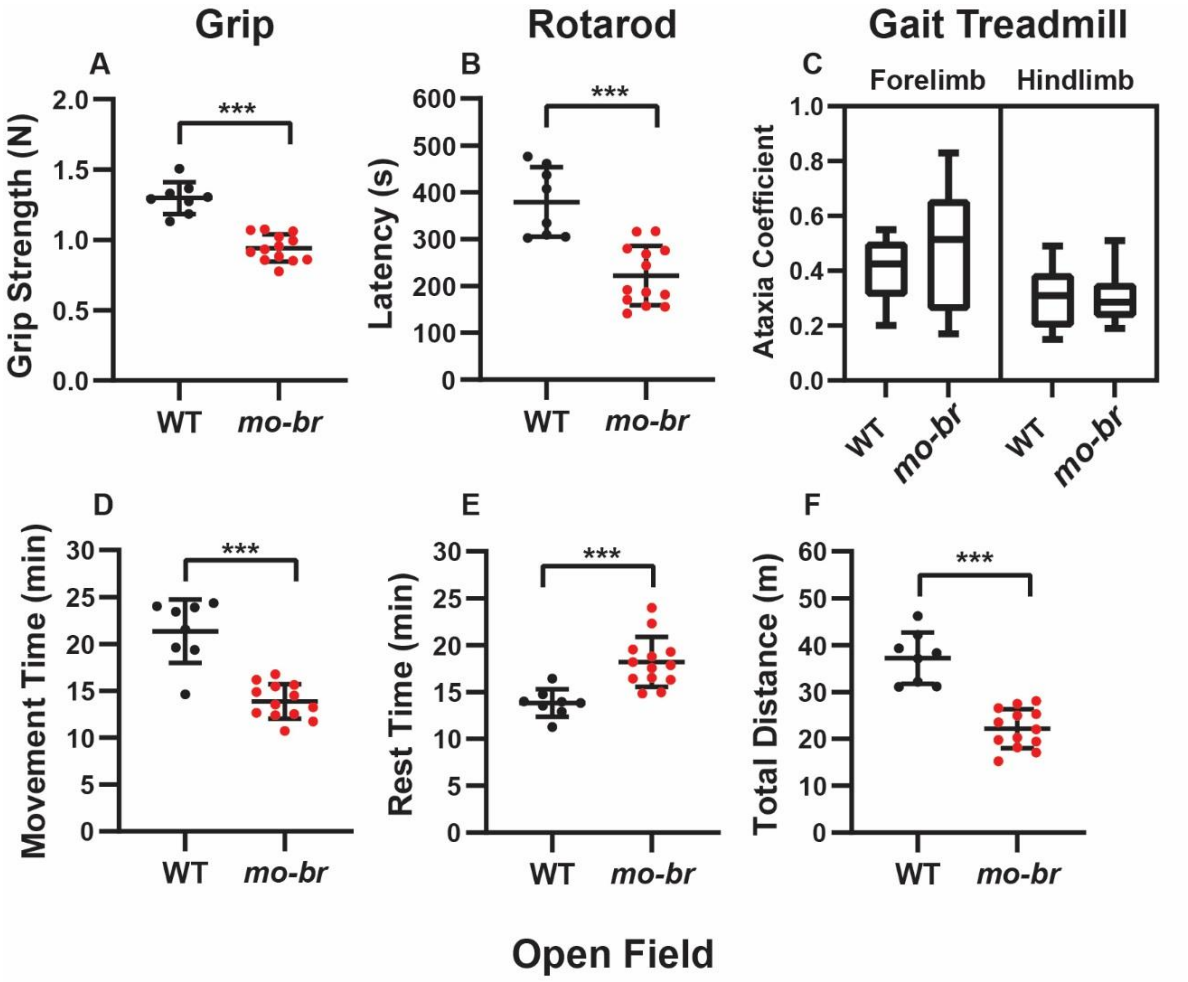


**Figure 3-12: Neuromotor tests of 10 week old mice**

Mice were assessed by grip strength, rotarod, gait treadmill, and open field at 10 weeks of age. **A)** Forelimb grip strength. **B)** Rotarod. **C)** Gait Treadmill. DigiGait™ generated ataxia coefficients of shoulder and pelvic girdles were statistically insignificant. **D-F)** Open Field. Movement time, rest time, and total distance. Cohorts consisted of WT $n = 8$ and *mo-br* $n = 13$. Data reported as mean ± SD with statistical significance assessed by unpaired t-test. ***$p < 0.001$.

**Table 3-6: Gait parameters at 10 week assessment in WT and *mo-br* males.**

| Gait Parameters | | | | | | |
|---|---|---|---|---|---|---|
| **Limb Girdle** | **Fore Limb** | | | **Hind Limb** | | |
| **Cohorts** | **WT** | ***mo-br*** | **p-value** | **WT** | ***mo-br*** | **p-value** |
| **Stride (s)** | **0.284 ± 0.016** | **0.257 ± 0.008** | **< 0.001** | **0.285 ± 0.017** | **0.258 ± 0.008** | **< 0.001** |
| **Swing (s)** | **0.116 ± 0.009** | **0.096 ± 0.008** | **< 0.001** | **0.113 ± 0.006** | **0.097 ± 0.015** | **0.001** |
| **Brake (s)** | 0.048 ± 0.010 | 0.054 ± 0.019 | 0.316 | **0.021 ± 0.006** | **0.033 ± 0.010** | **< 0.001** |
| **Propel (s)** | 0.120 ± 0.017 | 0.107 ± 0.023 | 0.079 | **0.151 ± 0.011** | **0.129 ± 0.009** | **< 0.001** |
| **Stance (s)** | 0.168 ± 0.019 | 0.161 ± 0.011 | 0.105 | **0.172 ± 0.013** | **0.162 ± 0.012** | **0.020** |
| **Stride Frequency** | **3.600 ± 0.171** | **3.953 ± 0.134** | **< 0.001** | **3.550 ± 0.232** | **3.936 ± 0.127** | **< 0.001** |
| **Stride Length (cm)** | **6.817 ± 0.383** | **6.161 ± 0.200** | **< 0.001** | **6.833 ± 0.398** | **6.206 ± 0.182** | **< 0.001** |
| **Stance Width (cm)** | 1.667 ± 0.225 | 1.672 ± 0.259 | 0.963 | **2.583 ± 0.264** | **2.244 ± 0.313** | **0.027** |
| **Step Angle (°)** | 62.283 ± 2.440 | 65.033 ± 9.499 | 0.496 | 58.833 ± 8.209 | 57.289 ± 7.511 | 0.674 |
| **Paw Angle (°)** | 7.000 ± 6.4000 | 9.139 ± 7.601 | 0.386 | 16.658 ± 4.846 | 18.117 ± 5.804 | 0.438 |
| **Paw Area ($cm^2$)** | **0.363 ± 0.059** | **0.447 ± 0.126** | **0.031** | 0.773 ± 0.108 | 0.859 ± 0.161 | 0.094 |
| **Ataxia Coefficient** | 0.406 ± 0.112 | 0.495 ± 0.231 | 0.205 | 0.313 ± 0.111 | 0.315 ± 0.087 | 0.944 |

Data reported as mean ± SD with statistical significance assessed by one-way ANOVA with post hoc Tukey's HSD test or Welch one-way ANOVA with post hoc Tukey's HSD test.

### 3.7. Brain Histology

Brain sections of vehicle and HIS-$Cu^{2+}$ treated mice at 2 weeks of age showed marked, diffuse neurodegeneration of cortical and hippocampal neurons (Fig. 3-13A) (Fig. 3-14A).

In the hippocampus, necrotic pyramidal neurons represented 10.5% of 3200 counted cells in vehicle and 4.9% in HIS-$Cu^{2+}$ *mo-br* mice. ES-$Cu^{+2}$ preserved cortical and hippocampal neurons with hippocampal regions showing no signs of necrosis as characterized by pyknotic nuclei (Fig. 3-13A).

The Purkinje neuron layer in the cerebellum was also preserved. (Fig. 3-14B). Brain structures examined at 10 weeks of age revealed preserved brain structures and no distinct differences between WT and ES- $Cu^{2+}$ treated *mo-br* mice (Fig. 3-13B) (Fig. 3-15A-C).

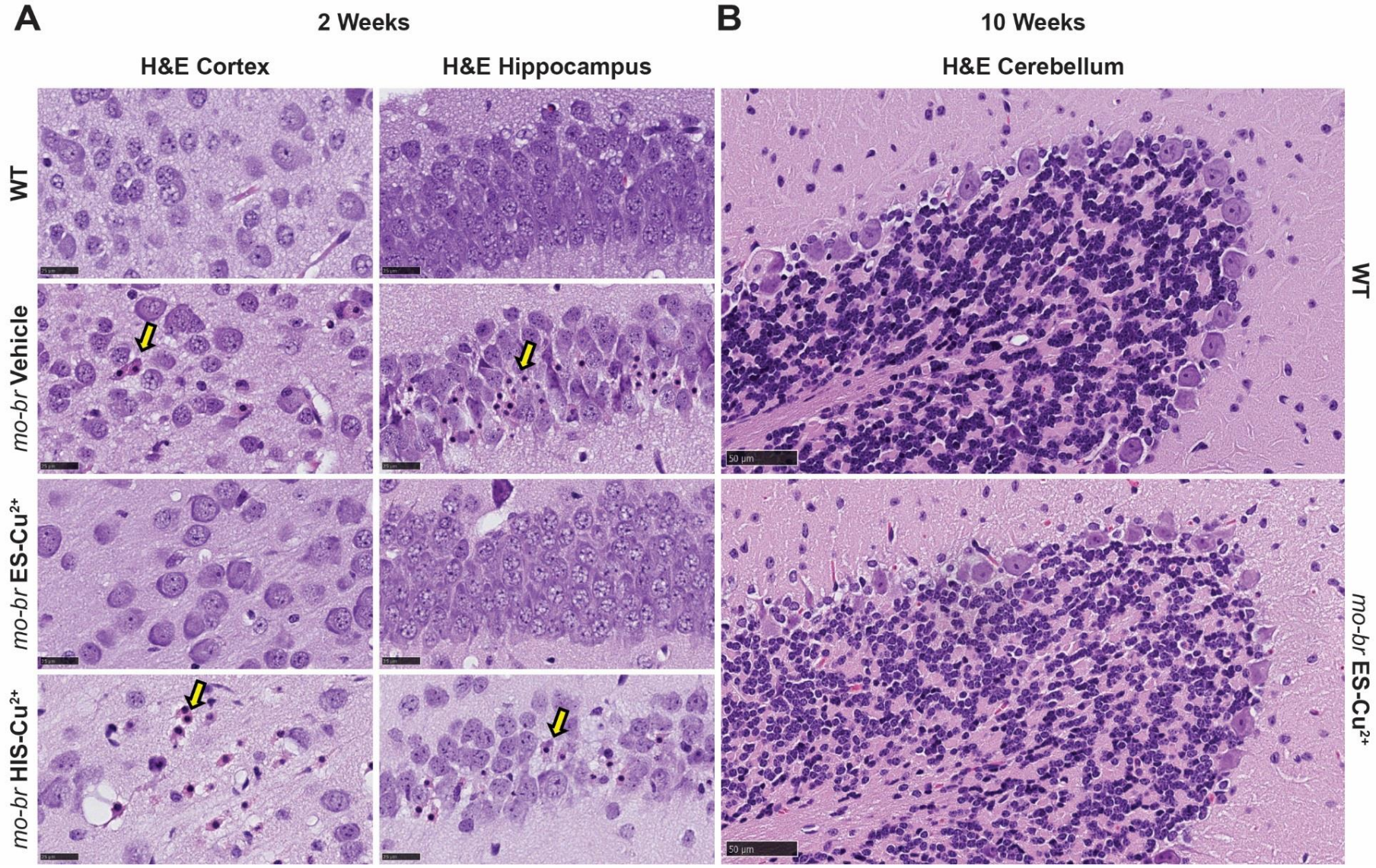
A
2 Weeks
H&E Cortex
H&E Hippocampus
B
10 Weeks
H&E Cerebellum
WT
mo-br Vehicle
mo-br ES-Cu2+
mo-br HIS-Cu2+
WT
mo-br ES-Cu2+
50 µm
50 µm

**Figure 3-13: Neuropathology of 2 and 10 week old mice.**

**A)** Cortex and hippocampus from PND 14 WT and *mo-br* mice administered vehicle, ES- $Cu^{2+}$ or HIS- $Cu^{2+}$. Somatomotor cortical neurons in *mo-br* vehicle and HIS-$Cu^{2+}$cohorts exhibit marked, diffuse neurodegenerative changes characterized by numerous pyknotic nuclei with eosinophilic cytoplasm (yellow arrows). In the hippocampus, the pyramidal neuron layer of region CA1 demonstrates degenerative changes including necrotic neurons in vehicle and HIS-$Cu^{2+}$ *mo-br* mice (yellow arrows). **B)** Cerebellar peduncles from PND 70 WT and *mo-br* ES-$Cu^{2+}$ mice revealed preservation of continuous Purkinje neuron layer. Scale bars represent 25 µm in cortical and hippocampal H&E slides. Scale bars represent 50 µm in cerebellar H&E slides.

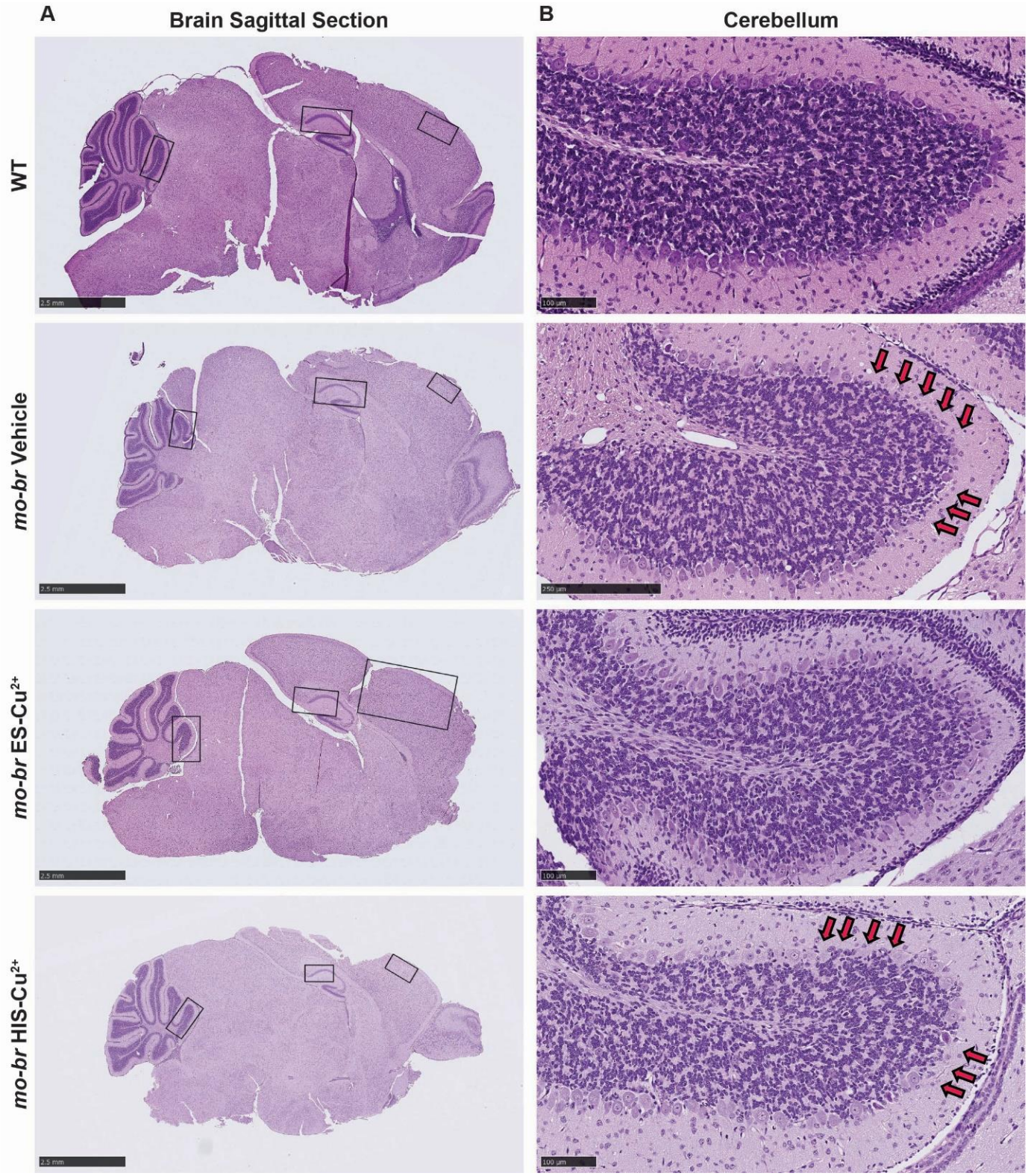
A
Brain Sagittal Section
B
Cerebellum
WT
mo-br Vehicle
mo-br ES-Cu2+
mo-br HIS-Cu2+
2.5 mm
100 µm
250 µm

**Figure 3-14: Additional neuropathology in 2 week old mice.**

**A**) Sagittal whole brain sections analyzed among cohorts. Surveyed areas represented by rectangular boxes (leftmost – cerebellum Fig. 14B, middle – hippocampus Fig. 13A, and rightmost – cortex Fig. 13A). Scale bars represent 2.5 mm. **B)** Cerebellum: Purkinje neuron layers are discontinuous (red arrows) and marked by rare necrotic nuclei in *mo-br* vehicle and HIS-$Cu^{2+}$ cohorts. Normal tissue architecture is preserved in *mo-br* ES-$Cu^{2+}$ mice. Scale bars represent 100 μm.

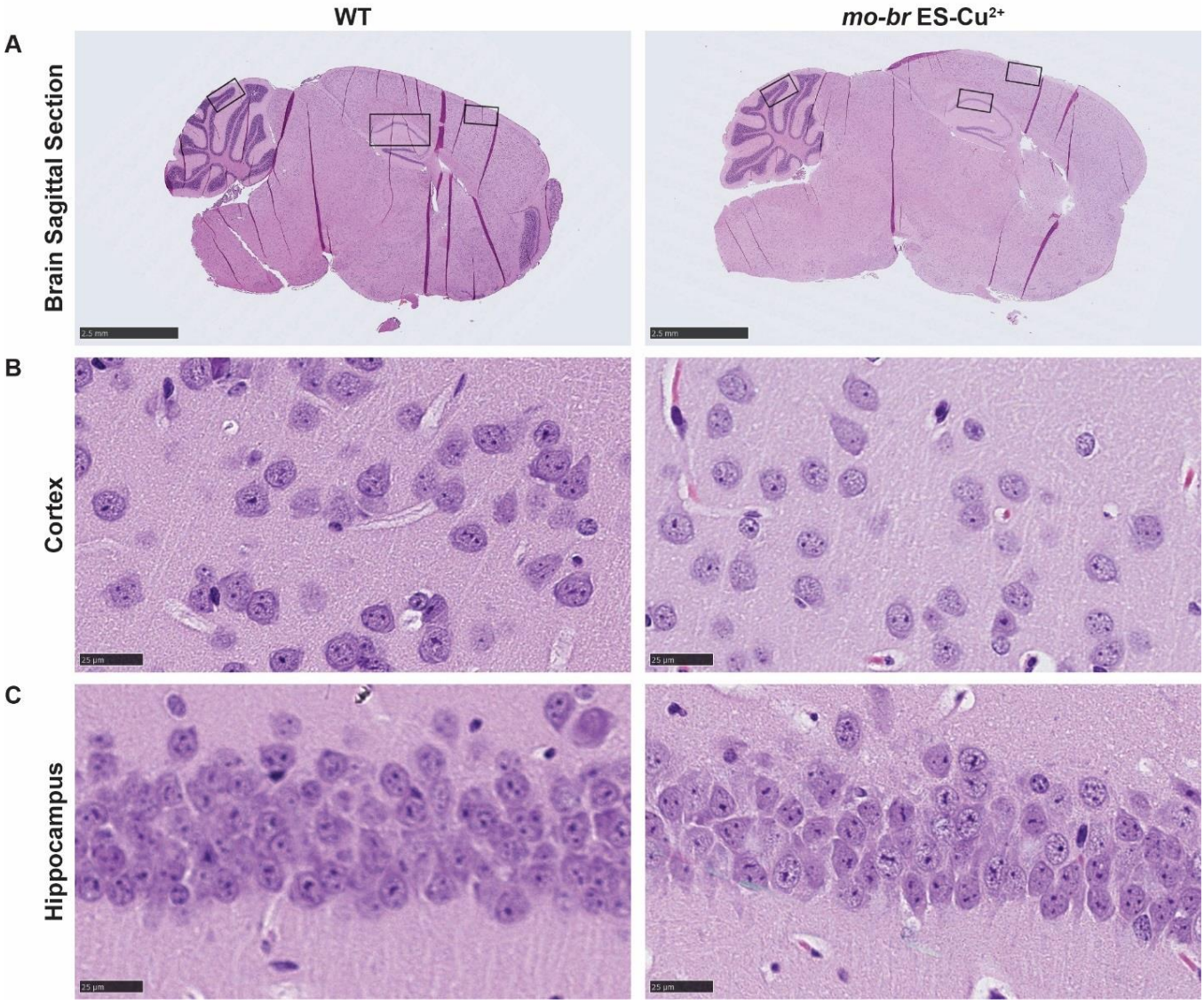


**Figure 3-15: Additional neuropathology in 10 week old mice.**

**A)** Sagittal brain sections analyzed among cohorts. Surveyed areas represented by rectangular boxes (leftmost – cerebellum Fig. 3-13B, middle – hippocampus Fig. 3-15C, and rightmost – cortex Fig. 3-15B). Scale bars represent 2.5 mm. **B)** Cortex: Neuroprotective effects of ES-$Cu^{2+}$ treatment persisted to 10 week assessment. Scale bars represent 25 µm. **C)** Hippocampus: Pyramidal neurons preserved. Scale bars represent 25 µm.

### 3.8. Biochemical Markers of ES-$Cu^{2+}$ Therapy

Two week old mice treated with ES-$Cu^{2+}$ showed normalized serum [Cu] (Fig. 3-16A) with increased brain [Cu] from the vehicle baseline of 22% of WT, to 41% (0.45 vs 0.82 $\mu g \cdot g^{-1}$, $p < 0.01$) compared to 24% with HIS-$Cu^{2+}$ (0.48 $\mu g \cdot g^{-1}$). ES-$Cu^{2+}$ proved superior to HIS-$Cu^{2+}$ at delivering Cu to brain tissue ($p < 0.01$) (Fig. 3-16B). Necropsy at 2 weeks showed significant decrease in total brain mass in *mo-br* animals treated with vehicle and HIS-$Cu^{2+}$ (-16% and -12%) (Fig. 3-16C) (Table 3-7, 3-8). ES-$Cu^{2+}$ normalized brain mass comparable to WT littermates (< 2% difference between WT and *mo-br* ES-$Cu^{2+}$ cohorts) (Fig. 3-16C) (Table 3-7).

Mitochondrial COX1 levels exhibited a 14% improvement with ES-$Cu^{2+}$ intervention (30% vs 16%, $p = 0.03$) (Fig. 3-16D, E). We did not observe any significant correction in COX1 levels in vehicle or HIS-$Cu^{2+}$ treated mice (17%, $p = 0.99$) (Fig. 3-16D, E). Though overall brain [Cu] was about 2.5-fold lower in ES-$Cu^{2+}$ cohort as compared to WT (0.75 vs 1.95 $\mu g \cdot g^{-1}$), the mitochondrial-specific delivery mechanism of ES-$Cu^{2+}$ could explain the degree of COX1 metalation. We also observed significant improvements in [Cu] and COX1 levels in hearts of ES-$Cu^{2+}$ treated *mo-br* mice as seen in previously described ES treatment in cardiac *Ctr1* KO mice (Fig. 3-17). SOD1 levels remained unchanged (Fig. 3-18).

At 10 weeks, COX1 levels in ES-$Cu^{2+}$ mice improved to 42% of WT. (Fig. 3-16F, G). Serum [Cu] reverted to earlier established *mo-br* baseline of 28% of WT (0.48 vs 1.73 $\mu g \cdot mL^{-1}$) (Fig. 3-16H). In the brain, Cu levels declined from 41% to 34% of WT (1.57 vs 4.64 $\mu g \cdot g^{-1}$) (Fig. 3-16J) but brain weights remained indistinguishable (0.448 vs 0.432 g, $p = 0.23$) (Fig. 3-16I) (Table 3-7, 3-8).

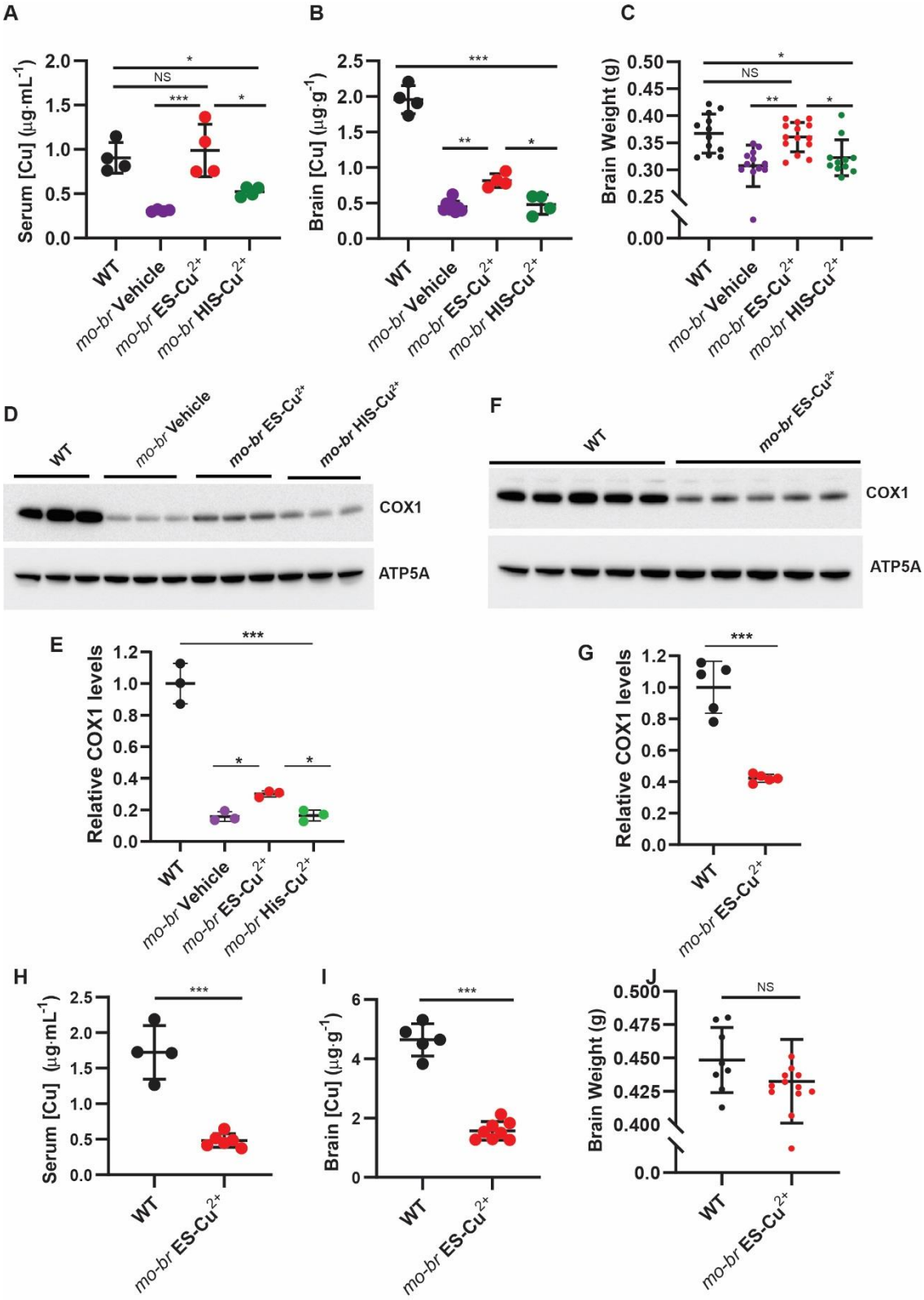
A
Serum [Cu] (µg·mL-1)
2.0
1.5
1.0
0.5
0.0
*
NS
***
*
WT
mo-br Vehicle
mo-br ES-Cu2+
mo-br HIS-Cu2+
B
Brain [Cu] (µg·g-1)
2.5
2.0
1.5
1.0
0.5
0.0
***
**
*
WT
mo-br Vehicle
mo-br ES-Cu2+
mo-br HIS-Cu2+
C
Brain Weight (g)
0.50
0.45
0.40
0.35
0.30
0.25
0.00
*
NS
**
*
WT
mo-br Vehicle
mo-br ES-Cu2+
mo-br HIS-Cu2+
D
WT
mo-br Vehicle
mo-br ES-Cu2+
mo-br HIS-Cu2+
COX1
ATP5A
F
WT
mo-br ES-Cu2+
COX1
ATP5A
E
Relative COX1 levels
1.2
1.0
0.8
0.6
0.4
0.2
0.0
***
*
*
WT
mo-br Vehicle
mo-br ES-Cu2+
mo-br His-Cu2+
G
Relative COX1 levels
1.2
1.0
0.8
0.6
0.4
0.2
0.0
***
WT
mo-br ES-Cu2+
H
Serum [Cu] (µg·mL-1)
2.5
2.0
1.5
1.0
0.5
0.0
***
WT
mo-br ES-Cu2+
I
Brain [Cu] (µg·g-1)
6
4
2
0
***
WT
mo-br ES-Cu2+
J
Brain Weight (g)
0.500
0.475
0.450
0.425
0.400
0.0
NS
WT
mo-br ES-Cu2+

**Figure 3-16: ES-$Cu^{2+}$ rescues biochemical phenotypes in 2 and 10 week old *mo-br* mice.**

**A)** Serum [Cu] at PND 14. (All cohorts *n* = 4) **B)** Brain [Cu] at PND 14. (All cohorts *n* = 4) **C)** Brain weights at PND 14. (WT *n* = 12, *mo-br* Vehicle *n* = 12, *mo-br* ES-$Cu^{2+}$+ *n* = 14, *mo-br* HIS-$Cu^{2+}$ *n* = 11, **D-E)** Brain COX1 at PND 14 (All cohorts *n* = 3). **F-G)** Brain COX1 at PND 70 (All cohorts *n* = 5) **H)** Serum [Cu] at PND 70. (WT *n* = 4, *mo-br* ES-$Cu^{2+}$ *n* = 6) **I)** Brain [Cu] at PND 70. (WT *n* = 5, *mo-br* ES-$Cu^{2+}$ *n* = 8) **J)** Brain weights at PND 70. (WT *n* = 8, *mo-br* ES-$Cu^{2+}$ *n* = 13). Data reported as mean ± SD with statistical significance assessed by one-way ANOVA or Welch one-way ANOVA with post hoc Tukey's HSD test. NS = not significant $*p < 0.05$, $**p < 0.01$, $***p < 0.001$. Western images analyzed with ImageJ software.

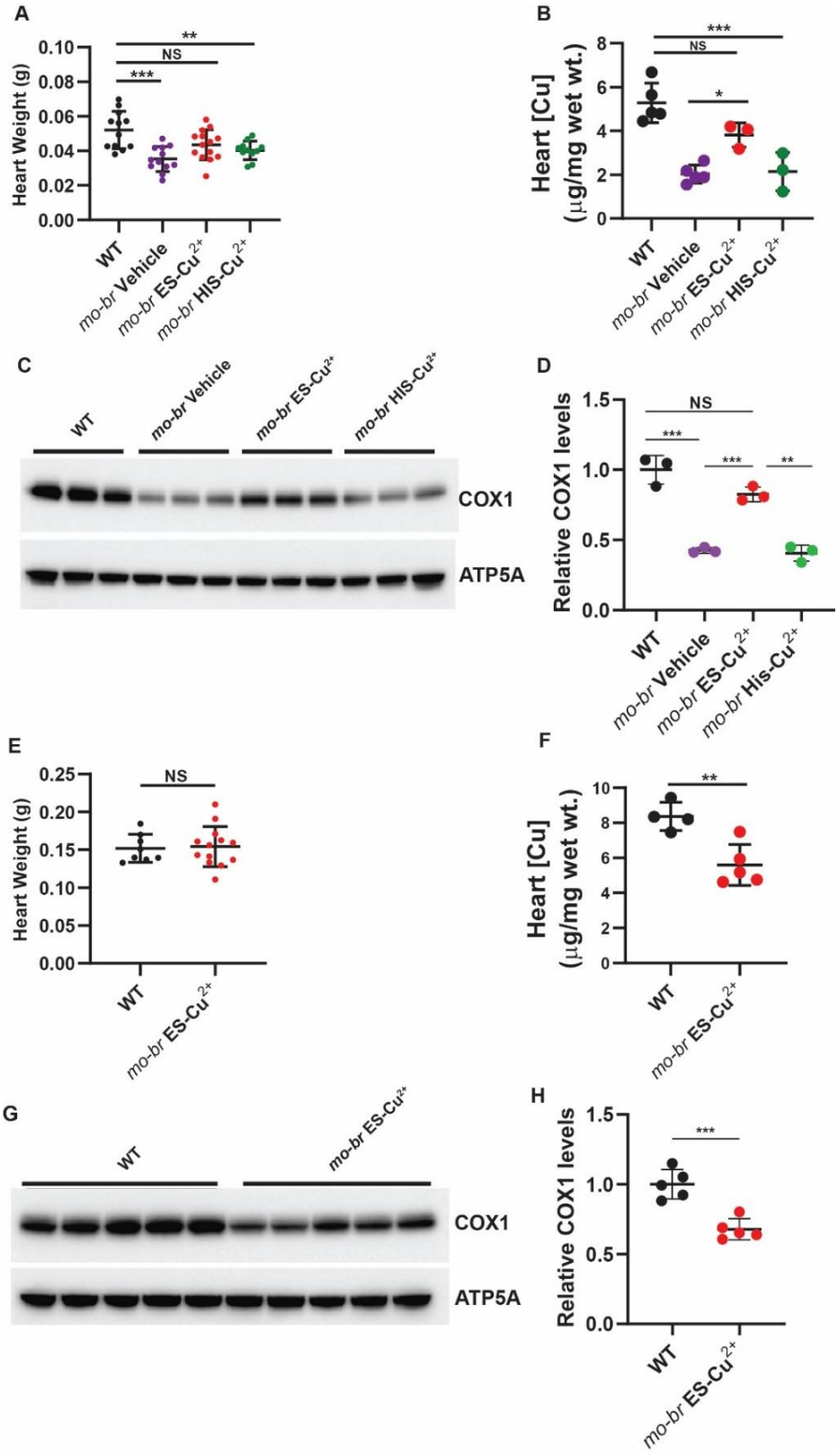
A
Heart Weight (g)
0.10
0.08
0.06
0.04
0.02
0.00
**
NS
***
WT
mo-br Vehicle
mo-br ES-Cu2+
mo-br HIS-Cu2+
B
Heart [Cu] (µg/mg wet wt.)
8
6
4
2
0
***
NS
*
WT
mo-br Vehicle
mo-br ES-Cu2+
mo-br HIS-Cu2+
C
WT
mo-br Vehicle
mo-br ES-Cu2+
mo-br HIS-Cu2+
COX1
ATP5A
D
Relative COX1 levels
1.5
1.0
0.5
0.0
NS
***
***
**
WT
mo-br Vehicle
mo-br ES-Cu2+
mo-br His-Cu2+
E
Heart Weight (g)
0.25
0.20
0.15
0.10
0.05
0.00
NS
WT
mo-br ES-Cu2+
F
Heart [Cu] (µg/mg wet wt.)
10
8
6
4
2
0
**
WT
mo-br ES-Cu2+
G
WT
mo-br ES-Cu2+
COX1
ATP5A
H
Relative COX1 levels
1.5
1.0
0.5
0.0
***
WT
mo-br ES-Cu2+

**Figure 3-17: Heart biochemistry *mo-br* mice.**

**A)** Heart weight at PND 14: *Mo-br* ES-$Cu^{2+}$ treatment normalizes heart weight compared to WT (0.043 vs 0.052 g, $p = 0.06$). (Cohorts $n = 12, 12, 14, \& 11$). **B)** Heart [Cu] at PND 14: ES-$Cu^{2+}$ treatment increased heart [Cu] from baseline vehicle levels of 2.0 to 3.8 $\mu g \cdot g^{-1}$ ($p = 0.02$) and proved superior to HIS-$Cu^{2+}$ (2.1 $\mu g \cdot g^{-1}$, $p = 0.01$). ES-$Cu^{2+}$ normalize heart [Cu] to WT levels (5.3 $\mu g \cdot g^{-1}$, $p = 0.06$). ES-$Cu^{2+}$ improved [Cu] from 38% to 72% of WT levels—an approximate increase of 34%. For comparison, HIS-$Cu^{2+}$ improved mean heart [Cu] by only 2% (2.1 $\mu g \cdot g^{-1}$, $p = 0.98$). (Cohorts $n = 5, 5, 3, \& 3$). **C)** COX1 at PND 14. **D)** COX1 Relative levels at PND 14: ES-$Cu^{2+}$ improved COX1 abundance by 41.6% relative to vehicle (0.835 vs 0.406, $p = 0.002$). HIS-$Cu^{2+}$ did not significantly improve COX1 abundance (0.426, $p = 0.98$). **E)** Heart weight at PND 70 (Cohorts $n = 8 \& 13$). **F)** Heart [Cu] PND 70: Heart [Cu] declined to 67% of WT (5.6 vs 8.4 $\mu g \cdot g^{-1}$, $p < 0.01$). (Cohorts $n = 4 \& 5$). **G)** COX1 at PND 70. **H)** COX1 Relative levels at PND70: ES-$Cu^{2+}$ *mo-br* adults 67.9% of WT ($p < 0.001$). (NS = not significant, $*p < 0.05$, $**p < 0.01$, $***p < 0.001$). All data reported as mean ± SD. Statistical analysis reported as one-way ANOVA or Welch ANOVA with post hoc Tukey's multiple comparisons test or unpaired t-test.

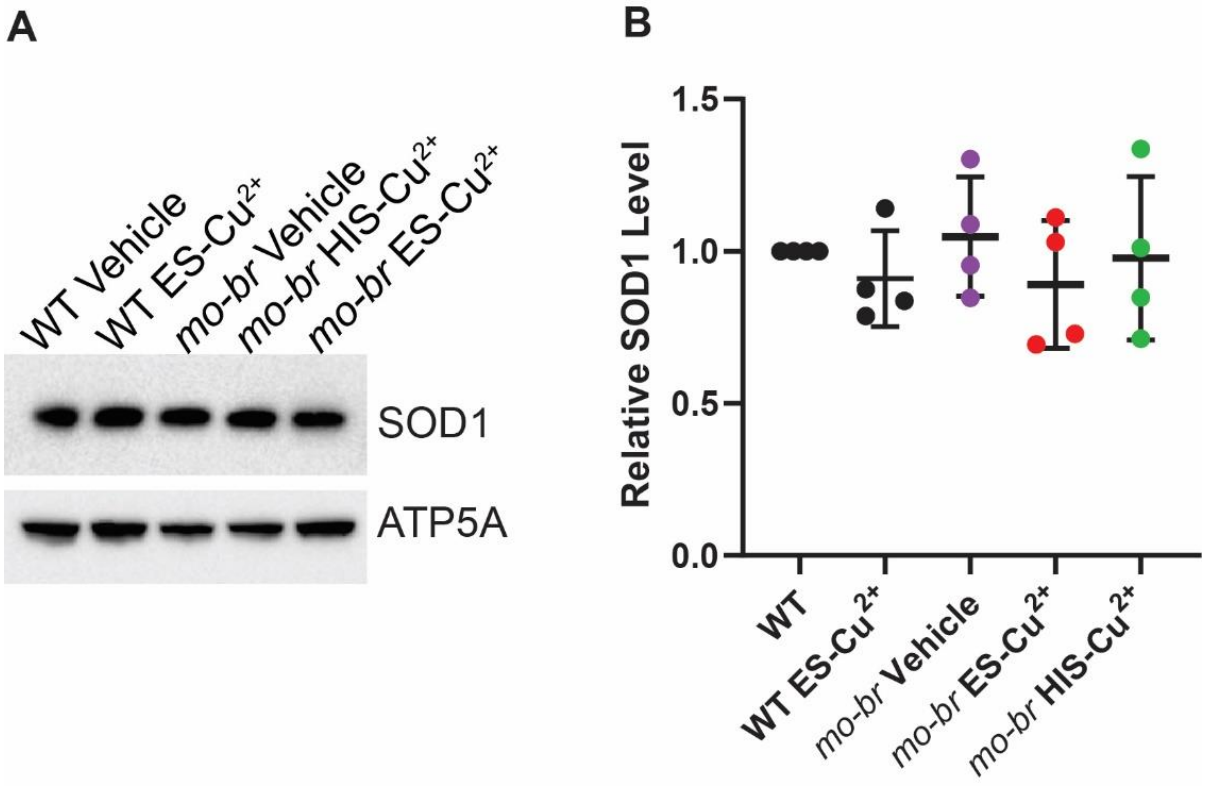


**Figure 3-18: Effects of ES treatment on SOD1 levels in *mo-br* mice.**

**A)** Representative Western blot depicting SOD1 abundance in brain tissue of two-week-old mice. **B)** Quantification of relative abundance ($n = 4$). No significance found between cohorts ($p > 0.01$). All data reported as mean ± SD. Statistical analysis reported as one-way ANOVA with post hoc Tukey's multiple comparisons test. Western images analyzed using ImageJ software.

**Table 3-7: Body, brain, and heart weights at 2 & 10 week necropsy.**

| 2 Weeks | | Organ Weights (g) | | | | | |
|---|---|---|---|---|---|---|---|
| | | Body Weight | | Brain | | Heart | |
| Cohort | *n* | Mean | p-value | Mean | p-value | Mean | p-value |
| WT Vehicle | 12 | 8.0 ± 0.9 | - | 0.3669 ± 0.0362 | - | 0.0520 ± 0.0052 | - |
| WT ES-$Cu^{2+}$ | 11 | **7.2 ± 1.0** | **0.03** | 0.3784 ± 0.0438 | 0.93 | 0.0589 ± 0.0047 | 0.11 |
| *mo-br* ES-$Cu^{2+}$ | 14 | **5.1 ± 0.7** | **< 0.01** | 0.3603 ± 0.0274 | 0.95 | 0.0435 ± 0.0087 | 0.09 |
| *mo-br* His-$Cu^{2+}$ | 11 | **4.7 ± 0.7** | **< 0.01** | **0.3220 ± 0.0336** | **0.01** | **0.0403 ± 0.0054** | **< 0.01** |
| *mo-br* Vehicle | 12 | **3.9 ± 0.5** | **< 0.01** | **0.3070 ± 0.0386** | **< 0.01** | **0.0353 ± 0.0072** | **< 0.01** |
| **10 Weeks** | | **Organ Weights (g)** | | | | | |
| | | **Body Weight** | | **Brain** | | **Heart** | |
| **Cohort** | ***n*** | **Mean** | **p-value** | **Mean** | **p-value** | **Mean** | **p-value** |
| WT Vehicle | 8 | 30.7 ± 1.5 | - | 0.4484 ± 0.0245 | - | 0.1519 ± 0.0184 | - |
| WT ES-$Cu^{2+}$ | 7 | 30.8 ± 2.2 | 0.99 | 0.4523 ± 0.0316 | 0.95 | 0.1513 ± 0.0155 | 0.99 |
| *mo-br* ES-$Cu^{2+}$ | 13 | **25.2 ± 2.6** | **< 0.01** | 0.4523 ± 0.0315 | 0.33 | 0.1542 ± 0.0265 | 0.97 |

All data reported as mean ± SD. Statistical analysis reported as one-way ANOVA with post hoc Tukey's multiple comparisons test for each organ analyzed.

**Table 3-8: Thymus, lungs, kidney, liver, and spleen weights at 2 & 10 week necropsy**

| 2 Weeks | | Organ Weights (g) | | | | | | | | | |
|---|---|---|---|---|---|---|---|---|---|---|---|
| | | Thymus | | Lungs | | Kidney | | Liver | | Spleen | |
| **Cohort** | ***n*** | **Mean** | **p-value** | **Mean** | **p-value** | **Mean** | **p-value** | **Mean** | **p-value** | **Mean** | **p-value** |
| **WT Vehicle** | 12 | 0.0602 ± 0.0130 | - | 0.1001 ± 0.0126 | - | 0.0545 ± 0.0545 | - | 0.3277 ± 0.1194 | - | 0.0352 ± 0.0139 | - |
| **WT ES-$Cu^{2+}$** | 11 | 0.0607 ± 0.0091 | 0.99 | 0.0940 ± 0.0146 | 0.65 | **0.0678 ± 0.0118** | **0.02** | 0.3869 ± 0.0387 | 0.41 | 0.0496 ± 0.0106 | 0.06 |
| ***mo-br* ES-$Cu^{2+}$** | 14 | **0.0442 ± 0.0123** | **0.01** | **0.0812 ± 0.0174** | **< 0.01** | 0.0501 ± 0.0107 | 0.92 | 0.2647 ± 0.0448 | 0.32 | 0.0282 ± 0.0096 | 0.5 |
| ***mo-br* His-$Cu^{2+}$** | 11 | **0.0427 ± 0.0097** | **< 0.01** | 0.0880 ± 0.0230 | 0.19 | 0.0479 ± 0.0120 | 0.44 | 0.3255 ± 0.0735 | 0.99 | 0.0351 ± 0.0112 | 0.99 |
| ***mo-br* Vehicle** | 12 | **0.0143 ± 0.0085** | **< 0.01** | **0.0621 ± 0.0221** | **< 0.01** | **0.0300 ± 0.0065** | **< 0.01** | **0.1298 ± 0.0278** | **< 0.01** | **0.0070 ± 0.0039** | **< 0.01** |
| **10 Weeks** | | **Organ Weights (g)** | | | | | | | | | |
| | | **Thymus** | | **Lungs** | | **Kidney** | | **Liver** | | **Spleen** | |
| **Cohort** | ***n*** | **Mean** | **p-value** | **Mean** | **p-value** | **Mean** | **p-value** | **Mean** | **p-value** | **Mean** | **p-value** |
| **WT Vehicle** | 8 | 0.0494 ± 0.0079 | - | 0.2073 ± 0.0143 | - | 0.1883 ± 0.0351 | - | 1.3956 ± 0.0823 | - | 0.0879 ± 0.0057 | - |
| **WT ES-$Cu^{2+}$** | 7 | 0.0459 ± 0.0110 | 0.98 | 0.1988 ± 0.0137 | 0.44 | 0.2009 ± 0.0160 | 0.59 | 1.3937 ± 0.0713 | 0.99 | **0.0936 ± 0.0054** | **0.01** |
| ***mo-br* ES-$Cu^{2+}$** | 13 | 0.0497 ± 0.0161 | 0.45 | **0.1751 ± 0.0335** | **< 0.01** | 0.1818 ± 0.0308 | 0.89 | **1.2178 ± 0.1270** | **< 0.01** | **0.1162 ± 0.0348** | **0.03** |

All data reported as mean ± SD. Statistical analysis reported as one-way ANOVA with post hoc Tukey's multiple comparisons test for each organ analyzed.

### 3.9. Discussion

While deficiencies in Cu transport and processing adversely affect numerous important biological pathways, the most profound pathological changes occur owing to perturbation of the electron transport chain *(5, 6)*. Specifically, CcO requires Cu for assembly and catalytic activity of two subunits COX1 and COX2 *(1)*. CcO dysfunction secondary to Cu deficiency results in cardiomyopathy, neurodegeneration, and premature death *(13, 14)*. ES at relatively low dose, stopped early mortality, and conferred near normal cardiac and brain histology while improving COX1 abundance in Cu deficient cardiac-specific *Ctr1* KO and *mo-br* mice *(29)*.

In the cardiac *Ctr1* KO mouse, affected animals possess elevated serum [Cu] *(20)*; allowing for in vivo ES-$Cu^{2+}$ complex formation and redistribution of Cu across CTR1-deficient cardiomyocyte membranes to mitochondria for metalation of CcO without supplementation of exogenous Cu. ES treatment completely reversed the delayed growth and slowed disease progression in these mice. ES treated mice exhibited improved survival at PND 26. Heart COX1 levels improved from 34% baseline to 66% (+28%) with a corresponding normalization of heart weight and reduced cardiomyocyte area despite only modest improvement in total tissue Cu levels.

HIS-$Cu^{2+}$ clinical trials for Menkes disease have shown mixed results. While there was some improvements in survival and clinical markers, it was primarily for a subset of patients with mutations that display residual ATP7A activity *(14, 15)*.

The *mo-br* mouse, possessing little residual transporter functionality *(22)*, only marginally benefits from HIS-$Cu^{2+}$ therapy. In contrast, ES-$Cu^{2+}$ significantly improves total brain tissue [Cu] levels compared to HIS-$Cu^{2+}$ with improved outcomes for survival, restoration of growth, preservation of neurological structures, tissue Cu delivery, and COX1 abundance. Two doses of ES-$Cu^{2+}$, equaling approximately 4 μg of Cu by PND 10, rescued *mo-br* males and improved median survival from 14 to 203 days.

The 14% improvement in brain COX1 level in two-week-old mice sufficiently preserved key neurological structures, such as cortical and hippocampal neurons. Preservation of brain structures and COX1 persisted past the two-week assessment. At ten weeks of age, the ES-$Cu^{2+}$ treated *mo-br* mice demonstrated normal brain structures and increased COX1 metalation with only small defects in gross neuromotor function as determined by open field, rotarod, grip strength, and gait treadmill.

Our in vivo results indicate the mechanism of ES-mediated Cu relocalization may not be limited to the mitochondria. Morphological changes in fur pigmentation and whisker structure indicate improvement in the secretory pathway cuproenzymes tyrosinase and sulfhydryl oxidase, enzymes whose metalation requires ATP7A activity in the Golgi complex. Partial improvement in other secretory pathway cuproenzymes, such as dopamine-β-hydroxylase and lysyl oxidase, could further explain the beneficial effects given the profound deficiency of most Cu-utilizing systems associated with Menkes disease.

Administration of ES or ES-$Cu^{2+}$ complex in a 1:1 stoichiometry and appropriate formulation exhibited good pharmacokinetic properties, low toxicity, and efficacy. Our results indicated ES corrects defective CTR1 and ATP7A membrane Cu transport with beneficial, targeted improvement of mitochondrial CcO metalation owing to the ES-$Cu^{2+}$ complex's unique mechanism of selective mitochondrial Cu release. The membrane-permeating properties of ES, coupled with its directed release mechanism, make this agent a good candidate for drug repurposing as a Cu courier for disorders impacting metalation of CcO. Our results in cardiac *Ctr1* KO and *mo-br* mice indicated ES or ES-$Cu^{2+}$ holds promise as a potential, efficacious therapeutic agent for the treatment of hereditary Cu deficiency disorders.

## 3.10. Materials & Methods

Materials and Methods as reported in Supplementary Material for Guthrie et al., Elesclomol alleviates Menkes pathology and mortality by escorting Cu to cuproenzymes in mice. *Science.* 2020 May 8; 368(6491): 620-625.

doi: 10.1126/science.aaz8899

Supple. NIHMS1594772-supplement-Supplementary_Science.pdf

GUID: BA310408-997A-4A17-ACAB-02771366F04C.

### 3.10.1. Reagents

Elesclomol (> 98.8%) was purchased from Accel Pharmtech (E. Brunswick, NJ). Captisol®, a proprietary β-cyclodextrin SBE derivative, was purchased from CyDex Pharmaceuticals, Inc. (Lenexa, KS). Methocel™ A15 LV, a proprietary carboxymethyl cellulose, was purchased from Dow, Inc. (Midland, MI). All other chemicals and reagents were purchased from Sigma-Aldrich unless otherwise noted.

### 3.10.2. Synthesis of Elesclomol-$Cu^{2+}$ Complex

The copper complex of ES was synthesized as described by Yadav et al, *J Inorg Biochem*. 2013/PMID: 23707906. Briefly, to a stirred solution of 6.0 mmol ES in ethanol, excess $CuCl_2 \cdot 2H_2O$ was added and stirred at room temperature for one hour to allow complete 1:1 stoichiometric complexation. Crude solid was precipitated by the addition of water and collected by filtration. The solid was dissolved in methylene chloride and filtered. The methylene chloride solution was further washed three times with water followed by acetone, dried with $Na_2SO_4$, and a solid recovered following solvent removal in a rotary evaporator. Solid was further purified by two rounds of crystallization from acetonitrile followed by a final, 48-hour lyophilization yielding a fine, dark reddish-brown powder. Powder was stored at 4°C for pharmacological formulations.

### 3.10.3. Synthesis of Copper Histidine Complex

The copper complex of histidine was synthesized as described by Gala et al, *Molecules.* 2014/PMID: 24434671. Briefly, to a stirred solution of 0.2 mmol pharmaceutical grade L-histidine in 100 mM HEPES buffer pH 7.4, $CuCl_2 \cdot 2H_2O$ (17.05 mg) was added and stirred at room temperature for three hours to allow complete 2:1 stoichiometric complexation. The resulting dark blue solution was filtered to remove particulates and stored at 4°C for use as a 50 mM HIS-$Cu^{2+}$ stock solution for pharmacological formulations.

### 3.10.4. *In vivo* Pharmacokinetics and Toxicological

*Formulation:* Phase solubility assays were conducted to determine suitability of vehicles for ES and ES-$Cu^{2+}$ complex in Methocel™ A15-LV and Captisol® per technical materials. Briefly, 500 µL Captisol® preps at 40%, 20%, 10%, and 5% (w/v) were mixed with 5, 2.5, 1.25, and 0.63 mg ES or ES-$Cu^{2+}$ powder in micro centrifuge tubes. Solutions were sonicated and continuously agitated overnight with micro spin bars at 30°C to ensure maximum dissolution. Samples were centrifuged at 6000 rpm for 2 hours to pellet out undissolved material. Solvated ES and ES-$Cu^{2+}$ was quantified by LC-MS. A similar protocol was followed for Methocel™ at 2.0%, 1.0%, 0.5%, and 0.25% (w/v) utilizing 2% DMSO final concentration as an excipient. Methocel™ poorly solubilized ES-$Cu^{2+}$ but adequately solubilized ES and was used for cardiac *Ctr1* KO mouse experiments. 20% Captisol® aqueous vehicle was used for ES-$Cu^{2+}$ administration for *mo-br* mouse experiments.

*ES & ES-$Cu^{2+}$ Tolerability:* Cohorts of five C57BL/6 adult female mice averaging 20 g were administered 25 mg/kg ES, 7.25 mg/kg ES-$Cu^{2+}$, 3.625 mg/kg ES-$Cu^{2+}$, 0.5% Methocel™ vehicle or 20% Captisol® vehicle via 400 µL subcutaneous injection. Mice were monitored daily for signs of acute toxicity, injection site reaction, and changes in total body weight. Body weight measurements were conducted on day 0, 5, and 10 of protocol and analyzed as percent change from initial weight. Vehicle, ES, and ES-$Cu^{2+}$ cohorts were then compared.

*ES & ES-$Cu^{2+}$ Pharmacokinetics:* C57BL/6 adult mice averaging 20 g were administered ES subcutaneously in 0.5% Methocel™, 2% DMSO aqueous vehicle at 10 mg/kg. ES-$Cu^{2+}$ was administered as a single bolus dose by intravenous, subcutaneous, or oral routes formulated in 20% Captisol® aqueous vehicle at 3.625 (IV), 7.25 (SubQ), and 10.875 (Oral) mg/kg. Serial blood sampling was conducted at 0, 0.05, 0.25, 0.5, 1, 2, 4, 8, and 24 hours with each time point representing a biological triplicate. Whole blood was collected in heparinized tubes and spun down at 2200 rpm for five minutes. Plasma was collected and frozen at -80°C until quantitative analysis by LC-MS. Non-compartmental and compartmental analysis was conducted using PKSolver software as described in Zhang et al, *Comput Methods Programs Biomed.* 2010/PMID: 20176408. Intravenous and/or subcutaneous PK parameters were generated in PKSolver using a single (Methocel™, ES) or type 2a 2-compartment (Captisol®, ES-$Cu^{2+}$) model. Oral route was not modeled due to poor systemic exposure. Bioavailability was calculated manually using the following equation:

$$F_{abs} = [(AUC_{0\text{-}inf})_{Oral/SQ} \text{ X } D_{IV}]/[(AUC_{0\text{-}inf})_{IV} \text{ X } D_{Oral/SQ}] \text{ X } 100\%$$

### 3.10.5. Brain Elesclomol-$Cu^{2+}$ Exposure

Cohorts of six postnatal age 7 day pups and adult C57BL/6 mice were administered ES-$Cu^{2+}$ as a single bolus dose at 7.25 mg/kg via subcutaneous injection in 20% Captisol®. Two mice of each age group were administered vehicle only. Mice were euthanized by isoflurane overdose and thoracotomy. Blood was removed by cardiocentesis and carcasses perfused with 20-50 mL normal saline. Brains were harvested, flash frozen with liquid nitrogen, and stored at -80°C pending analysis.

### 3.10.6. LC-MS Quantification in Plasma and Brain

*Plasma Processing:* Plasma collected from mice was thawed and 100 µL extracted with two 500 µL volumes of acetonitrile. Samples were spun down at 2200 rpm for five minutes and supernatant transferred to clean 1.7 mL micro centrifuge tube. Solvent was evaporated in a Vacufuge™ (Eppendorf™) concentrator at 45°C for 3 hours. Plasma extracts were reconstituted in 100 µL acetonitrile + 0.1% formic acid spiked with 100 ng/mL fluconazole internal standard. Constitution of standards involved spiking of ES/ES-$Cu^{2+}$ in control plasma ranging from 1000 ng/mL to 1.93 ng/mL followed by identical processing to correct for matrix effects. All samples were run as biological triplicates and technical duplicates.

*Brain Processing:* Brain tissue was mechanically pulverized by ball milling using a CryoMill (Retsch® Newtown, PA). Homogenate was collected and extracted with 36 µL of extraction buffer consisting of 75% acetonitrile, 25% methanol + 0.2% formic acid spiked with 100 ng/mL fluconazole internal standard per milligram of tissue. 4 µL of ultrapure water per milligram of tissue was added and mixture vortexed for 30 s. Mixture was then centrifuged at 6000 rpm, 4°C and supernatant collected for analysis. Constitution of standards involved spiking of ES or ES-$Cu^{2+}$ in control brain homogenate ranging from 1000 ng/mL to 1.93 ng/mL followed by identical processing to correct for matrix effects. All samples were run as biological triplicates and technical duplicates.

*LC-MS Protocol:* ES and ES-$Cu^{2+}$ in plasma and brain were detected and quantified on a triple quadrupole mass spectrometer (Quantiva, Thermo Scientific, Waltham, MA) coupled to a binary pump HPLC (UltiMate 3000, Thermo Scientific). MS parameters were optimized for the target compound under direct infusion at 5 µL $min^{-1}$ to identify the SRM transitions (precursor/product fragment ion pairs). Samples were maintained at 4 °C on an autosampler before injection. The injection volume was 10 µL. Chromatographic separation was achieved on a Hypersil Gold 5 µm 50 x 3 mm column (Thermo Scientific) maintained at 30 °C using a solvent gradient method. Solvent A was 0.1% formic acid in water. Solvent B was 0.1% formic acid in acetonitrile. The gradient method used was 0-1.6 min (20% B to 80% B), 1.6-4 min (80% B) and 4-5 min (80% B to 20% B). The flow rate was 0.5 mL $min^{-1}$. Sample acquisition and analysis was performed with TraceFinder 3.3 (Thermo Scientific).

### 3.10.7. Cardiac *CTR1* Knockout Mice

The cardiac-specific *Ctr1* deletion mouse (*Ctr1*$^{hrt/hrt}$) was generated by crossing *Ctr1*$^{flox/flox}$ mice (Nose et al, *Cell Metab.*, 2006/PMID:16950140) with mice expressing Cre recombinase driven by the promoter of cardiac-expressed α-Myosin Heavy Chain (MHC) obtained from the Jackson Laboratory as performed previously (Kim et al, *Cell Metab.*, 2010/PMID: 20444417). Age-matched *Ctr1*$^{flox/+}$ or *Ctr1*$^{flox/flox}$ siblings not expressing Cre served as control animals. All mouse genotypes were confirmed by performing *Ctr1* excision genotyping PCR on cardiac tissue as previously described in Kim et al 2010 and cardiac *Ctr1* protein levels in selected mice were determined by immunoblot. All mice were maintained on the C57BL/6 genetic background. All animal procedures were performed in accordance with the National Institutes of Health Guide and approved by the Institutional Animal Care and Use Committee (IACUC) at the University of Maryland, College Park (Protocol # R-APR-18-14).

### 3.10.8. *Mottled-brindled* Mice

Heterozygous C57BL/6-*Atp7A*$^{+/mo\text{-}br}$ /J females and wildtype C57BL/6-*Atp7A*$^{+/y}$/J males were procured from the Jackson Laboratory. Mice were housed in an OptiMice® animal care system with 14/10 hour light-dark cycle. Breeding for experimental and colony maintenance purposes involved random sibling crosses between carrier females and wild-type males. Cage and nutritional enrichment in the form of nestlets, shepherd

huts, and Love Mash® (Bio-Serv) reproductive supplement was provided in addition to Teklad 4% fat standard diet (Envigo) and water *ad libitum*. Litter size for experimental pairs was reduced to 3-4 pups by culling of females. On post-natal day 5, tail snip biopsies of males were used to confirm genotypes of pigment deficient mice. Genomic DNA was isolated and amplified using PCR forward primer (5' TTAATCTATAGGGCAAAACCT) and reverse primer (5' GAGTTCAGAGTTACAATAGTG 3') containing the *mo-br* 6-bp deletion followed by electrophoretic separation on a polyacrylamide gel. All breeding and experimental procedures were approved by the Texas A&M University IACUC under protocols #2017-0380 and #2018-0069.

### 3.10.9. Administration of Elesclomol to Cardiac *Ctr1* Knockout Mice

*ES Formulation & Delivery:* 10 mg/kg body weight ES or 0.5% Methocel™ vehicle (final 2% DMSO) was subcutaneously administered to cardiac *Ctr1* KO and WT control mice every three days until post-natal day 26 after which dosing frequency was reduced to once weekly until post-natal day 54. Weight adjusted amounts of ES were first dissolved in DMSO and mixed with Methocel™ solution to reach a 2% final DMSO concentration. Mouse body weight was recorded daily from post-natal day 5 to 26 then weekly from 26 to 54. Survival and growth curves were generated from observational data. Subsequent subsets of mice on post-natal day 10 and 26 were harvested for histological and biochemical analysis.

### 3.10.10. Administration of substances to *mo-br* Mice

*ES Formulation & Delivery:* 2X stock solution of ES was prepared by wetting 2.5 mg ES base with 10 mL 20% Captisol® solution. Slurry was sonicated for 5 min. at 30°C and continuously mixed at constant temperature for 3 hours to ensure complete dissolution. Material was filtered and stored at 4°C yielding a stock of 250 µg/mL. Final formulation involved 1:2 dilution of stock with Captisol® to 125 µg/mL with adjustment of pH to 7.4 with 0.2 N NaOH. ES final product was sterilized by 0.2 µm filtration. Each 100 µL subcutaneous dose contained 12.5 µg ES. Pups received injections on postnatal days 7 and 10 for a total ES dose of 25 µg.

*ES-$Cu^{2+}$ Formulation & Delivery:* 2X stock solution of ES-$Cu^{2+}$ was prepared by wetting 2.9 mg complex with 10 mL 20% Captisol® solution. Slurry was sonicated for 5 min. at 30°C and continuously mixed at constant temperature for 3 hours to ensure complete dissolution. Material was filtered and stored at 4°C yielding a stock of 290 µg/mL. Final formulation involved 1:2 dilution of stock with Captisol to 145 µg/mL with adjustment of pH to 7.4 with 0.2 N NaOH. ES-$Cu^{2+}$ final product was sterilized by 0.2 µm filtration. Each 100 µL subcutaneous dose contained 14.5 µg ES-$Cu^{2+}$ (12.5 µg ES, 2 µg $Cu^{2+}$). Pups received injections on postnatal days 7 and 10 for a total ES-$Cu^{2+}$ dose of 29 µg (25 µg ES, 4 µg $Cu^{2+}$).

*HIS-$Cu^{2+}$ Formulation & Delivery:* 72 µL of 50 mM (16.3 mg/mL) HIS-$Cu^{2+}$ in 100 mM HEPES was added to a stirring solution of 9.93 mL 20% Captisol®. pH was adjusted to 7.4 using 0.2 N NaOH and filter sterilized. Final formulation concentration was 116.7 µg/mL. Each 100 µL subcutaneous dose contained 11.67 µg HIS-$Cu^{2+}$ (9.67 µg Histidine, 2 µg $Cu^{2+}$) and 20 µg inert Captisol®. Final HEPES concentration was negligible at 0.72 mM. Pups received injections on postnatal days 7 and 10 for a total HIS-$Cu^{2+}$ dose of 23.3 µg (19.34 µg HIS, 4 µg $Cu^{2+}$).

All formulation work was conducted in a class II, type 2a laminar flow biosafety cabinet. All reagents were of pharmaceutical or cell culture grade. Each 100 µL treatment contained 20 µg inert Captisol® delivered by a 27G, 0.5cc allergy syringe with permanently attached needle (BD Biosciences, San Jose, CA).

### 3.10.11. Growth Curves and Kaplan-Meier Survival Plot

Treated pups were weighted daily from PND 5 to PND 70 (10 weeks) and monitored for survival. The primary growth and survival study endpoints concluded on PND 70. Mice at 10 weeks were then divided into groups for behavioral, biochemical, and histological assessment. A subset of WT ($n$ = 5), WT ES-$Cu^{2+}$ ($n$ = 4), and ES-$Cu^{2+}$ *mo-br* ($n$ = 11) mice were monitored without further manipulation until PND 245 (35 weeks) in order to calculate median survival. Only observations and weekly weightings were conducted for this subset between weeks 11 – 35.

Growth curves and Kaplan-Meier survival plots were generated from body weight and survival data. To assess immediate effects of interventions, additional pups were treated on PND 7 and 10 for biochemical and histological characterization of intervention effects.

### 3.10.12. Locomotor Function

The following protocols were conducted utilizing WT ($n$ = 8) and ES-$Cu^{2+}$ treated *mo-br* ($n$ = 13) mice between 10-13 weeks of age at the TAMU Rodent Preclinical Phenotyping Core (College Station, TX). Mice were randomly assessed during mid-light cycle in environmentally controlled settings. Mice were allowed to acclimate for 1 hour before activity initiation.

*Open Field Assessment:* Mice were placed in open field chambers (Tru Scan Activity System 2.0, Coulbourn Instruments) for 30 minutes. Test chambers and sensor plates were disinfected between runs. Animals completing assessment were temporarily housed in holding cages before returning to home housing. Data for each mouse were collected and averaged for three trials over a six-day period of time with one rest day between assessments. Vector traces and measured parameters were exported to Excel for processing and data analysis.

*Forelimb Strength Assessment:* Mice were suspended by the tail and allowed to grasp a horizontally orientated metal mesh plate consisting of 1 mm diameter wire connected to a Chatillon force meter. Gentle horizontal force was applied to the mouse until maximum grip strength is achieved and the mouse released the plate. Average maximum force (N) of three trials separated by rest periods of 15 minutes were recorded in Excel for data analysis.

*Rotarod Assessment:* Mice were trained on the rotarod (UGO Basile model 7650) for three sessions at constant rotation of 4 rpm the week before testing. To assess motor performance, mice were placed on an accelerating rotarod (4 rpm to 40 rpm 5 min.) for a maximum of 420 seconds. Latency to fall or passive rotation (s) was recorded and averaged for three trials per session with three sessions over a six day period of time.

*DigiGait™ Assessment:* Gait assessment was conducted as described by Lambert et al, *Behav Brain Res.* 2015/PMID: 25116252 with modifications. Briefly, mice were trained for five consecutive days before data collection on the DigiGait™ system. Training sessions included three runs per day separated by a 2-hour rest interval. Mice began training at 12 cm/s which was accelerated to 24 cm/s over a two-minute interval. Avoidance behavior was corrected by gentle nudging of mice with the rear bumper. Most animals exhibited rhythmic gait at 24 cm/s. Between runs, the belt and chamber were sterilized. Data collection occurred 4 days after completion of training and involved securing mice in the chamber and initializing the treadmill immediately at 24 cm/s.

DigiGait™ Imaging Software was used to acquire and process video collected in 30 s intervals. Sequences containing 6-10 continuous strides were chosen for analysis in DigiGait™ Analyzer. Temporal and spatial gait parameters were collected for each assessed mouse and exported to Excel.

### 3.10.13. Necropsy & Histology

WT and *mo-br* treatment cohorts at 2 weeks and 10 weeks were euthanized by isoflurane overdose and thoracotomy. Blood samples for serology were collected by cardiocentesis.

*Histological Samples:* Before organ harvest, mice were perfused through the left ventricle of the heart after severing of the right atrium with 10% neutral buffered formalin. Brains, hearts, livers, kidneys, and spleens were collected, fixed in formalin, and sent to the Texas Veterinary Medical Diagnostic Lab (College Station, TX) for analysis by a blinded pathologist. Reports and digital slides were returned for each sample set.

*Brain Digital Slides:* NDP Viewer was used to review sagittal sections of brain (H&E stain) in order to generate high resolution images. Percent pyknotic neurons of the CA1-3 region of the hippocampus at 40X-80X magnification were generated by counting 400 nuclei in each brain hemisphere (800 nuclei per biological replicate, $n = 4$ per cohort; 3200 total per cohort). Qualitative assessment of cortex and cerebellum was provided in

the pathologist's report along with detailed analysis of the Purkinje cell layer of the cerebellar peduncles.

*Organ Digital Slides:* NDP Viewer was used to review longitudinal and cross sections of liver, kidney, heart, and spleen (H&E stain) in order to generate high resolution images. Qualitative assessment of organs was provided in the pathologist's report.

### 3.10.14. Biochemistry

WT and *mo-br* treatment cohorts at 2 weeks and 10 weeks were euthanized and blood collected as previously described. Before organ harvest, mice were perfused through the left ventricle of heart with normal saline. Brains, hearts, thymus, lungs, livers, spleens, and kidneys were harvested, washed, trimmed, weighted, and flash frozen with liquid nitrogen. Samples were stored at -80°C pending analysis.

*Copper Measurement:* Tissue and serum copper levels were measured by using a PerkinElmer DRC II inductively coupled plasma (ICP) mass spectrometer. Intact tissue samples were washed with 100 μM EDTA-containing water, weighed, and digested with 40% nitric acid (TraceSELECT; Sigma) at 90°C for 18 h, followed by digestion with 1% hydrogen peroxide (Ultratrace analysis; Sigma) at 90°C for 4 h. Samples were diluted in ultrapure metal-free water (TraceSELECT; Sigma) and analyzed by ICP-MS. Copper

standard solutions were prepared by appropriate dilutions of commercially available mixed metal standards (BDH Aristar Plus).

*Immunoblotting:* Tissue samples were homogenized on ice in RIPA extraction buffer (50 mM Tris (pH 7.4), 150 mM NaCl, 1% NP-40, 0.5% sodium deoxycholate, 0.1% SDS supplemented with a 1× cOmplete protease inhibitor cocktail (Roche, Indianapolis, IN) and centrifuged at 4°C for 15 min at 14,000 × g to obtain a supernatant. Protein concentration of the supernatant was determined using BCA assay (Pierce BCA Protein Assay), and indicated protein (20 μg) samples were separated by SDS-PAGE and blotted onto a polyvinylidene difluoride membrane. Membranes were treated for 1 hr in blocking buffer containing 5% nonfat milk dissolved in Tris-buffered saline with 0.1% Tween 20 (TBST-milk), followed by overnight incubation with primary antibody in TBST-milk at 4°C. Primary antibodies were used at the following dilutions: COX1, 1:5000 (14705; Abcam); ATP5A, 1: 10,000 (14748; Abcam); SOD1, 1:5000 (PA1-30195; Invitrogen).

### 3.10.15. *ATP7A* Knockout B16 Melanoma Cells

The B16 melanoma cells were obtained from American Type Culture Collection (ATCC®, B16-F10 CRL-6475™). *ATP7A* KO CellTiter-Glo Luminescent Viability assay (Promega Cat. #G9241) cells were generated by transfecting wild-type B16 cells with a CRISPR-Cas9/GFP construct targeting Exon 16 of ATP7A

[5'-CCCATGGAACCCCAGTAGTGAA-3'] (Sigma-Aldrich), using Lipofectamine 2000. GFP-positive cells were isolated using a Beckman Coulter MoFlo CDP and individual clones were screened for ATP7A protein by immunofluorescence and immunoblot analyses. Cells were grown in complete medium consisting of Dulbecco's modified Eagle's medium (Life Technologies) supplemented with 10% (v/v) fetal bovine serum, 2 mM glutamine and 100 units/ml penicillin and streptomycin (Life Technologies, Carlsbad, CA) in 5% $CO_2$ at 37°C.

*Tyrosinase Activity (Qualitative): ATP7A* KO cells were treated with DMSO, 25 μM $CuCl_2$, or 1 nM ES for 3 days prior to trypsinization, washing, and pelleting. Pigment content of pellet was recorded following visual inspection.

### 3.10.16. *CTR1* Knockout H9c2 Cells

The *CTR1* KO H9c2 cells were generated as described in Soma et al. *Proc Natl Acad Sci U S A* (2018)/PMID 30038027. Briefly, rat H9c2 cells (ATCC®, CLR-1446™) were generated by transfecting wild-type H9c2 cells with a lentiCRISPRv2 construct targeting Exon 1 of CTR1 (Addgene Cat. #52961). Two days after transfection, cells were plated in puromycin selection media. Disruption of *CTR1* was confirmed by genomic sequencing.

*Oxygen consumption rate measurements:* Oxygen consumption rate (OCR) measurements were carried out as previously described (Gohil et al., *Nat Biotech.* 2010/ 20160716) with minor modifications. Briefly, rat H9c2 control and *CTR1* KO cardiomyocytes were treated with DMSO or 1 nM elesclomol for three days in high glucose DMEM growth media supplemented with 10% FBS (Sigma) and 1 mM sodium pyruvate (Life Technologies). The cells were then seeded in XF24-well cell culture microplates (Agilent Technologies) at 20,000 cells/well in 250 µl of growth media with DMSO or 1 nM elesclomol and incubated at 37 °C, 5% CO2 for ~20 h. Before the measurements were made, 525 µl of the pre-warmed growth medium was added to each well and cells were incubated at 37 °C for 30 min. OCR measurements were carried out in intact cells using Seahorse XF24 Extracellular Flux Analyzer (Agilent Technologies). Mix, wait and measure durations were set to 2, 2 and 2 min, respectively. For the mitochondrial stress test, oligomycin, carbonyl cyanide 3-chlorophenylhydrazone (CCCP) and antimycin A were sequentially injected to achieve final concentrations of 0.5, 10 and 1 µM, respectively. Immediately after the assay, the cell culture microplates were washed thrice with 500 µl PBS and 25 µl RIPA lysis buffer (25mM Tris. HCl pH 7.6, 150mM NaCl, 1% NP-40, 1% sodium deoxycholate, 0.1% SDS) was added to each well and incubated on ice for 30 min. Protein concentration in each well was measured by BCA assay (Thermo Scientific), and the OCR values were normalized to protein content.

*ATP measurement*: Rat H9c2 control and *Ctr1* KO cardiomyocytes were treated for 3 days with DMSO or 1 nM elesclomol in No glucose DMEM media supplemented with 10 mM galactose, 10% FBS (Sigma) and 1 mM sodium pyruvate (Life Technologies) were seeded in 96 well plates at 5,000 cells/well. After ~20 h of growth ATP levels were assayed by CellTiter-Glo Luminescent Viability assay (Promega Cat. #9241) according to the manufacturer's instructions.

### 3.10.17. Statistical analysis and software

Statistical analysis was conducted using XLSTAT, GraphPad Prism, and Excel. One-way ANOVA/Welch ANOVA with post hoc Tukey's HSD test and t-test were used to determine significance among cohorts unless otherwise specified. PKSolver was used to analyze PK data and generate models. GraphPad Prism 8 was used to generate growth curves, Kaplan-Meier plot, and preliminary figures. ImageJ was used to quantitatively analyze Western blots. Final figures were processed in Adobe Illustrator.

### 3.11. Acknowledgments

We thank H. McGuire and R. McAdams for rodent husbandry and tissue processing assistance; P. Trivedi for optimizing *mo-br* genotyping protocol; C. Klemashevich and S. Shankar from Texas A&M University Integrated Metabolomics Analysis Core (IMAC) for mass spectroscopy technical expertise. We thank M. Anguiano from Texas Veterinary Medicine Diagnostics Lab (TVMDL) for brain histology technical help.

**Funding:** This work was supported by the Chancellor's Research Initiative, Texas A&M University System (J.C.S.), Welch Foundation grants A-0015 (J.C.S), A-1810 (V.M.G.) and National Institutes of Health grants R01GM111672 (V.M.G.), R01DK110195 (B.E.K).

**Author Contributions:** L.M.G. established *mo-br* rodent colony, husbandry/breeding, drug formulations, PK/Tox experiments, developed interventional protocols, efficacy studies, behavioral studies, and wrote the manuscript. A.S., T.C.S., S.S., M.Z., H.F.G, B.L., and E.N. assisted in husbandry and biological sample processing for PK/Tox, histology, and biochemical experiments. S.S. and M.Z. performed tissue copper, and biochemical studies. A.A. and C.D.V. synthesized ES-$Cu^{2+}$ complex. V.S. and M.J.P. developed the *ATP7A*$^{-/-}$ B16 melanoma cell line and provided technical expertise. F.R.L. performed histopathology sectioning, generation of digital slide sets, and analysis.

S.Y. and B.E.K. established cardiac *Ctr1* KO rodent colony, husbandry/breeding, efficacy studies, histology, and biochemical studies. V.M.G. and J.C.S. developed the concept of ES drug therapy for hereditary copper disorders, provided administrative and technical expertise, undertook data analysis, and helped write the manuscript.

**Competing Interests:** Authors declare no competing interests.

**Data and Materials:** All data is available from the main and supplementary materials.

### 3.12. References


1. B. E. Kim, T. Nevitt, D. J. Thiele, Mechanisms for copper acquisition, distribution and regulation. *Nat Chem Biol.* ***4(3)***, 176-185 (2008).
2. L. M. Gaetke, H. S. Chow-Johnson, C. K. Chow, Copper: toxicological relevance and mechanisms. *Arch Toxicol.* ***88(11)***, 1929-1938 (2014).
3. E. D. Harris, Cellular copper transport and metabolism. *Annu Rev Nutr.* ***20(1)***, 291-310 (2000).
4. N. J. Robinson, D. R. Winge, Copper metallochaperones. *Annu Rev Biochem.* ***79***, 537-562 (2010).
5. I. Valnot et al., Mutations of the SCO1 gene in mitochondrial cytochrome c oxidase deficiency with neonatal onset hepatic failure and encephalopathy. *Am J Hum Genet.* ***67(5)***, 1104-1109 (2000).
6. L. C. Papadopoulou et al., Fatal infantile cardioencephalomyopathy with COX deficiency and mutations in SCO2, a COX assembly gene. *Nat Genet.* ***23(3)***, 333-337 (1999).
7. S. G. Kaler, Inborn errors of copper metabolism. *Handb Clin Neurol.* ***113***, 1745-1754 (2013).
8. H. Ohrvik, D. J. Thiele, How copper traverses cellular membranes through the mammalian copper transporter, Ctr1. *Ann N Y Acad Sci.* ***1314***, 32-41 (2014).
9. B. S. Choi, W. Zheng, Copper transport to the brain by the blood-brain barrier and blood-CSF-barrier. *Brain Res.* ***1248***, 14-21 (2009).

10. S. G. Kaler, ATP7A-related copper transport diseases: emerging concepts and future trends. *Nat Rev Neurol.* ***7(1)***, 15-29 (2011).
11. H. Kodama, Y. Murata, M. Kobayashi, Clinical manifestations and treatment of Menkes disease and its variants. *Pediatr Int.* ***41(4)***, 423-429 (1999).
12. M. Sparaco, A. Hirano, M. Hirano, S. DiMauro, E. Bonilla, Cytochrome *c* oxidase deficiency and neuronal involvement in Menkes' kinky hair disease: immunohistochemical study. *Brain Pathol.* ***3(4)***, 349-354 (1993).
13. S. Zlatic et al., Molecular basis of neurodegeneration and neurodevelopment defects in Menkes Disease. *Neurobiol Dis.* ***81***, 154-161 (2015).
14. S. G. Kaler et al., Neonatal diagnosis and treatment of Menkes disease. *N Engl J Med.* ***358(6)***, 605-614 (2008).
15. J. H. Kim et al., Novel mutations and clinical outcomes of copper-histidine therapy in Menkes disease patients. *Metab Brain Dis.* ***30(1)***, 75-81 (2015)
16. S. Soma et al., Elesclomol restores mitochondrial function in genetic models of copper deficiency. *Proc Natl Acad Sci U S A.* ***115(32)***, 8161-8166 (2018).
17. A. S. Grillo et al., Restored iron transport by a small molecule promotes absorption and hemoglobinization in animals. *Science* ***356****(6338),* 608-616 (2017).
18. M. D. Garrick et al., A direct comparison of divalent metal-ion transporter (DMT1) and hinokitiol, a potential small molecule replacement. *Biometals* ***(32)***, 745-755 (2019).

19. J. Lee, J. R. Prohaska, D. J. Thiele, Essential role for mammalian copper transporter Ctr1 in copper homeostasis and embryonic development. *Proc Natl Acad Sci U S A.* ***98(12)***, 6842-6847 (2001).

20. B. E. Kim et al., Cardiac copper deficiency activates a systemic signaling mechanism that communicates with the copper acquisition and storage organs. *Cell Metab.* ***11(5)***, 353-363 (2010).

21. M. J. Niciu et al., Altered ATP7A expression and other compensatory responses in a murine model of Menkes disease. *Neurobiol Dis.* ***27(3)*** 278-291 (2007).

22. A. Grimes, C. J. Hearn, P. Lockhart, D. F. Newgreen, J. F. Mercer. Molecular basis of the brindled mouse mutant (Mo(br)): a murine model of Menkes disease. *Hum Mol Genet.* ***6(7)***, 1037-1042 (1997).

23. A. Donsante et al., ATP7A gene addition to the choroid plexus results in long-term rescue of the lethal copper transport defect in a Menkes disease mouse model. *Mol Ther.* ***19(12)***, 2114-2123 (2011).

24. M. R. Haddad et al., rAAV9-rsATP7A plus subcutaneous copper histidinate advance survival and outcomes in a Menkes disease mouse model. *Mol Ther Methods Clin Dev.* ***10***, 165-178 (2018).

25. S. G. Kaler, Neurodevelopment and brain growth in classic Menkes disease is influenced by age and symptomatology at initiation of copper treatment. *J. Trace Elem Med Biol.* ***28(4)***, 427-430 (2014).

26. J. W. Pyatskowit, J. R. Prohaska, Copper deficient rats and mice both develop anemia but only rats have lower plasma and brain iron levels. *Comp Biochem Physiol C Toxicol Pharmacol.* ***147(3)***, 316-323 (2008).

27. S. R. Setty et al., Cell-specific ATP7A transport sustains copper-dependent tyrosinase activity in melanosomes. *Nature.* ***454(7208)***, 1142-1146 (2008).

28. J. M. Gillespie, Keratin structure and changes with copper deficiency. *Australas J Dermatol.* ***14(3)***, 127-131 (1973).

29. M. Bourens, A. Barrientos, A *CMC1*-knockout reveals translation-independent control of human mitochondrial complex IV biogenesis. *EMBO Rep.* ***18(3)***, 477-494 (2017).

30. A. A. Yadav, D. Patel, X. Wu, B. B. Hasinoff, Molecular mechanisms of the biological activity of the anticancer drug elesclomol and its complexes with Cu(II), Ni(II), and Pt(II). *J Inorg Biochem.* ***126***, 1-6 (2013).

31. M. Nagai et al., The oncology drug elesclomol selectively transports copper to the mitochondria to induce oxidative stress in cancer cells. *Free Radic Biol Med.* ***52(10)***, 2142-2150 (2012).

32. R. K. Blackman et al., Mitochondrial electron transport is the cellular target of the oncology drug elesclomol. *PLoS One.* ***7(1)***, e29798 (2012).

33. P. Tsvetkov et al., Mitochondrial metabolism promotes adaptation to proteotoxic stress. *Nat Chem Biol.* ***15(7)***, 681-689 (2019).

# Chapter 4

# Conclusions

# 4. CONCLUSIONS

## 4.1. Future Works

ES-$Cu^{2+}$ demonstrated a significant survival benefit in juvenile mice. The interventional protocol devised during the course of this dissertation work increased brain [Cu] with modest improvement in CcO as quantified by COX1/2 levels. Future studies may be needed to assess the benefit of further copper supplementation. Initial improvement in tissue [Cu] at PND 14 declined with age. Possible later supplementation with either ES or ES-$Cu^{2+}$ may further improve survival and neurological function in these mice.

Proposed future study: ES/ES-$Cu^{2+}$ Booster Schedule and Effects.

We observed phenotypic changes as well as connective tissue abnormalities in rescued *mo-br* male mice with improvement in neuromotor function. The lack of complete phenotypic rescue was expected given our proposed mechanism of ES-mediated release of copper within the mitochondria without release mechanism in the Golgi. Surprisingly, mice in our treatment arm demonstrated some improvement of secretory pathway cuproenzymes with marked changes in whisker keratin structure and localized production of melanin pigments. There may be additional pathways of copper transport or target of ES-$Cu^{2+}$ that could explain this beneficial "off-target" effect.

Further elucidation of copper biochemistry and potential ES-$Cu^{2+}$ reductases could potentially allow better repletion of secretory pathway cuproenzymes. Connective tissue defects, owning to lysyl oxidase deficiency, manifested as marfanoid habitus and inguinal hernia as noted by veterinary care technicians. Further, several seemingly healthy adults suddenly died of unknown causes. Attempts to necropsy mice in a timely manner yielded inconclusive results though large thoracic and abdominal hematomas were noted. This could be due to large vessel dissection—a known fatal outcome of multiple connective tissue disorders including Marfan syndrome. Restoration of lysyl oxidase function was attempted but failed due to assay development issues. Understanding the effects of ES therapy may be of critical importance for long-term medical management of Menkes patients.

Proposed future study: Elucidation of ES-$Cu^{2+}$ Partial restoration of pigment and keratin structure. *In vitro* or *in vivo.*

Proposed future study: Histological examination of aorta for histological signs of connective tissue defects.

Proposed future study: ES/ES-$Cu^{2+}$ Effect on LOX in *mo-br* model.

DBH functional activity and catecholamine ratios were not determined during the course of this work due to assay development challenges. Given the neurocognitive symptoms and dysautonomia caused by DBH deficiency, understanding how ES-$Cu^{2+}$ affects this key cuproenzyme is needed.

Proposed future study: DBH activity in CNS and endocrine systems.

Proposed future study: Catecholamine ratios.

The results of our work successfully establish proof of concept that ES can function as a copper ionophore with targeted restoration of copper and cuproenzyme levels in difficult to access bodily compartments such as the brain. Practically, wildtype lifespan was reconstituted in nearly 50% of interventional protocol mice in our long-term observation arm. The utility of ES-$Cu^{2+}$ for the treatment of MD has now successfully been demonstrated in both zebrafish and mice.

Adaptation to human use, as part of either a clinical trial or compassionate use protocol requires dose-finding trials to adapt murine levels to pediatric dose, frequency, and route. Pharmacokinetics are notoriously difficult in pediatric populations due to the need for age and weight adjustments. Careful consultation, modeling, and additional animal experimentation will be required before first-in-human applications.

Proposed future study: ES/ES-$Cu^{2+}$ Pediatric Pharmacokinetics.

Proposed future study: ES/ES-$Cu^{2+}$ Pediatric Pharmacodynamics.

While most Aims outlined in our research proposal were met during the time of this dissertation research, questions pertaining to copper biology, transport, and mechanism of ES-$Cu^{2+}$ beneficial effects still remain. This body of work hopefully establishes a foundation for use of ES or similar chemical analogs for the restoration of copper homeostasis in the context of disordered copper transport diseases.

### 4.2. ES-$Cu^{2+}$ Clinical Trial Design

Below is a list of primary and secondary outcome measures for a theoretical elesclomol clinical trial. Included is a discussion of outcome measures, clinical tools, and laboratory assessment of intervention in children with pathologic *ATP7A* variants.

Given the diverse nature of allelic variants with varying degrees of residual functionality, consultation with a medical geneticist and lab capable of targeted exome sequencing is recommended.

Primary and Secondary Outcome Measures for Elesclomol Trial

1) Denver Developmental Screening Test (DDST) II [Global Development] – Primary Outcome
    a. Pros
        i. Historical with High Degree of Clinician Familiarity
        ii. Moderately Easy to Collect Data & Non-Invasive
        iii. Assesses Multiple Aspects of Development
    b. Cons
        i. Long Time Commitment: Assuming intervention before 1 month of age, serial assessments could range from 2 to 36 months.
        ii. Qualitative Data
        iii. Requires cooperation of typically uncooperative children.

2) CDC or WHO Growth Charts including weight, length, and head circumference with ratios. [Growth] – Primary Outcome
    a. Pros
        i. Historical with Universal Clinician Familiarity
        ii. Easy to Collect Data & Non-Invasive
        iii. Quantitative Data
        iv. Statistic Already Collected for Well-Child Visits

b. Cons

i. Long Time Commitment: Individual time points are much less valuable than long-term trends. High quality data would involve at least 18 months of monitoring. Evidence of failure to thrive (FTT) involves significant percentile crossing observed over multiple time points.

3) Imaging (Cranial MRI) [Central CNS Dysfunction] – Primary Outcome

a. Pros

i. Some Historical Data with Moderate Degree of Clinician Familiarity. Brain appears normal at or near birth followed by progressive cerebral and cerebellar degeneration, white matter changes, and ventricular expansion. T1 weighted images often show elevated intensity of basal ganglia preceding global CNS changes. Tortuous vessels and large vessel pathology well-recognized marker of connective tissue disease.

ii. Qualitative/Quantitative Data

iii. Can be combined with other procedures (i.e. MR angiography) to assess connective tissue aspect of disease progression.

b. Cons

i. Long Time Commitment: Changes from base-line begin subtly and intensify over time. Minimum 18 month commitment.

ii. Expensive: Will require multiple imaging studies to document progressive changes.

iii. Expertise-Intensive: Will require pediatric radiologist/neurologist for data interpretation.

iv. Difficult Data Collection: MR imaging requires approximately 30 minutes of stillness from typically uncooperative children. Pediatric MRI typically requires sedation.

4) Biochemical Markers of Copper Status – Primary Outcome

a. Pros (Serum, CSF, Urine)

i. Historical Data with Moderate Degree of Clinician Familiarity. Such tests should include serum and CSF ceruloplasmin and total copper levels with or without catecholamine ratios.

ii. Direct, Early Measure of Intervention Success.

iii. Can be Collected in A Serial Manner to Provide Rapid Measure of Treatment.

iv. Inexpensive Compared to Imaging Studies.

b. Cons

i. Invasive, Often Distressing to Child & Parents.

ii. Clinical Laboratory Intensive.

iii. Moderate Specimen Collection Difficulty (CSF).

5) Long Term Survival – Primary Outcome
    a. Pros
        i. Historical Data.
        ii. Easy to Collect & Interpret Data.
    b. Cons
        i. Long Time Commitment.
        ii. Not Suitable as Sole Primary Outcome Due to Ethical Reasons: If used, should be in conjunction with items #1-3.

6) Nerve Conduction Studies [Peripheral Neuropathy] – Secondary Outcome
    a. Pros
        i. Some Historical Data with Moderate Degree of Clinician Familiarity: Enables clinician to monitor progressive motor decline and assess functional impact of intervention.
        ii. Easy to Collect & Interpret Data.
        iii. Quantitative Data.
    b. Cons
        i. Somewhat Invasive.
        ii. Can be Difficult to Assess in Small Children.

7) Clinical Tests for Dysautonomia [Autonomic Dysfunction] – Secondary Outcome(s)

a. Pros

    i. Some Historical Data with Universal Degree of Clinician Familiarity.

    ii. Easy to Collect & Interpret Data.

    iii. Non-Invasive.

    iv. Includes normal tests and procedures including heart rate, blood pressure, pupillary response, neurogenic bladder, constipation, etc.

b. Cons

    i. Very Young Patients Tend to be Uncooperative.

    ii. Qualitative Data with High Variability.

8) Serum Chemistries [Toxicity] – Secondary Outcome

a. Pros

    i. Historical Data with Universal Clinician Familiarity.

    ii. Easy Data Interpretation.

    iii. Quantitative and Trend-Oriented.

    iv. Inexpensive.

    v. Should be Collected and Monitored Anyway in Chronically Ill Children.

b. Cons

    i. Invasive

    ii. Biomarkers insensitive to acute/subacute changes in copper status.

9) Urinalysis [Toxicity] – Secondary Outcome

    a. Pros

        i. Historical Data with Universal Clinician Familiarity.

        ii. Easy Data Interpretation.

        iii. Non-Invasive.

        iv. Quantitative and Trend-Oriented.

        v. Inexpensive.

        vi. Should be Collected and Monitored Anyway in Chronically Ill Children.

    b. Cons

        i. Difficult Specimen Collection.

10) Other Clinical Laboratory (CBC, Iron Studies, CMP etc.) – Secondary Outcome

    a. Pros

        i. Provides Well-Rounded Clinical Narrative.

        ii. Inexpensive.

    b. Cons

        i. Questionable, Often Conflicting Historical Data.

        ii. Invasive but Can Be Paired with Other Hematological Specimen Collections.